AN EXPERIMENTAL STUDY OF THE PRINTED-CIRCUIT CIRCULAR DISC ANTENNA

A Thesis

Presented to the Faculty of

The Department of Electrical Engineering

University of Houston

In Partial Fulfillment

of the Requirements for the Degree

Master of Science in Electrical Engineering

---

by

Mark D. Walton

December 1976

ACKNOWLEDGEMENT

To Dr. L. C. Shen and Dr. Stuart A. Long, who patiently guided the research, I would like to express my appreciation and gratitude. I would also like to thank Dr. G. W. Batten for serving on the committee and Margaret Coward for typing this thesis.

AN EXPERIMENTAL STUDY OF THE PRINTED-CIRCUIT, CIRCULAR DISC ANTENNA

An Abstract of a Thesis
Presented to the Faculty of
The Department of Electrical Engineering
University of Houston

In Partial Fulfillment
of the Requirements for the Degree
Master of Science in Electrical Engineering

---

by
Mark D. Walton
December 1976

ABSTRACT

Using Watkins'[1] dominant mode design for a circular resonant structure in microstrip, several circular disc radiators were fabricated on a copper-clad laminate of teflon/glass using conventional printed-circuit board etching techniques. The input impedance and far field patterns of these antennas were measured as a function of feed position and dielectric thickness. The effect of a cross-polarizing of the radiators was also measured assuming that Watkins' surface current distribution on the disc for the n=1 mode would result in a linearly polarized radiation. Finally, a comparison between the measured and theoretical radiation properties is presented for various combinations of antenna feed position and dielectric thickness.

TABLE OF CONTENTS

Page

CHAPTER I

INTRODUCTION

With the introduction of the printed-circuit board to the electronics industry, came great reductions in circuit weight and complexity. In many cases involving spacecraft or aircraft, antennas which are lightweight and simple to fabricate are of primary concern to the designer. Recently, printed circuit technology has been applied to the fabrication of printed-circuit board antennas.[2,3] Not only are these antennas lightweight and easy to fabricate, but also they are low-profile and extremely reproduceable. These antennas are fabricated using standard printed-circuit board etching techniques. The printed-circuit antenna now offers a homogeneous technology for the fabrication of communication systems since it is now possible to design the antenna, feed network, phase shifters, and associated circuitry on the same printed-circuit board. This type of technology will offer to the engineer great reductions in the size, weight, and cost of communication systems.

The printed-circuit, circular disc antenna shown in Figure 1 was chosen to be analyzed experimentally with the ultimate goal being to verify or disprove the validity of Watkins' zeroth-order theory for various dielectric substrate thicknesses and antenna feed positions.

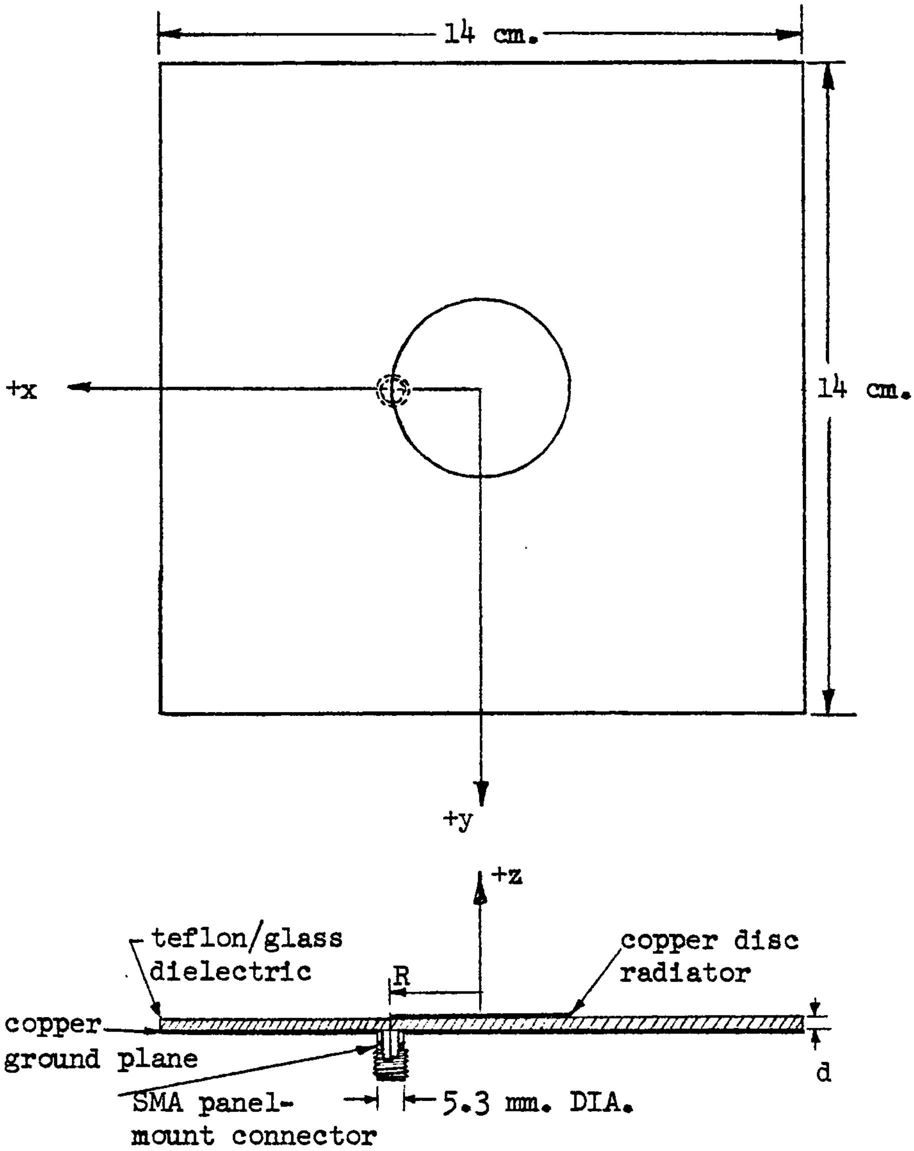

Figure 1: The Printed-Circuit, Circular Disc Antenna in An Edge-Fed Configuration

CHAPTER II

DESIGN AND CONSTRUCTION OF THE ANTENNAS

II.1 Zeroth-Order Theory

From a close observation of Figure 1, one can see that the area between the outer edges of the disc and the ground plane form an aperture through which radiation may occur. This must be so if a disc over a ground plane separated by a dielectric sheet is to behave like an antenna. In Watkins' analysis of circular resonant structures in microstrip, he assumed that the distance between the disc and the ground plane was very small compared to a wavelength in the dielectric material, i.e. $kd \ll \lambda$. With the relationship between the radiator/ground plane separation and wavelength established, Watkins made two additional assumptions in his analysis. He stated fringe effects at the edge of the disc are negligible and radiation from the aperture formed by the edge of the disc and the ground plane is much smaller than the stored energy in the parallel-plate region. These three assumptions are basic to the zeroth-order theory, although they may seem inappropriate if the disc/ground plane configuration is to be used as a radiating device. However, Watkins' theory does provide a starting point for an experimental study of the printed-circuit, circular disc antenna.

II.2 Design Considerations

The antennas were designed such that for a given disc radius, R, resonance occurred for the lowest order or n=1 mode. From Watkins, this radius is given by:

$$R(\text{cm}) = 1.84118 \times \frac{30}{2\pi f\sqrt{\varepsilon_r}} \tag{1}$$

where: f = frequency in gigahertz

ε_r = relative dielectric constant

Several commercial companies offer a wide variety of copper-clad dielectric materials in various thicknesses and with various relative dielectric constants. A teflon/glass substrate material with a relative dielectric constant of approximately 2.45 was chosen* because of its availability and its desirable physical characteristics. The teflon/glass substrate is not brittle as is a substrate material like Rexolite, and tolerances on its thickness can be accurately maintained.

Before a design radius, R, could be established, other factors had to be considered. First, the cost of the copper-clad dielectric board prohibited a circular disc radiator that was excessively large, because it was decided that the width and height of the square ground plane would be at least three times larger than the diameter of the disc. Second, the availability of suitable test equipment which operated at the chosen design frequency had to be considered. This test equipment included signal sources, a network analyzer, directional couplers, crystals, pyramidal horn antennas, power meters, receivers, and an anechoic chamber. The anechoic chamber was designed to operate in the range from 2 to 4 gigahertz, and this frequency range was well within the design limits of the other test equipment that was available. In order to investigate the broadband characteristics of the printed-circuit, circular disc antenna, an operating frequency of approximately 3.0 gigahertz, a frequency close to

*made by 3M Company, St. Paul, Minn.

the midpoint of the 2 to 4 gigahertz range, was chosen.

Letting: $\varepsilon_r = 2.45$

$f = 3.0$ GHz

$$R = 1.84118 \times \frac{30}{2\pi(3.0)\sqrt{2.45}}$$

$R \simeq 1.87$ cm

or

$D \simeq 3.74$ cm

Using a disc diameter of 3.74 cm would mean the dimensions on the ground plane would have to be at least 11.2 cm X 11.2 cm. A ground plane of this size would certainly not be prohibitive.

II.3 Design of the Antennas

Measured test data on the electrical and physical characteristics of the copper-clad dielectric materials was sent with each sample that had a different dielectric substrate thickness. This data is shown in Table II.1. In order to accurately evaluate the effects of different dielectric substrate thicknesses on the circuit and radiation properties

K-6098-11 Product Number	Dissipation Factor @ X-band	Dielectric Constant @ X-band	Substrate Thickness		
			Ave.	Min.	Max.
LX-1004	-	2.47	0.16 cm	-	-
LX-1030	.0018	2.48	0.0296 in. 0.075 cm.	0.0291 in. 0.074 cm.	0.0299 in. 0.076 cm.
LX-1010	.0020	2.45	0.0143 in. 0.036 cm.	0.0142 in. 0.036 cm.	0.0144 in. 0.036 cm.

Table II.1 - Manufacturer's Data on
3 Thicknesses of Copper-Clad Dielectric Board

of the printed-circuit, circular disc antenna, it was desirable that each copper-clad board have the same relative dielectric constant. From Table II.1, one can see that this was almost accomplished. The manufacturer would only guarantee in their ordering brochure that each copper-clad board would have a relative dielectric constant within a certain tolerance of ±.04. Therefore, the actual dielectric constant of each sheet was not known until the time of delivery. This variation in relative dielectric constant produced a negligible change in the calculation of the resonant frequency for the n=1 mode of a given size radiator. A circular disc with a radius of 1.88 cm was chosen for this experimental investigation. Solving equation (1) for frequency, one has:

$$f(\text{GHz}) = 1.84118 \times \frac{30}{2\pi R \sqrt{\varepsilon_r}} \tag{2}$$

For

$\varepsilon_r = 2.45 \rightarrow \quad f = 2.987$ GHz

$\varepsilon_r = 2.47 \rightarrow \quad f = 2.975$ GHz

$\varepsilon_r = 2.48 \rightarrow \quad f = 2.969$ GHz

Thus the worst case difference in relative dielectric constants for the three sheets that were used accounted for a 0.6% change in the calculated resonant frequency.

II.4 Construction of the Antennas

As was mentioned earlier, a disc radius of 1.88 cm was used in the design regardless of the dielectric substrate thickness or the position of the feed point. The physical properties of each antenna are shown in Table II.2.

Antenna #	R (cm)	Relative Dielectric Constant	Dielectric Thickness (cm)	Feed Point
1	1.88	2.47	0.16	R
2	1.88	2.47	0.16	3/4 R
3	1.88	2.47	0.16	1/2 R
4	1.88	2.48	0.075	R
5	1.88	2.48	0.075	3/4 R
6	1.88	2.48	0.075	1/2 R
7	1.88	2.45	0.036	R
8	1.88	2.45	0.036	3/4 R
9	1.88	2.45	0.036	1/2 R

Table II.2 Physical Properties of the Printed-Circuit, Circular Disc Antennas

Thus, three separate antennas which were fed at different points were fabricated on each of three copper-clad substrate materials of different thickness. This accomplished two things. First, the effects of moving the feed point to three separate locations on a substrate material with the same thickness could be experimentally investigated. The first, second, and third feed point were respectively located at R, 3/4 R, and 1/2 R, where R, the radius, was measured from the center of the disc. Second, the effects of changing the dielectric substrate thickness for radiators that were fed at the same point could be evaluated.

All nine circular disc radiators were fabricated using conventional photographic etching techniques[4]. Nine separate copper-clad boards were cut to dimensions of approximately 14 cm by 14 cm. Each board was coated with photoresist on both sides and then spun in a low temperature oven to dry the photoresist. A rubylith masque was made for each side of the printed-circuit board. One masque was made for the radiating disc and another masque was made for the feed-through hole in the ground plane. Each side of the board was exposed to an ultraviolet lamp for approximately 15 minutes with the appropriate masque accurately positioned over the printed-circuit board. A great deal of caution had to be exercised to make certain that the feed-through hole in the ground plane was accurately aligned with the feed position on the disc radiator. After exposure to the ultraviolet lamp, each copper-clad board was placed in a developing solution of thichloroethylene. Finally, the boards were placed in a mechanically agitated container of etching solution made of ferric chloride. After the etching process was completed, each printed-circuit board had a disc radiator with a radius of 1.88 cm etched on one side, and an appropriately located feed-through hole etched in the ground plane on the opposite side. The diameter of the feed-through hole was important because any discontinuity caused by the ground plane in the coaxial line of the SMA panel mount connector would affect the impedance measurements of the circular disc antenna.

CHAPTER III

MEASUREMENT OF THE INPUT IMPEDANCE OF THE ANTENNAS

III.1 The Network Analyzer System[5]

The network analyzer system shown in Figure 2 was used for all impedance measurements. This system consists of a sweep oscillator with an appropriate RF plug-in, a transducer, a harmonic frequency converter, a network analyzer mainframe, a polar display unit, and a precision x-y recorder.

The 8690B sweep oscillator provides a CW or a swept RF signal which can be leveled over the entire sweep range of the plug-in. However, a leveled source is not required by the network analyzer since there are two matched AGC (automatic gain control) amplifiers in the 8410A mainframe to compensate for any RF power fluctuations during a sweep. Regardless, to insure accurate results in this experimental study, the 8690B sweep oscillator was leveled externally with the use of a directional coupler and a crystal detector. As a precaution against spurious outputs and harmonic outputs, an in-line coaxial low pass filter was inserted in the RF path which leaves the sweep oscillator.

The transducer, placed as it is between the signal source and the harmonic frequency converter, has three functions. First, it has to split the incoming signal into a reference and test channel. Secondly, it has to provide the capability of extending the electrical length of the reference channel so that the distances that the reference and test signals travel are equal. Thirdly, it correctly connects the system for transmission or reflection measurements. Figure 2 shows the HP 8743A transducer configured for complex reflection coefficient measurements.

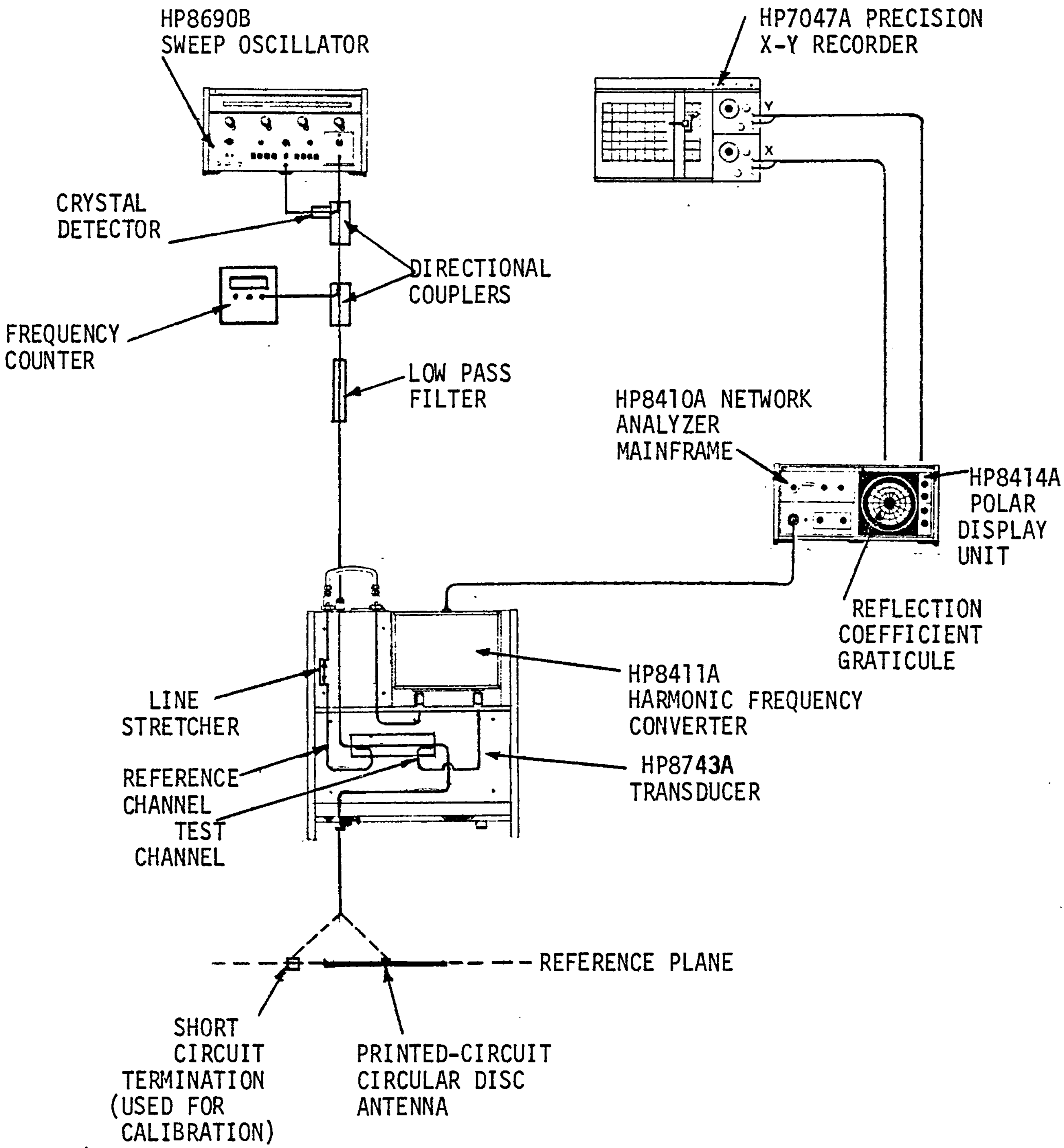

Figure 2: The Network Analyzer System

Input impedance can be obtained directly from the complex reflection coefficient by using the relation:

$$\frac{Z_{in}}{Z_o} = \frac{1 + \Gamma}{1 - \Gamma} \qquad (3)$$

where: $\frac{Z_{in}}{Z_o}$ = normalized input impedance

Z_o = characteristic impedance of the system (50Ω)

Γ = complex reflection coefficient

The HP 8411A harmonic frequency converter unit and the HP 8410A network analyzer mainframe serve as the core of the entire system. The test channel and reference channel information enter the harmonic frequency converter from the transducer where, by harmonic sampling, the input signals are converted to a fixed IF frequency. This enables low frequency circuitry in the network analyzer to measure amplitude and phase relationships. Through harmonic sampling, the system can operate over an extremely wide frequency range; in this case the range is 110 MHz to 18 GHz.

The amplitude and phase detectors are in the HP 8414A polar display unit. This unit provides a polar plot of complex reflection coefficients and can be used with either CW or swept frequency. The magnitude of the complex reflection coefficient of the device under test is read on the concentric circles, with $|\Gamma| = 0$ at the center of the display and $|\Gamma| = 1$ at the edge of the display. The phase angle of each point is read by noting where the radial line that passes through the point intersects the outside ring of the graticule.

Since divisions on the polar display graticule were rather coarse, a visual observation of the reflection coefficient points was not accurate. By using the HP 7047A precision x-y recorder, the reflection coefficient trace shown on the polar display unit could be accurately duplicated on a Smith chart. Copies of the precision x-y recorder Smith chart plots are shown in Appendix 1. From these plots, the magnitude and phase of the complex reflection coefficient was accurately determined, since the reflection coefficient graticule on the Smith chart has many more divisions than the reflection coefficient graticule on the polar display unit.

III.2 Calibration of the Network Analyzer System

Prior to the measurement of the input impedance of the printed-circuit, circular disc radiators, the network analyzer system was calibrated using a short-circuit termination. After initial calibration of the system, impedance measurements were begun on the printed-circuit circular disc antennas. Since the physical position of the short-circuit termination was established as the reference point for future impedance measurements, particular care had to be taken to insure that the reference plane chosen as the load position of the printed-circuit, circular disc antennas occurred at the same point in the system as did the short-circuit termination. Different reference points would cause an ambiguity in the measurements, since from the following relationship for a terminated lossless transmission line, one can observe that input impedance changes with position from the load.

$$Z(\ell) = Z_0 \frac{Z_L + jZ_0 \tan \beta\ell}{Z_0 + jZ_L \tan \beta\ell} \ (\Omega) \tag{4}$$

where $Z(\ell)$ = impedance at a distance ℓ looking toward the load (Ω)

Z_0 = characteristic impedance of the line (Ω)

Z_L = load impedance (Ω)

β = propagation constant (m^{-1})

ℓ = distance from the load (m)

The effective load position chosen for the printed circuit, circular disc antennas was the substrate ground plane, and this was made to coincide with the position of the short-circuit termination that was used in the system calibration.

III.3 Impedance Measurement Results

III.3a Tabulated Impedance Measurements

Tables III.1 through III.9 contain the results of the impedance measurements. Real and imaginary parts of impedance were calculated from the measured complex reflection coefficients by using equation (3). This task was simplified by writing a computer program on the Wang 720C Programmable Calculator. This computer program is included in Appendix 2. Tables III.1 through III.3 contain data that was taken on three printed-circuit, circular disc antennas that were fabricated on a substrate thickness of approximately 0.16 cm. The feed position of each radiator is denoted on each table. Tables III.4 through III.6 are pertinent to printed-circuit, circular disc antennas that were fabricated on a substrate thickness of approximately 0.075 cm. Tables III.7 through III.9 apply to circular disc antennas that were fabricated on a substrate material with a thickness of approximately 0.036 cm.

SUBSTRATE THICKNESS: .16 CM.

DIELECTRIC THICKNESS: 2.47

EDGE FED RADIATOR

FREQUENCY (GHZ)	REFLECTION COEFFICIENT MAGNITUDE	REFLECTION COEFFICIENT ANGLE	IMPEDANCE REAL PART	IMPEDANCE IMAGINARY PART
2.400	1.00	80	0	60
2.600	.93	56	8	93
2.680	.92	40	18	135
2.700	.91	38	22	142
2.710	.91	36	24	150
2.720	.91	32	30	169
2.730	.90	29	40	185
2.740	.89	27	50	196
2.750	.88	24	68	215
2.760	.86	21	97	230
2.770	.85	18	131	248
2.780	.84	14	195	269
2.790	.83	11	262	267
2.800	.82	7	367	224
2.810	.80	2	439	68
2.815	.79	0	426	0
2.820	.79	-2	417	-61
2.830	.77	-6	332	-131
2.840	.74	-11	239	-148
2.850	.73	-15	190	-154
2.860	.72	-20	146	-149
2.870	.71	-25	114	-138
2.880	.70	-32	84	-122
2.890	.68	-38	69	-107
2.900	.67	-44	57	-95
3.000	.66	-118	14	-28
3.100	.77	-173	7	-3
3.200	.89	156	3	11

Table III.1 Impedance Measurement Results

SUBSTRATE THICKNESS: .16 CM.

DIELECTRIC CONSTANT: 2.47

FEED POINT AT 3/4R

FREQUENCY (GHZ)	REFLECTION COEFFICIENT MAGNITUDE	REFLECTION COEFFICIENT ANGLE	IMPEDANCE REAL PART	IMPEDANCE IMAGINARY PART
2.400	1.00	94	0	47
2.600	.94	68	5	74
2.710	.90	45	18	118
2.720	.89	42	22	127
2.730	.88	38	29	140
2.740	.87	35	37	150
2.750	.86	32	46	162
2.760	.84	28	66	177
2.770	.83	25	84	190
2.780	.81	21	120	202
2.790	.80	17	164	213
2.800	.78	12	237	197
2.810	.77	8	300	158
2.820	.75	0	350	0
2.830	.72	-5	287	-74
2.840	.70	-10	229	-109
2.850	.68	-15	181	-118
2.860	.67	-21	139	-121
2.870	.66	-27	109	-115
2.880	.65	-34	84	-105
2.890	.64	-41	67	-94
2.900	.63	-49	53	-83
3.000	.68	-123	12	-25
3.100	.79	-168	6	-5
3.200	.89	167	3	6
3.400	.95	136	1	20

Table III.2 Impedance Measurement Results

SUBSTRATE THICKNESS: .16 CM.

DIELECTRIC CONSTANT: 2.47

FEED POINT AT 1/2R

FREQUENCY (GHZ)	REFLECTION COEFFICIENT MAGNITUDE	REFLECTION COEFFICIENT ANGLE	IMPEDANCE REAL PART	IMPEDANCE IMAGINARY PART
2.400	1.00	108	0	36
2.600	.93	85	4	54
2.760	.76	40	51	118
2.770	.74	35	67	127
2.780	.71	29	95	131
2.790	.68	22	133	126
2.800	.64	15	170	96
2.810	.60	6	192	38
2.818	.58	0	188	0
2.820	.57	-3	181	-15
2.830	.54	-13	148	-50
2.840	.50	-25	109	-61
2.850	.48	-35	87	-62
2.860	.46	-47	67	-57
2.870	.46	-60	52	-53
2.880	.46	-75	40	-45
2.890	.47	-88	33	-39
2.900	.49	-100	27	-34
3.000	.76	-175	7	-2
3.100	.87	159	4	9
3.200	.95	144	1	16

Table III.3 Impedance Measurement Results

SUBSTRATE THICKNESS: .075 CM.

DIELECTRIC CONSTANT: 2.48

EDGE FED RADIATOR

FREQUENCY (GHZ)	REFLECTION COEFFICIENT MAGNITUDE	REFLECTION COEFFICIENT ANGLE	IMPEDANCE REAL PART	IMPEDANCE IMAGINARY PART
2.500	.99	108	0	36
2.700	.94	80	4	59
2.790	.87	48	21	109
2.800	.86	42	28	125
2.810	.84	36	42	143
2.820	.82	29	69	167
2.830	.79	22	118	186
2.840	.76	15	193	180
2.850	.74	8	276	126
2.860	.72	0	307	0
2.870	.70	-10	229	-109
2.880	.69	-20	146	-131
2.890	.68	-31	91	-118
2.900	.67	-44	57	-95
3.000	.81	-141	6	-17
3.100	.90	179	3	0
3.400	.98	139	1	19

Table III.4 Impedance Measurement Results

SUBSTRATE THICKNESS: .075 CM.

DIELECTRIC CONSTANT: 2.48

FEED POINT AT 3/4R

FREQUENCY (GHZ)	REFLECTION COEFFICIENT MAGNITUDE	REFLECTION COEFFICIENT ANGLE	IMPEDANCE REAL PART	IMPEDANCE IMAGINARY PART
2.500	1.00	121	0	28
2.700	.93	94	3	47
2.780	.88	66	11	76
2.820	.81	42	38	120
2.830	.78	34	62	138
2.840	.75	26	102	153
2.850	.72	18	162	149
2.860	.69	10	224	102
2.869	.68	0	262	0
2.880	.66	-13	189	-99
2.890	.65	-25	118	-112
2.900	.65	-38	73	-100
2.910	.64	-50	50	-83
3.000	.81	-135	6	-20
3.100	.90	-171	3	-3
3.400	.98	153	1	12

Table III.5 Impedance Measurement Results

SUBSTRATE THICKNESS: .075 CM.

DIELECTRIC CONSTANT: 2.48

FEED POINT AT 1/2R

FREQUENCY (GHZ)	REFLECTION COEFFICIENT MAGNITUDE	REFLECTION COEFFICIENT ANGLE	IMPEDANCE REAL PART	IMPEDANCE IMAGINARY PART
2.500	.99	133	0	22
2.700	.92	113	3	33
2.800	.84	83	10	56
2.850	.66	44	58	94
2.860	.61	32	93	96
2.870	.56	18	138	70
2.875	.54	9	157	38
2.880	.52	0	158	0
2.885	.49	-13	133	-38
2.890	.48	-21	115	-51
2.900	.47	-43	73	-60
2.950	.67	-130	12	-22
3.000	.83	-163	5	-7
3.100	.92	171	2	4
3.400	.97	147	1	15

Table III.6 Impedance Measurement Results

SUBSTRATE THICKNESS: .036 CM.

DIELECTRIC CONSTANT: 2.45

EDGE FED RADIATOR

FREQUENCY (GHZ)	REFLECTION COEFFICIENT MAGNITUDE	REFLECTION COEFFICIENT ANGLE	IMPEDANCE REAL PART	IMPEDANCE IMAGINARY PART
2.600	.95	127	2	25
2.800	.86	90	7	49
2.850	.68	54	41	83
2.860	.63	42	65	92
2.870	.57	29	103	84
2.875	.54	20	128	67
2.880	.52	12	144	43
2.885	.49	0	146	0
2.890	.47	-9	133	-25
2.895	.46	-22	110	-48
2.900	.45	-35	86	-55
2.905	.45	-48	66	-55
2.910	.46	-60	52	-53
2.950	.68	-128	12	-23
3.000	.85	-163	4	-7
3.200	.98	162	1	8

Table III.7 Impedance Measurement Results

SUBSTRATE THICKNESS: .036 CM.

DIELECTRIC CONSTANT: 2.45

FEED POINT AT 3/4R

FREQUENCY (GHZ)	REFLECTION COEFFICIENT MAGNITUDE	REFLECTION COEFFICIENT ANGLE	IMPEDANCE REAL PART	IMPEDANCE IMAGINARY PART
2.600	.98	135	1	21
2.800	.83	94	9	46
2.840	.62	56	45	74
2.850	.55	42	72	76
2.855	.51	32	94	68
2.860	.48	24	109	55
2.865	.45	13	122	31
2.870	.42	0	122	0
2.875	.41	-14	112	-26
2.880	.40	-32	87	-44
2.885	.40	-44	72	-47
2.890	.41	-59	56	-47
2.900	.48	-86	33	-41
2.950	.80	-149	6	-13
3.100	.94	172	2	3
3.600	.99	150	0	13

Table III.8 Impedance Measurement Results

SUBSTRATE THICKNESS: .036 CM.

DIELECTRIC CONSTANT: 2.45

FEED POINT AT i/2R

FREQUENCY (GHZ)	REFLECTION COEFFICIENT MAGNITUDE	REFLECTION COEFFICIENT ANGLE	IMPEDANCE REAL PART	IMPEDANCE IMAGINARY PART
2.600	.98	145	1	16
2.800	.83	112	7	33
2.830	.63	88	22	47
2.840	.52	76	36	50
2.850	.38	59	57	43
2.855	.30	45	68	32
2.860	.24	30	73	19
2.864	.18	0	72	0
2.870	.18	-42	63	-15
2.875	.24	-80	48	-24
2.880	.31	-98	38	-25
2.900	.60	-136	14	-18
3.000	.94	175	2	2
3.200	.99	163	0	7

Table III.9 Impedance Measurement Results

III.3b Effects of the Dielectric Substrate Thickness on Input Impedance

Figures 3 through 8 graphically display the effects of the dielectric substrate thickness on the input impedance. Figures 3 and 4 show the effects on resistance and reactance, respectively, of edge-fed radiators etched on different substrate thicknesses. Two phenomena are immediately observable from these figures. First, the magnitude of the resistive and reactive component of input impedance decreases for decreasing substrate thickness. Secondly, the resonant frequency, or frequency at which the reactive component of impedance is zero, increases for decreasing substrate thickness. For edge fed radiators, resonance occurred at 2.815 GHz, 2.86 GHz and 2.885 GHz, for dielectric thicknesses of 0.16 cm, 0.075 cm and 0.036 cm, respectively.

Figures 5 and 6 are similar to Figures 3 and 4, respectively, except these figures pertain to radiators that were fed at 3/4 of a disc radius. Once again the magnitude of the resistance and reactance decreased for decreasing dielectric thickness. For these 3/4 R fed radiators, resonance occurred at 2.82 GHz, 2.869 GHz, and 2.87 GHz for substrate thicknesses of 0.16 cm, 0.075 cm, and 0.036 cm, respectively. Note that the difference in the resonance frequency of the radiator etched on the 0.075 cm substrate thickness and the radiator etched on the 0.036 cm substrate thickness is only 1 MHz.

Figures 7 and 8 display the resonance behavior of 1/2 R fed radiators etched on different substrate thicknesses. As was the case for radiators that were edge fed and 3/4 R fed, the magnitude of the resistance and reactance for 1/2 R fed radiators decreased with decreasing substrate thickness. However, the resonant frequency for 1/2 R fed radiators did not continuously increase for decreasing substrate

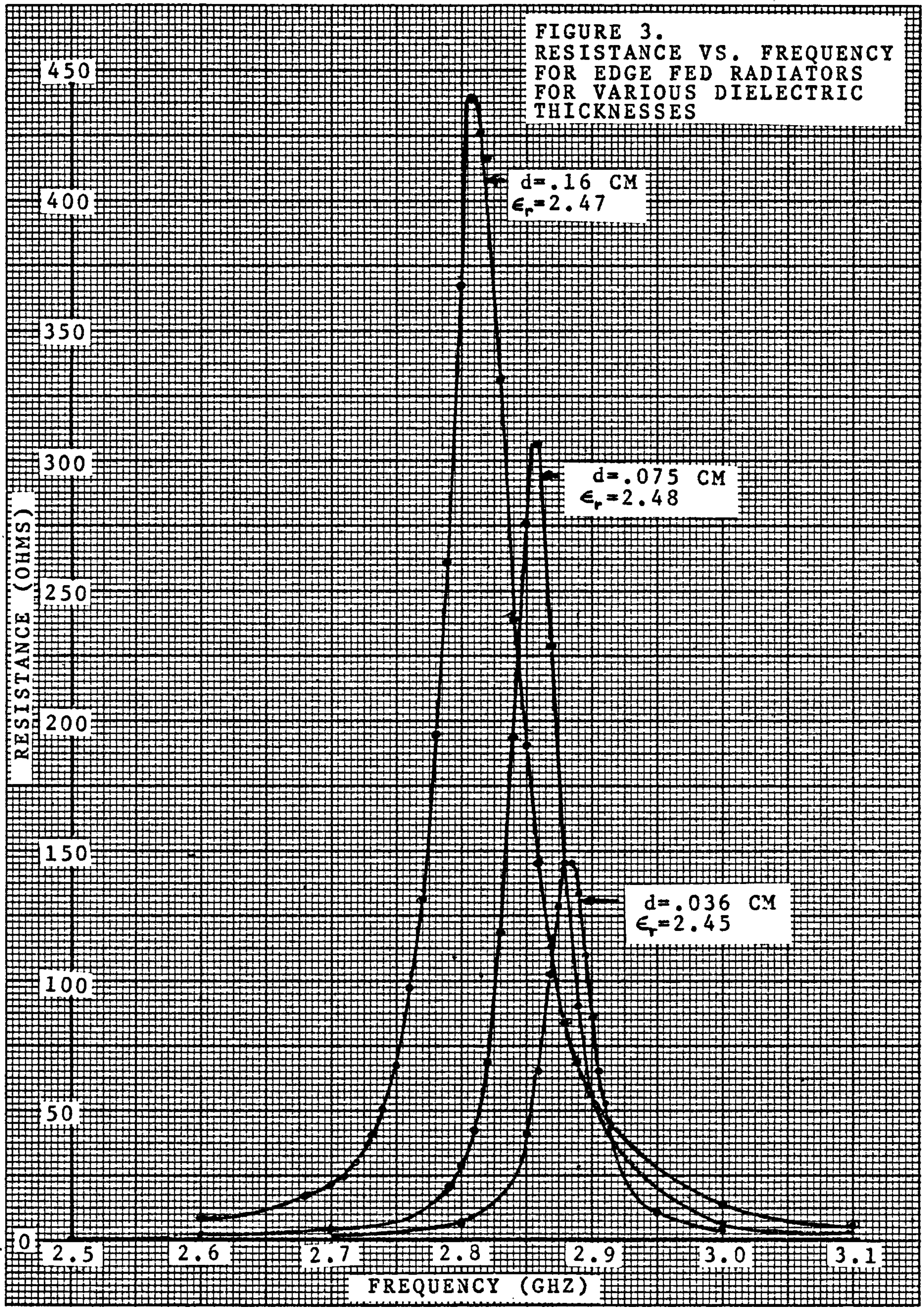
FIGURE 3.
RESISTANCE VS. FREQUENCY
FOR EDGE FED RADIATORS
FOR VARIOUS DIELECTRIC
THICKNESSES
d=.16 CM
ϵ_r=2.47
d=.075 CM
ϵ_r=2.48
d=.036 CM
ϵ_r=2.45
RESISTANCE (OHMS)
0
50
100
150
200
250
300
350
400
450
2.5
2.6
2.7
2.8
2.9
3.0
3.1
FREQUENCY (GHZ)

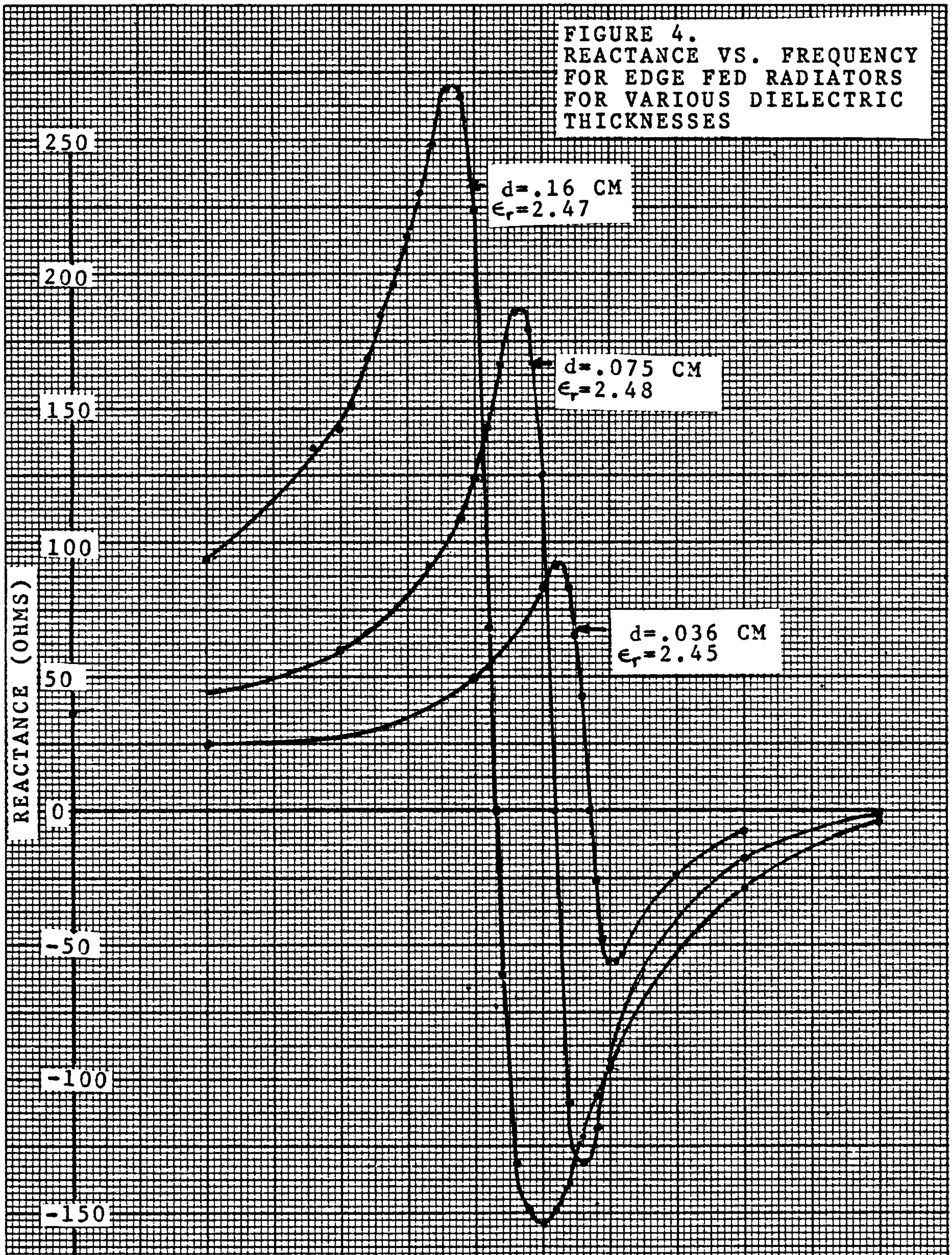
FIGURE 4.
REACTANCE VS. FREQUENCY
FOR EDGE FED RADIATORS
FOR VARIOUS DIELECTRIC
THICKNESSES
d=.16 CM
ϵ_r=2.47
d=.075 CM
ϵ_r=2.48
d=.036 CM
ϵ_r=2.45
250
200
150
100
50
0
-50
-100
-150
REACTANCE (OHMS)
2.5
2.6
2.7
2.8
2.9
3.0
3.1
FREQUENCY (GHZ)

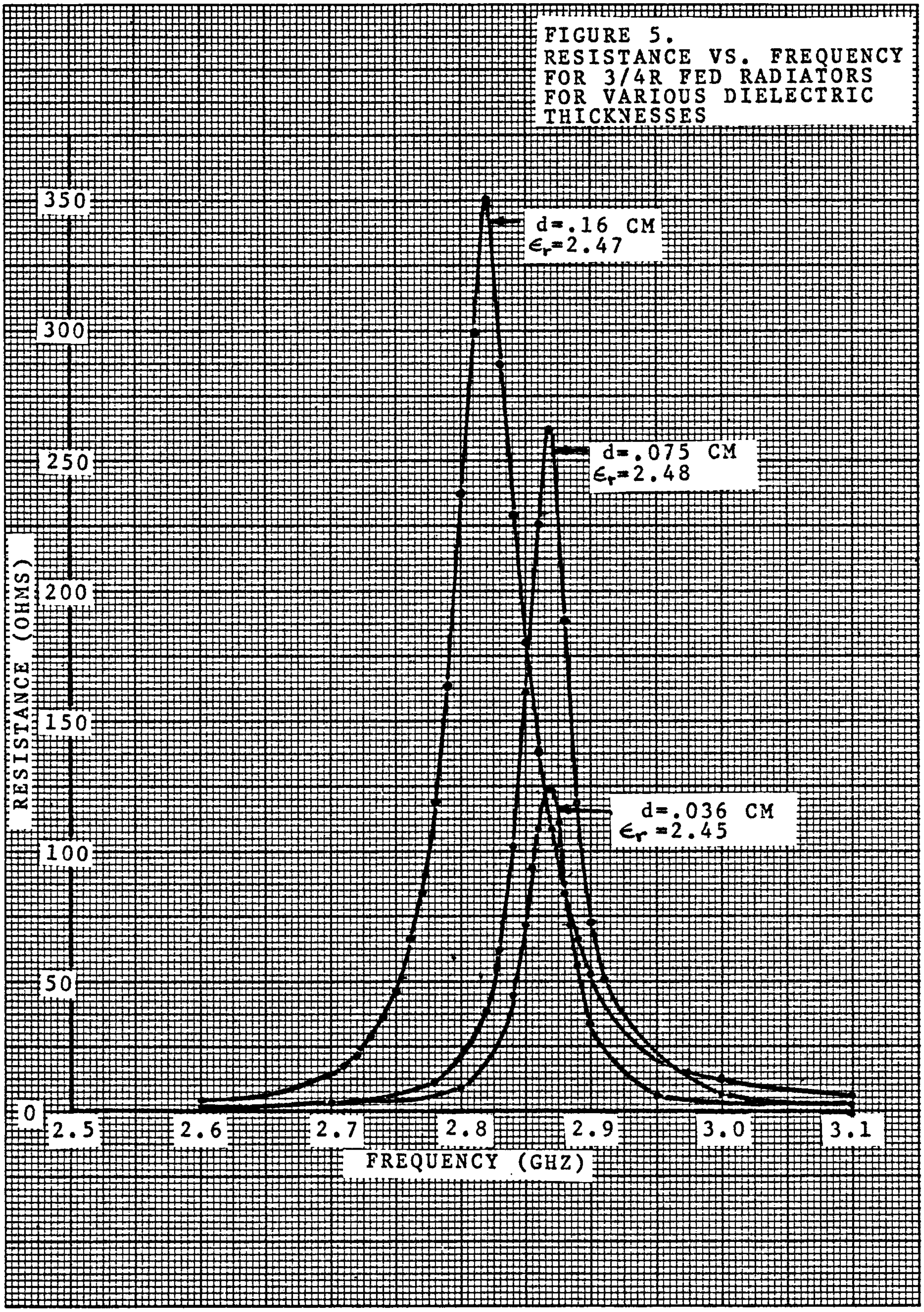
FIGURE 5.
RESISTANCE VS. FREQUENCY
FOR 3/4R FED RADIATORS
FOR VARIOUS DIELECTRIC
THICKNESSES
d=.16 CM
ϵ_r=2.47
d=.075 CM
ϵ_r=2.48
d=.036 CM
ϵ_r =2.45
RESISTANCE (OHMS)
350
300
250
200
150
100
50
0
2.5
2.6
2.7
2.8
2.9
3.0
3.1
FREQUENCY (GHZ)

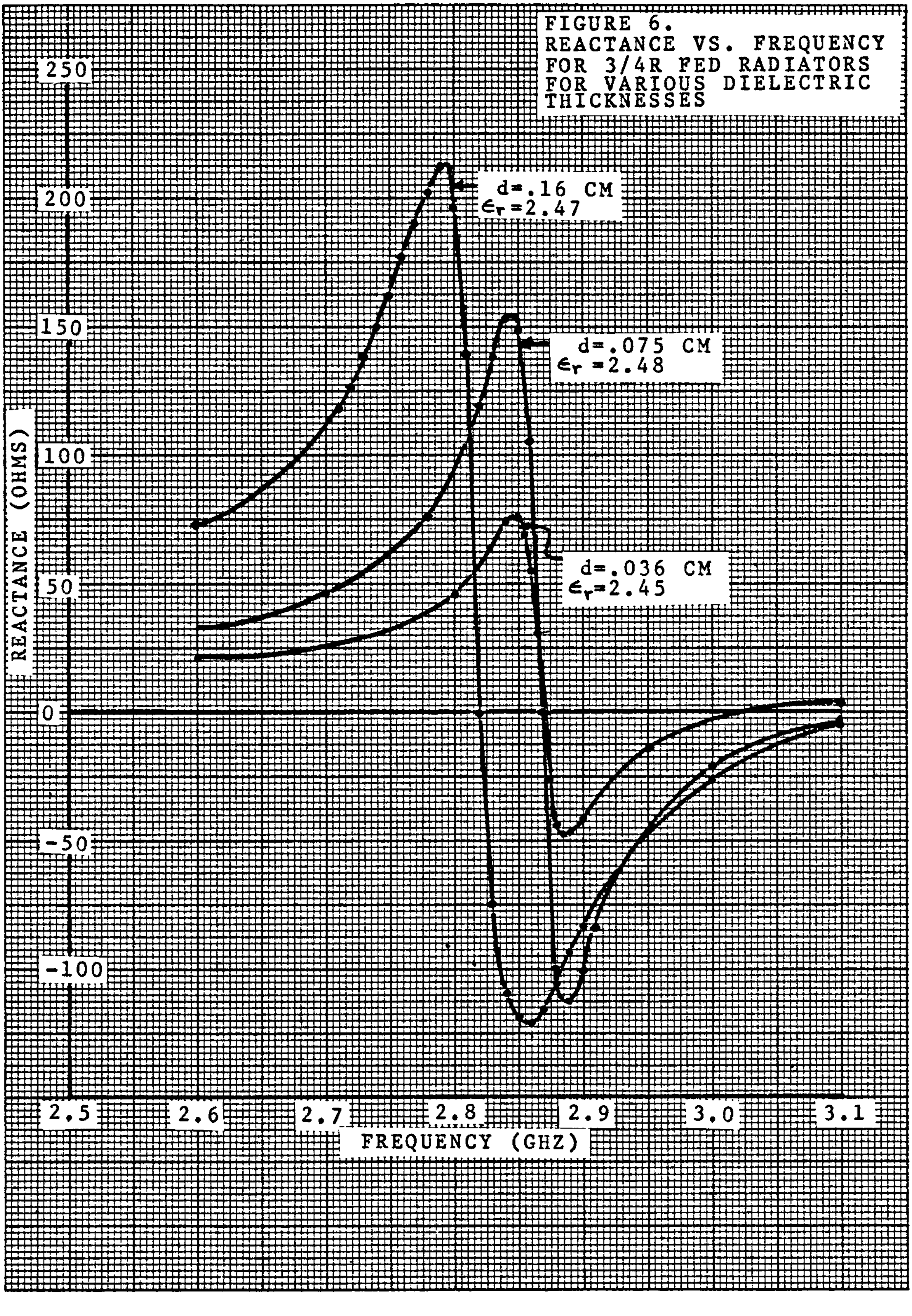
FIGURE 6.
REACTANCE VS. FREQUENCY
FOR 3/4R FED RADIATORS
FOR VARIOUS DIELECTRIC
THICKNESSES
d=.16 CM
ϵ_r=2.47
d=.075 CM
ϵ_r=2.48
d=.036 CM
ϵ_r=2.45
REACTANCE (OHMS)
250
200
150
100
50
0
-50
-100
2.5
2.6
2.7
2.8
2.9
3.0
3.1
FREQUENCY (GHZ)

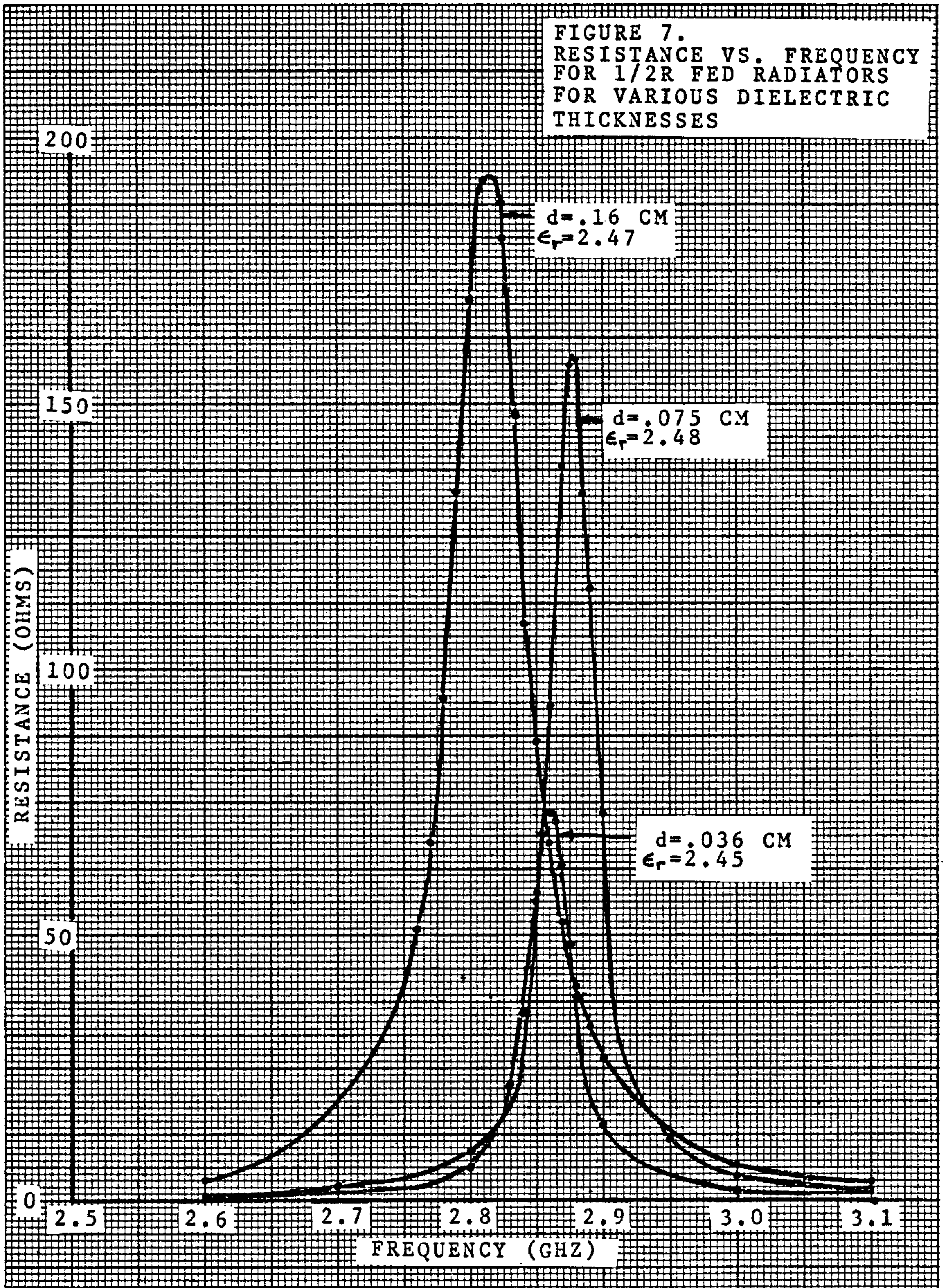
FIGURE 7.
RESISTANCE VS. FREQUENCY
FOR 1/2R FED RADIATORS
FOR VARIOUS DIELECTRIC
THICKNESSES
d=.16 CM
ϵ_r=2.47
d=.075 CM
ϵ_r=2.48
d=.036 CM
ϵ_r=2.45
RESISTANCE (OHMS)
0
50
100
150
200
2.5
2.6
2.7
2.8
2.9
3.0
3.1
FREQUENCY (GHZ)

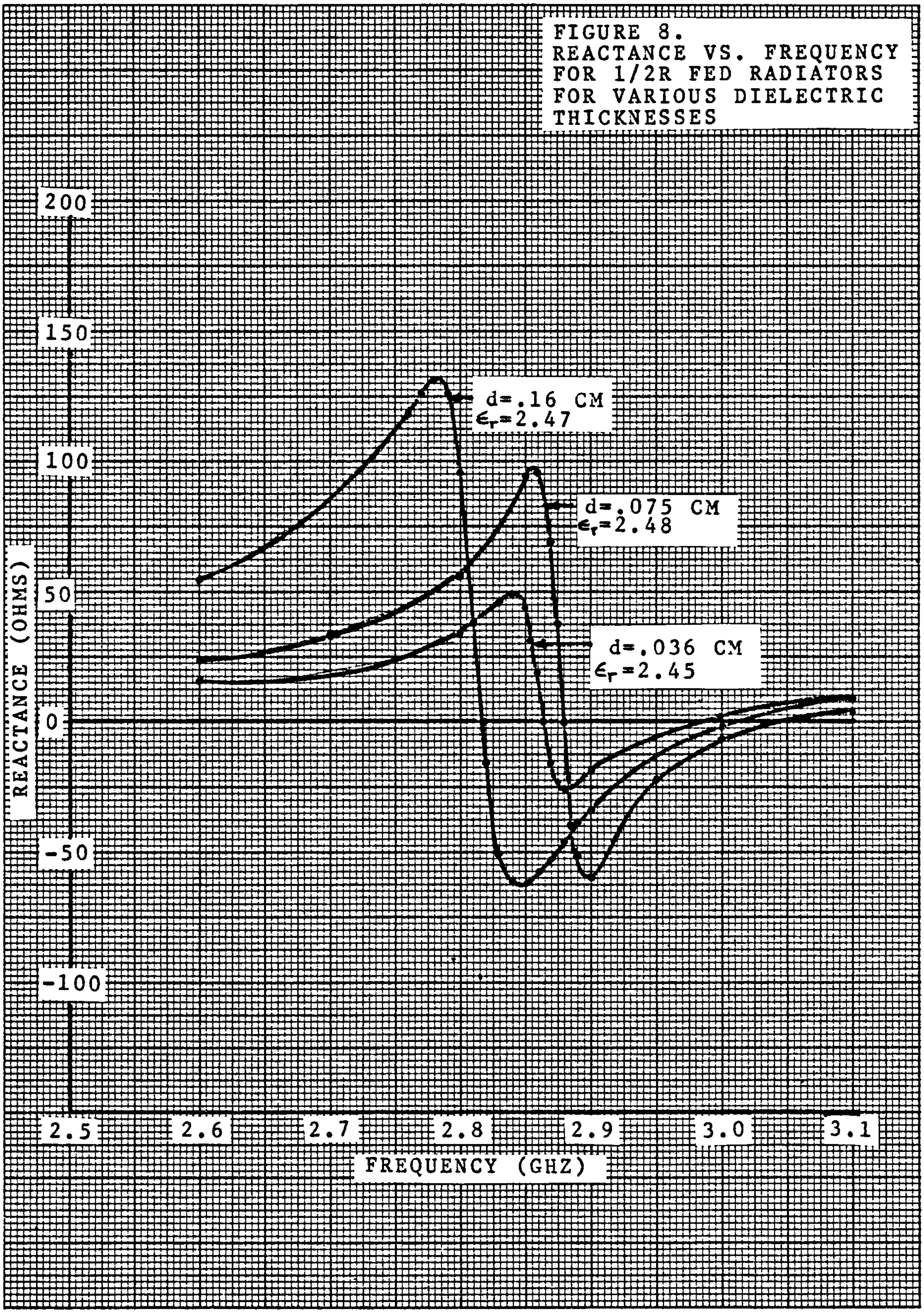
FIGURE 8.
REACTANCE VS. FREQUENCY
FOR 1/2R FED RADIATORS
FOR VARIOUS DIELECTRIC
THICKNESSES
d=.16 CM
ϵr=2.47
d=.075 CM
ϵr=2.48
d=.036 CM
ϵr=2.45
200
150
100
50
0
-50
-100
REACTANCE (OHMS)
2.5
2.6
2.7
2.8
2.9
3.0
3.1
FREQUENCY (GHZ)

thickness. This was evidenced by the fact that resonance occurred at 2.818 GHz for d = 0.16 cm, 2.88 GHz for d = 0.075 cm, and 2.864 GHz for d = 0.036 cm.

III.3c Effects of Feed Position on Input Impedance

Figures 9 through 14 graphically display the effects of moving the feed point of the radiators which have a substrate material with the same thickness. Figures 9 and 10 respectively show the resistance and reactance variations caused by moving the feed point of three radiators etched on a substrate material with d = 0.16 cm. One observation that is immediately noticeable is that the magnitude of the resistance and reactance decreases as the feed point is moved closer to the center of the disc. Upon close observation of the curves, one also notices that the resonant frequency of each radiator changes very little as the feed point is moved closer to the center of the disc.

Figures 11 and 12 respectively show resistance and reactance curves for three radiators etched on a substrate material with thickness d = 0.075 cm. Once again, the magnitude of the resistance and reactance of the antennas decreased as the feed point was moved closer to the center of the disc. Also, the resonant frequency gradually increased by 0.7% as the feed point was moved from R to 1/2 R.

Figures 13 and 14 contain graphs of the resistance and reactance, respectively, for three differently fed radiators etched on a dielectric material with a thickness of 0.036 cm. As was the case for thicker substrate materials, the magnitude of the resistance and reactance of the antennas decreased for feed positions located closer to the center of the disc. However, for the 0.036 cm substrate material, the resonance

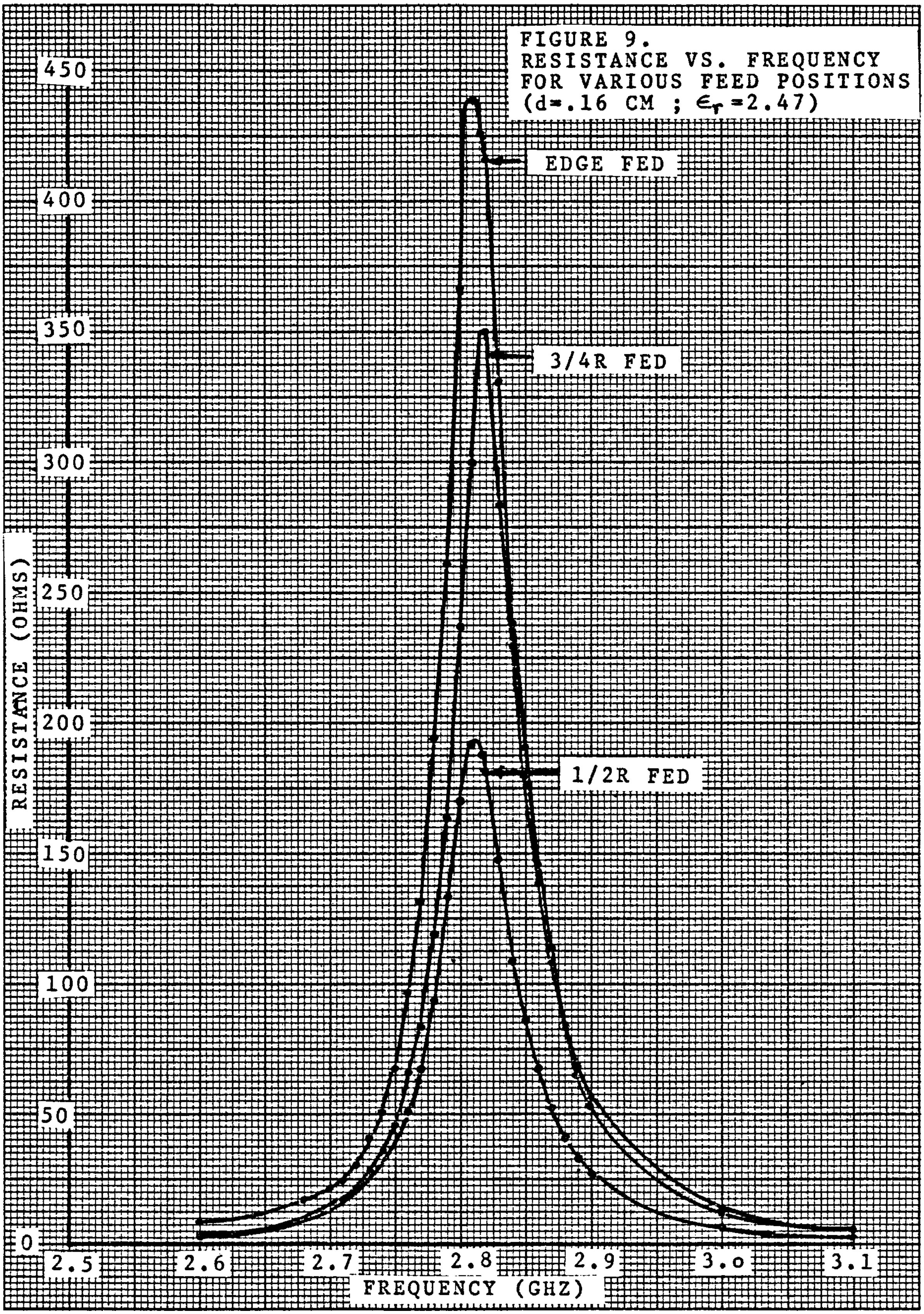
FIGURE 9.
RESISTANCE VS. FREQUENCY
FOR VARIOUS FEED POSITIONS
(d=.16 CM ; ϵ_r=2.47)
EDGE FED
3/4R FED
1/2R FED
RESISTANCE (OHMS)
0
50
100
150
200
250
300
350
400
450
2.5
2.6
2.7
2.8
2.9
3.o
3.1
FREQUENCY (GHZ)

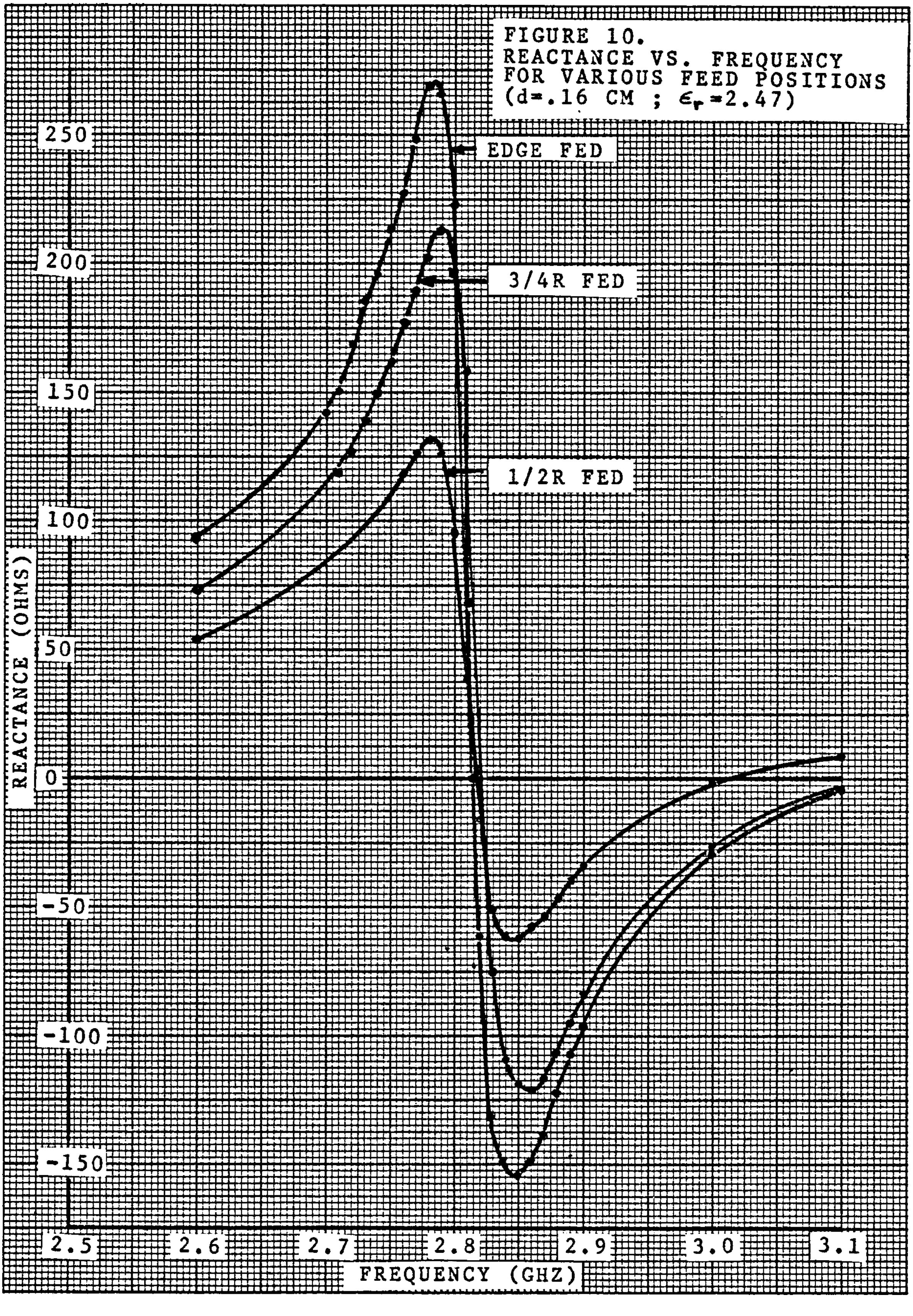
FIGURE 10.
REACTANCE VS. FREQUENCY
FOR VARIOUS FEED POSITIONS
(d=.16 CM ; ϵ_r=2.47)
EDGE FED
3/4R FED
1/2R FED
250
200
150
100
50
0
-50
-100
-150
REACTANCE (OHMS)
2.5
2.6
2.7
2.8
2.9
3.0
3.1
FREQUENCY (GHZ)

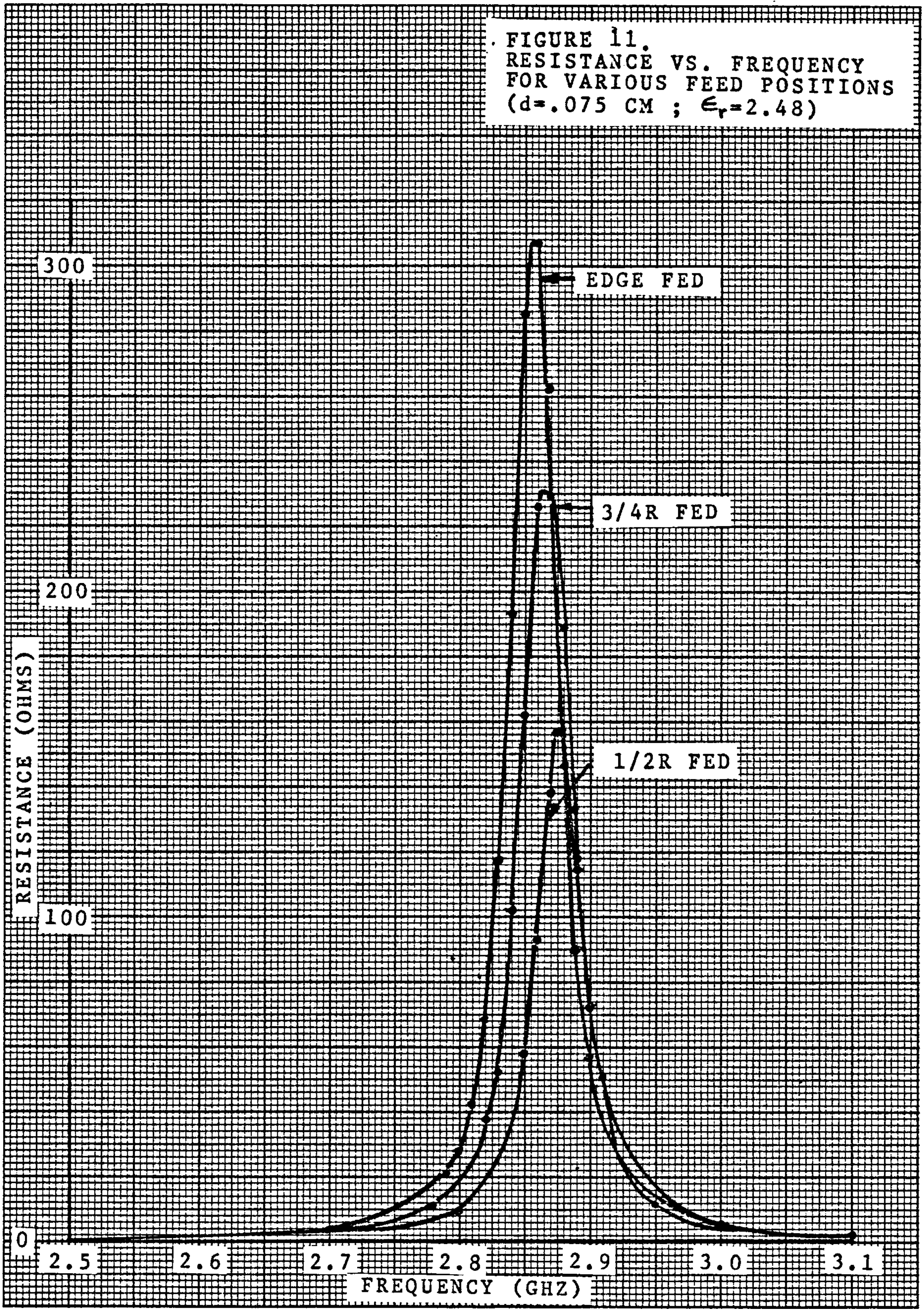
FIGURE 11.
RESISTANCE VS. FREQUENCY
FOR VARIOUS FEED POSITIONS
(d=.075 CM ; ϵ_r=2.48)
EDGE FED
3/4R FED
1/2R FED
300
200
100
0
RESISTANCE (OHMS)
2.5
2.6
2.7
2.8
2.9
3.0
3.1
FREQUENCY (GHZ)

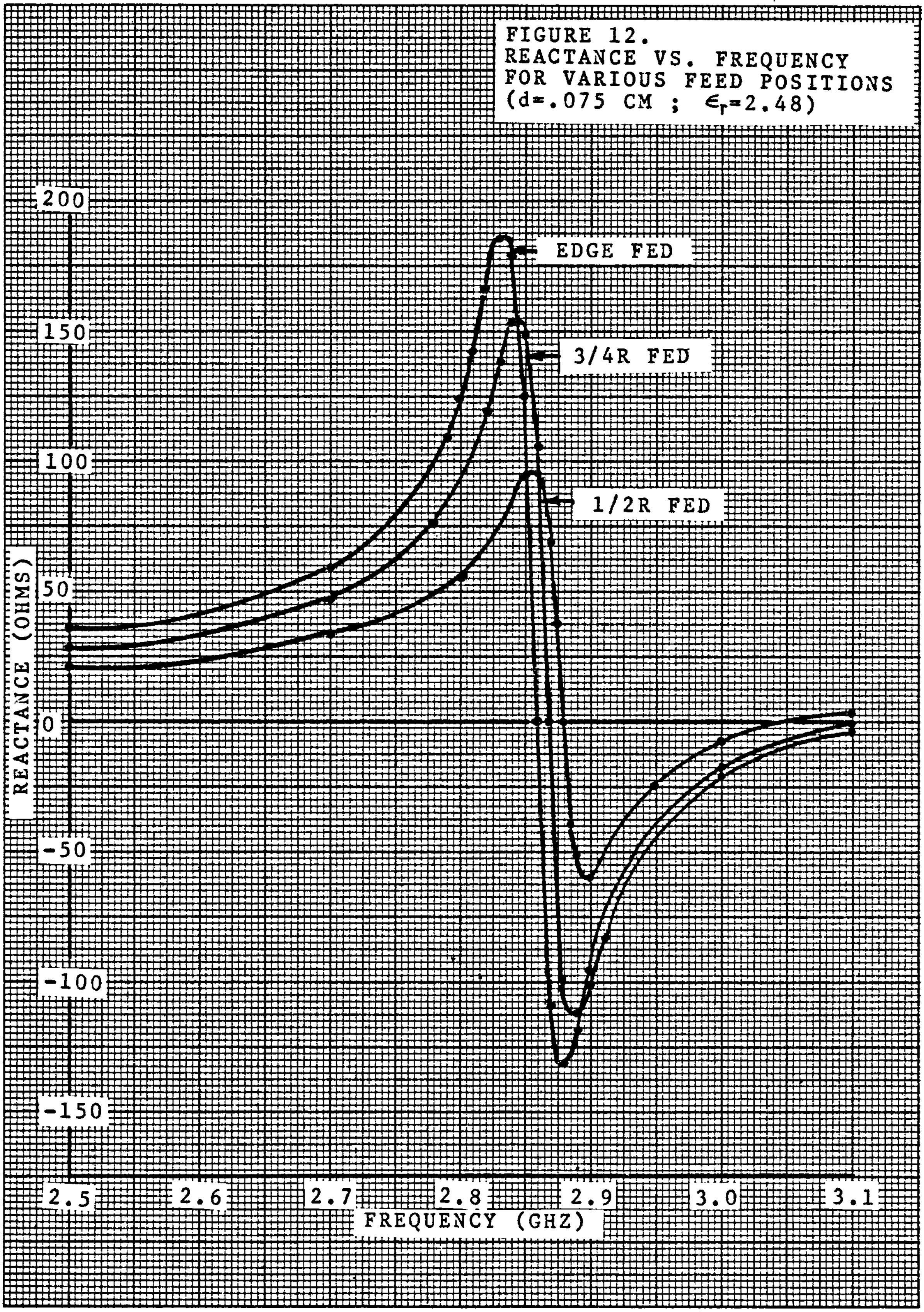
FIGURE 12.
REACTANCE VS. FREQUENCY
FOR VARIOUS FEED POSITIONS
(d=.075 CM ; ϵ_r=2.48)
EDGE FED
3/4R FED
1/2R FED
REACTANCE (OHMS)
200
150
100
50
0
-50
-100
-150
2.5
2.6
2.7
2.8
2.9
3.0
3.1
FREQUENCY (GHZ)

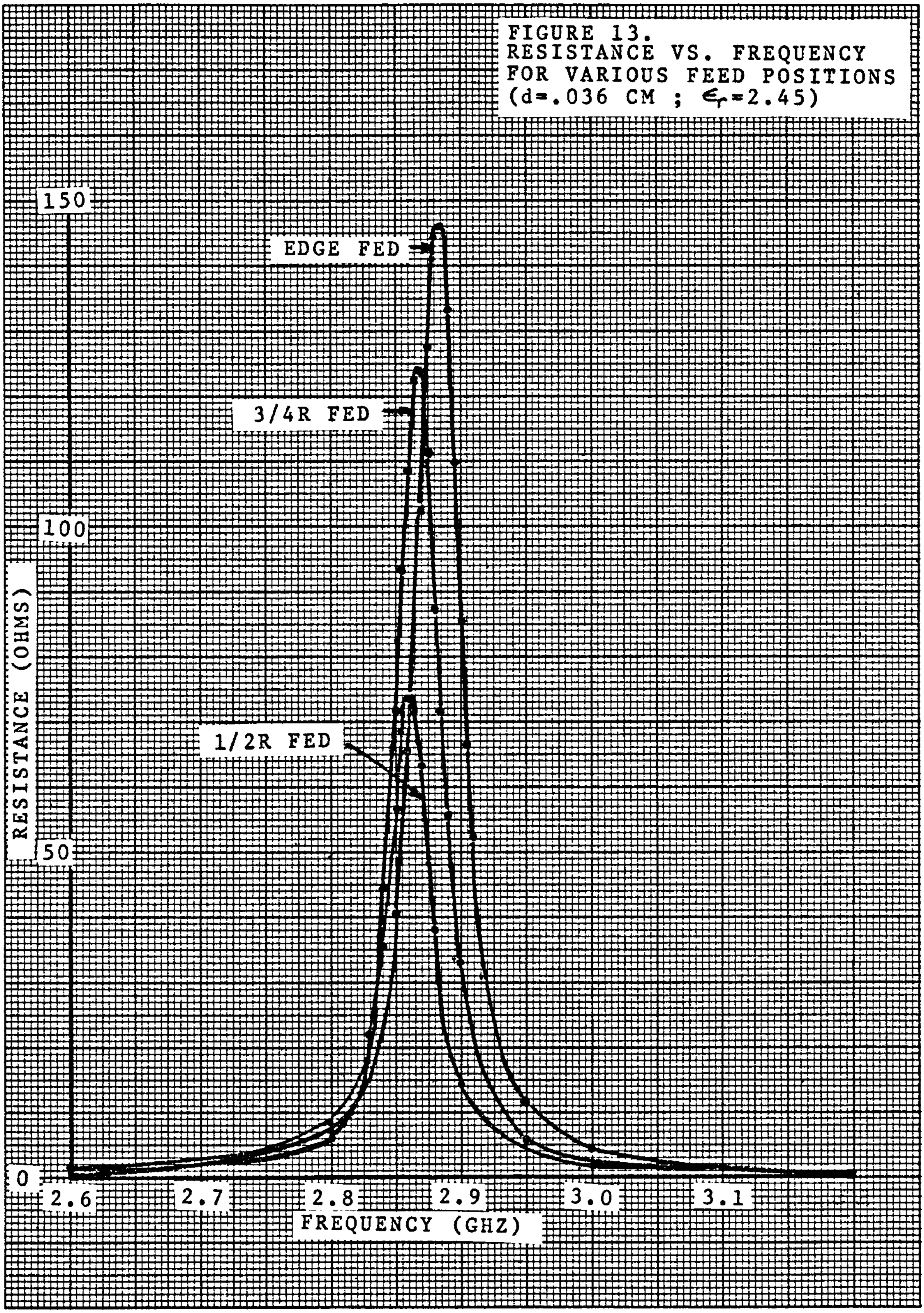

FIGURE 13.
RESISTANCE VS. FREQUENCY
FOR VARIOUS FEED POSITIONS
(d=.036 CM ; ϵ_r=2.45)

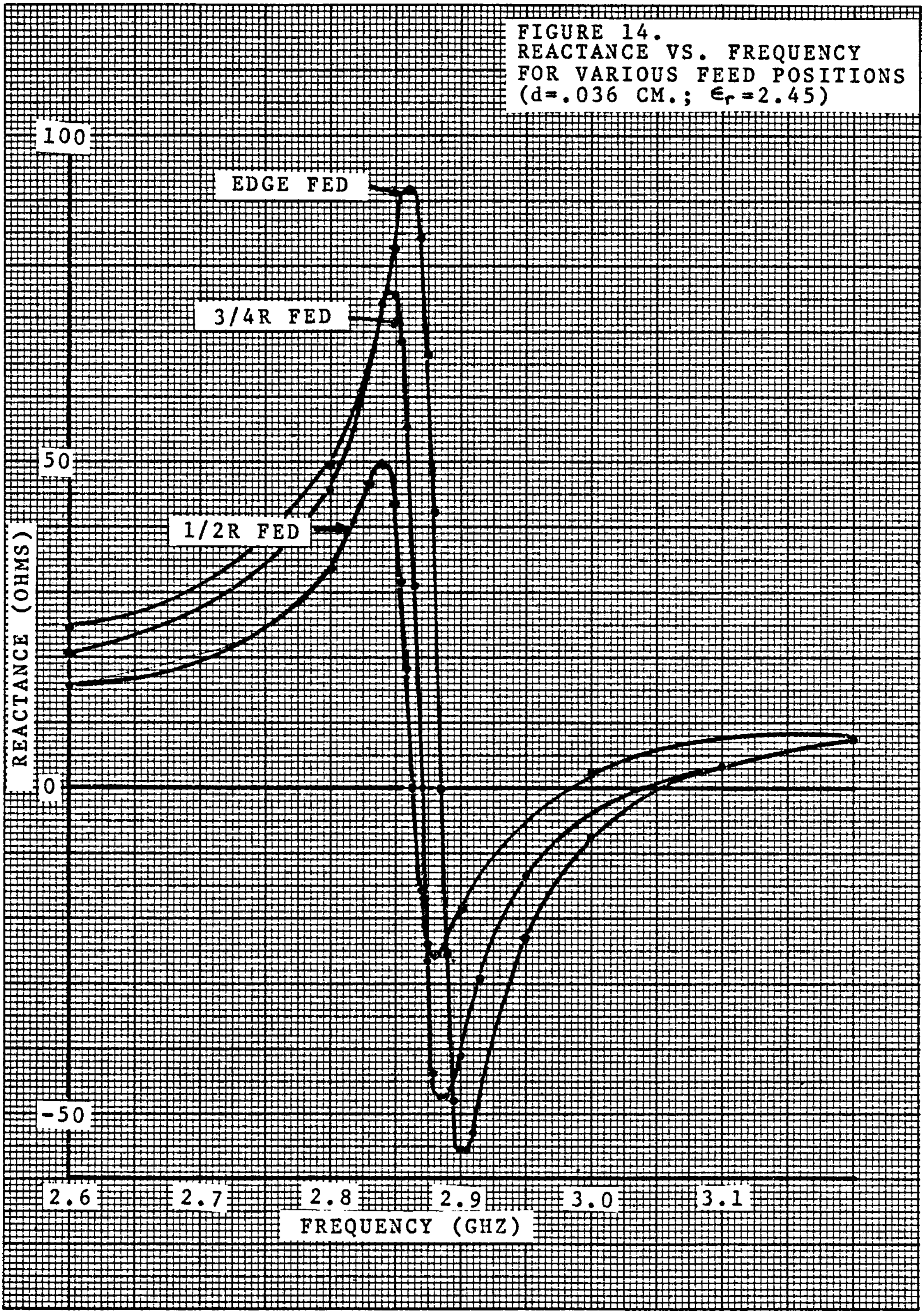
FIGURE 14.
REACTANCE VS. FREQUENCY
FOR VARIOUS FEED POSITIONS
(d=.036 CM.; ϵ_r=2.45)
EDGE FED
3/4R FED
1/2R FED
100
50
0
-50
REACTANCE (OHMS)
2.6
2.7
2.8
2.9
3.0
3.1
FREQUENCY (GHZ)

frequency continuously decreased by a total of 0.73% after successive feed positions from the disc edge to 1/2 R.

III.4 Comparisons Between Measured Results and the Zeroth-Order Theory

In order to minimize fringing effects and radiation, Watkins made the assumption that the dielectric thickness, d, was small compared to a wavelength in the dielectric, i.e., kd<<λ. Table III.10 compares the dielectric thicknesses of the three printed-circuit boards used in this investigation to the wavelength in the dielectric at the theoretical resonant frequency for the n=1 mode.

Dielectric Constant @ X-band	d (cm)	Calculated Resonant Frequency (GHz)	kd (radians)	$\frac{kd}{2\pi} = \frac{d}{\lambda}$	$\frac{\lambda}{d}$
2.47	0.16	2.975	0.156	0.025	40
2.48	0.075	2.969	0.073	0.012	83.3
2.45	0.036	2.987	0.035	0.006	166.7

Table III.10 Calculated Values of kd for Three Copper-Clad Dielectric Boards

From Table III.11, one is able to make several conclusions regarding the accuracy of Watkins' zeroth-order theory as it applies to the prediction of the resonant frequency for the printed-circuit, circular disc antenna. First, for all the antennas that were tested, the measured resonant frequency was lower than the theoretical resonant frequency, regardless of the substrate thickness or the feed position. For the edge fed radiators, the percentage error between measured

d (cm)	Dielectric Constant @ X-band	Feed Point Position	Measured Resonant Point (GHz)	Calculated Resonant Point (GHz)	% error $(\frac{\text{calc-meas}}{\text{meas.}} \times 100)$
0.160	2.47	R	2.815	2.975	5.68
0.160	2.47	3/4 R	2.820	2.975	5.50
0.160	2.47	1/2 R	2.818	2.975	5.57
0.075	2.48	R	2.860	2.969	3.81
0.075	2.48	3/4 R	2.869	2.969	3.48
0.075	2.48	1/2 R	2.880	2.969	3.09
0.036	2.45	R	2.885	2.987	3.54
0.036	2.45	3/4 R	2.870	2.987	4.08
0.036	2.45	1/2 R	2.864	2.987	4.29

Table III.11 Comparison Between Theoretical and Experimental Results

resonance and theoretical resonance decreased from 5.68% to 3.54% as the dielectric substrate thickness was decreased from 0.16 cm to 0.036 cm. This was not altogether true for the antennas which were 3/4 fed and 1/2 R fed, since for each of these feed points, the percentage error decreased as dielectric thickness was changed from 0.16 cm to 0.075 cm but increased as dielectric thickness was changed from 0.075 cm to 0.036 cm.

Discrepancies between measured and calculated resonances could only be attributed to violations of Watkins' assumptions for the zeroth-order theory and/or higher order modes in the region between the disc and ground plane being simultaneously present with the n=1 or dominant mode.

CHAPTER IV

MEASUREMENT OF THE RADIATION PROPERTIES OF THE ANTENNAS

IV.1 Test Configuration for Measuring the Far Fields of the Antennas

Figure 15 shows the test configuration used in the measurement of the far fields of the printed-circuit, circular disc antennas. To avoid the reception of unwanted signals during the pattern measurements, an anechoic chamber was used. With the use of microwave absorbing material inside the chamber, a free space condition was simulated. Details of the antenna ground plane are shown in Figure 16. Since the 0.91 m x 1.52 m ground plane was a finite structure, its edges were lined with microwave absorbing material to reduce edge effects due to diffraction. The effects of this material on the far field patterns are presented later in the polar plots of the antenna patterns.

IV.2 Far Field Pattern Measurements

IV.2a General Results of the Measurements

On every printed-circuit, circular disc antenna that was fabricated, two components of the electric field, $\overline{E}_\theta$ and $\overline{E}_\phi$, were measured as a function of θ for various ϕ planes. These components, $\overline{E}_\theta$ and $\overline{E}_\phi$, are shown in Figure 17. Note in Figure 17, that along the Z-axis ($\theta = 0$), $\overline{E}_\theta$ in the $\phi = 0$ plane is the same component of the electric field as $\overline{E}_\phi$ in the $\phi = 90°$ plane. Table IV.1 contains data pertinent to the far field measurements of each antenna. Note that during the far field

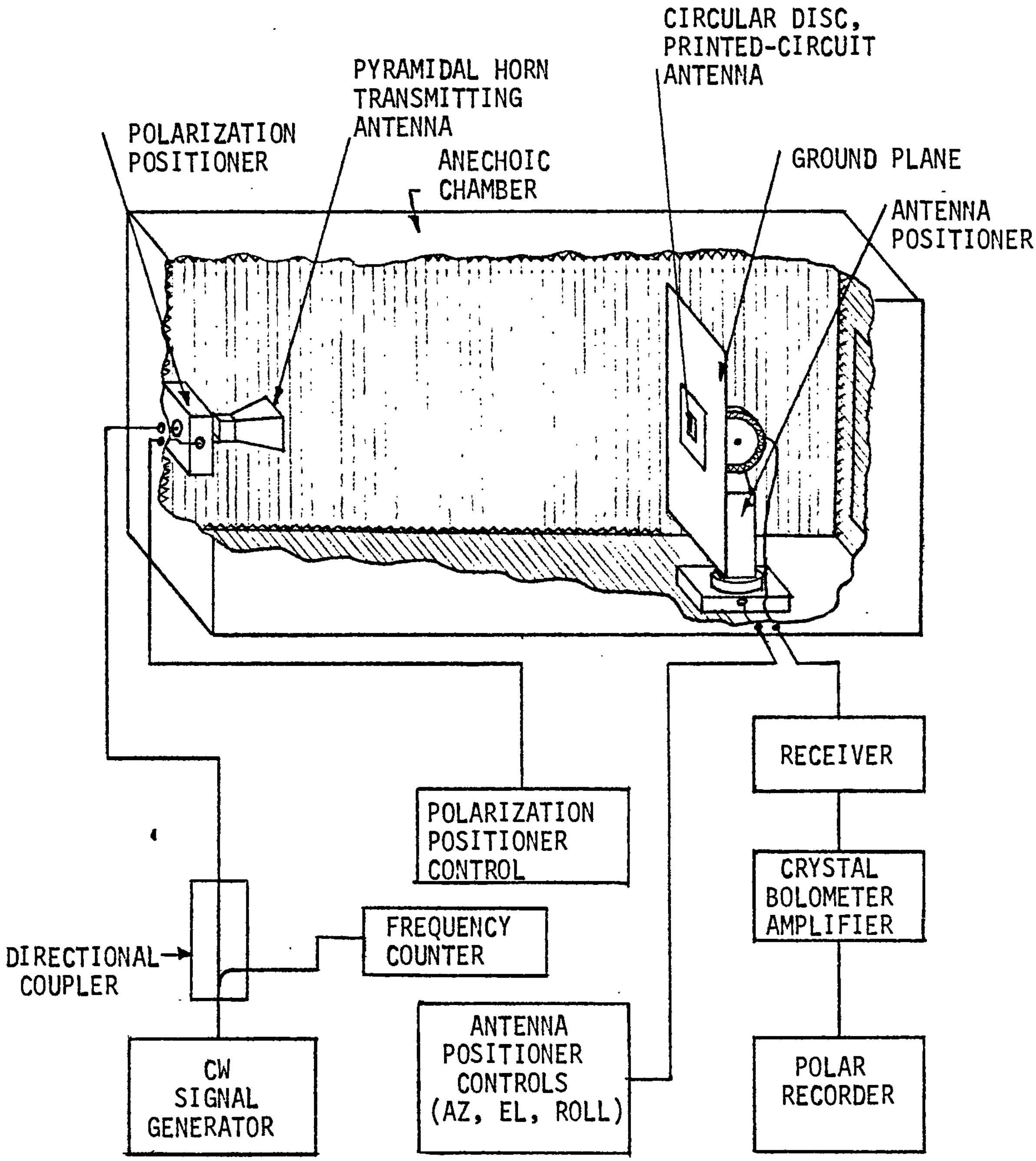

Figure 15: Test Configuration for Measuring the Far Fields

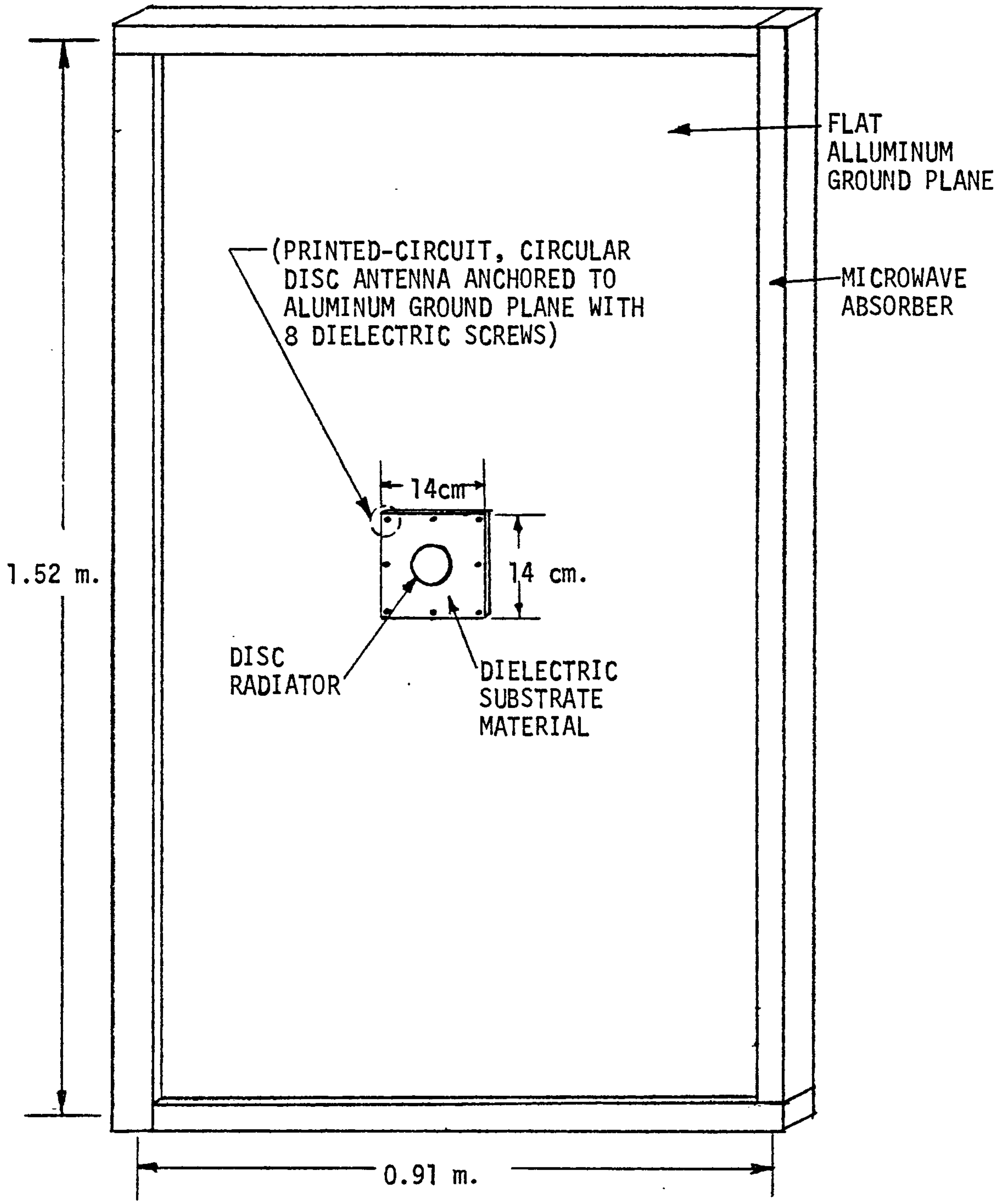

Figure 16: Antenna Ground Plane Details

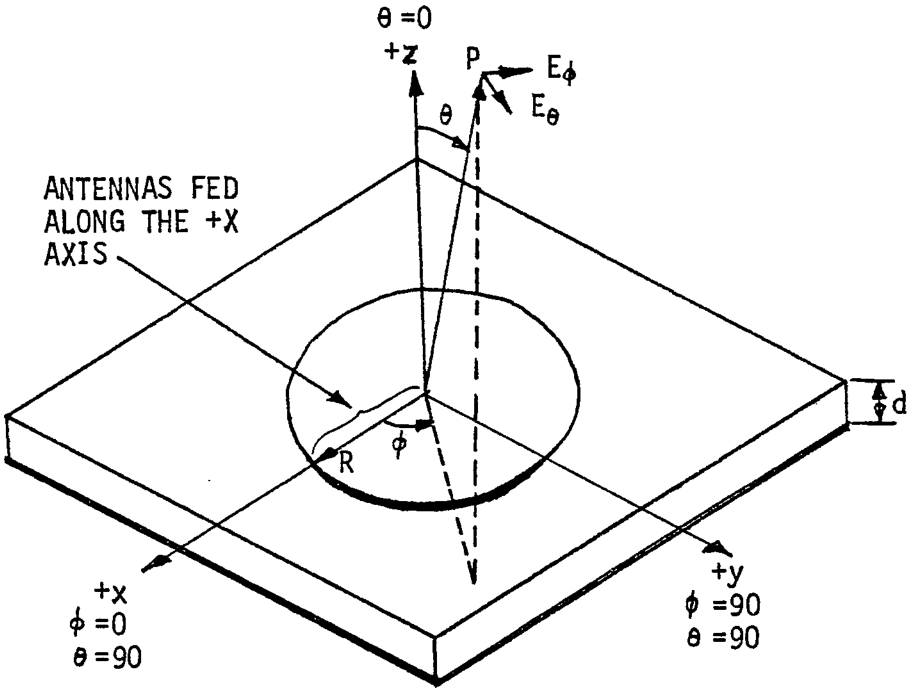

Figure 17: E_θ and E_ϕ Components of the Far Field

measurements, each radiator was fed at its measured resonant frequency.

Antenna #	Feed Point	Measured Resonant Frequency (GHz)	Substrate Thickness (cm)	Far Field Component that was Measured	ϕ Planes (deg.)	Ground Plane Configuration
1	R	2.815	0.16	$\lvert E_\theta \rvert$ vs θ	0,30,60,90	w/absorber
				$\lvert E_\phi \rvert$ vs θ	90,60,30,0	w/absorber
2	3/4 R	2.82	0.16	$\lvert E_\theta \rvert$ vs θ	0,30,60,90	w/absorber
				$\lvert E_\phi \rvert$ vs θ	90,60,30,0	w/absorber
3	1/2 R	2.818	0.16	$\lvert E_\theta \rvert$ vs θ	0,30,60,90	w/absorber
				$\lvert E_\phi \rvert$ vs θ	90,60,30,0	w/absorber
4	R	2.86	0.075	$\lvert E_\theta \rvert$ vs θ	0,30,60,90	w/o absorber
				$\lvert E_\phi \rvert$ vs θ	90,60,30,0	w/o absorber
				$\lvert E_\theta \rvert$ vs θ	0,30,60,90	w/absorber
				$\lvert E_\phi \rvert$ vs θ	90,60,30,0	w/absorber
5	3/4 R	2.869	0.075	$\lvert E_\theta \rvert$ vs θ	0,30,60,90	w/absorber
				$\lvert E_\phi \rvert$ vs θ	90,60,30,0	w/absorber
6	1/2 R	2.88	0.075	$\lvert E_\theta \rvert$ vs θ	0,30,60,90	w/absorber
				$\lvert E_\phi \rvert$ vs θ	90,60,30,0	w/absorber
7	R	2.885	0.036	$\lvert E_\theta \rvert$ vs θ	0,30,60,90	w/absorber
				$\lvert E_\phi \rvert$ vs θ	90,60,30,0	w/absorber
8	3/4 R	2.87	0.036	$\lvert E_\theta \rvert$ vs θ	0,30,60,90	w/absorber
				$\lvert E_\phi \rvert$ vs θ	90,60,30,0	w/absorber
9	1/2 R	2.8[illegible]4	0.036	$\lvert E_\theta \rvert$ vs θ	0,30,60,90	w/absorber
				$\lvert E_\phi \rvert$ vs θ	90,60,30,0	w/absorber

Table IV.1 Summary of Measured Far Field Patterns

Figures 18 through 23 apply to radiators etched on a 0.16 cm dielectric substrate. Figures 18 and 19 respectively show $|E_\theta|$ vs θ and $|E_\phi|$ vs θ for an edge-fed radiator which was being driven at its resonant frequency of 2.815 GHz. Figures 20 and 21 respectively show $|E_\theta|$ vs θ and $|E_\phi|$ vs θ for a 3/4 R fed radiator being driven at its resonant frequency of 2.82 GHz. Finally, Figures 22 and 23 show $|E_\theta|$ vs θ and $|E_\phi|$ vs θ for a 1/2 R fed radiator being driven at 2.818 GHz, its resonant frequency.

Figures 24 through 31 apply to radiators that were etched on a dielectric substrate material of 0.075 cm. Figures 24 and 25 are similar to Figures 26 and 27, respectively, with the exception being that Figures 24 and 25 show patterns that were measured on an edge-fed radiator mounted on a ground plane without absorber while Figures 26 and 27 show patterns that were measured on an edge-fed radiator mounted on a ground plane with absorber. Note that the absorber had virtually no effect on the patterns involving $|E_\phi|$ but that the absorber eliminated the fluctuations in the $|E_\theta|$ patterns. Morel [7] theoretically calculates far field patterns for $|E_\theta|$ vs θ and $|E_\phi|$ vs θ for the circular disc, printed-circuit antenna which are smooth. This smooth pattern for $|E_\theta|$ vs θ was obtained when the ground plane was lined with microwave absorber material. Figures 26 and 27 show $|E_\theta|$ vs θ and $|E_\phi|$ vs θ, respectively, for an edge-fed radiator being driven at its resonant frequency of 2.86 GHz. Figures 28 and 29, respectively, show $|E_\theta|$ vs θ and $|E_\phi|$ vs θ for a 3/4 R fed radiator at its resonant frequency of 2.869 GHz. Figures 30 and 31 show $|E_\theta|$ vs θ and $|E_\phi|$ vs θ, respectively, for a 1/2 R fed radiator being driven at 2.88 GHz, its resonant frequency.

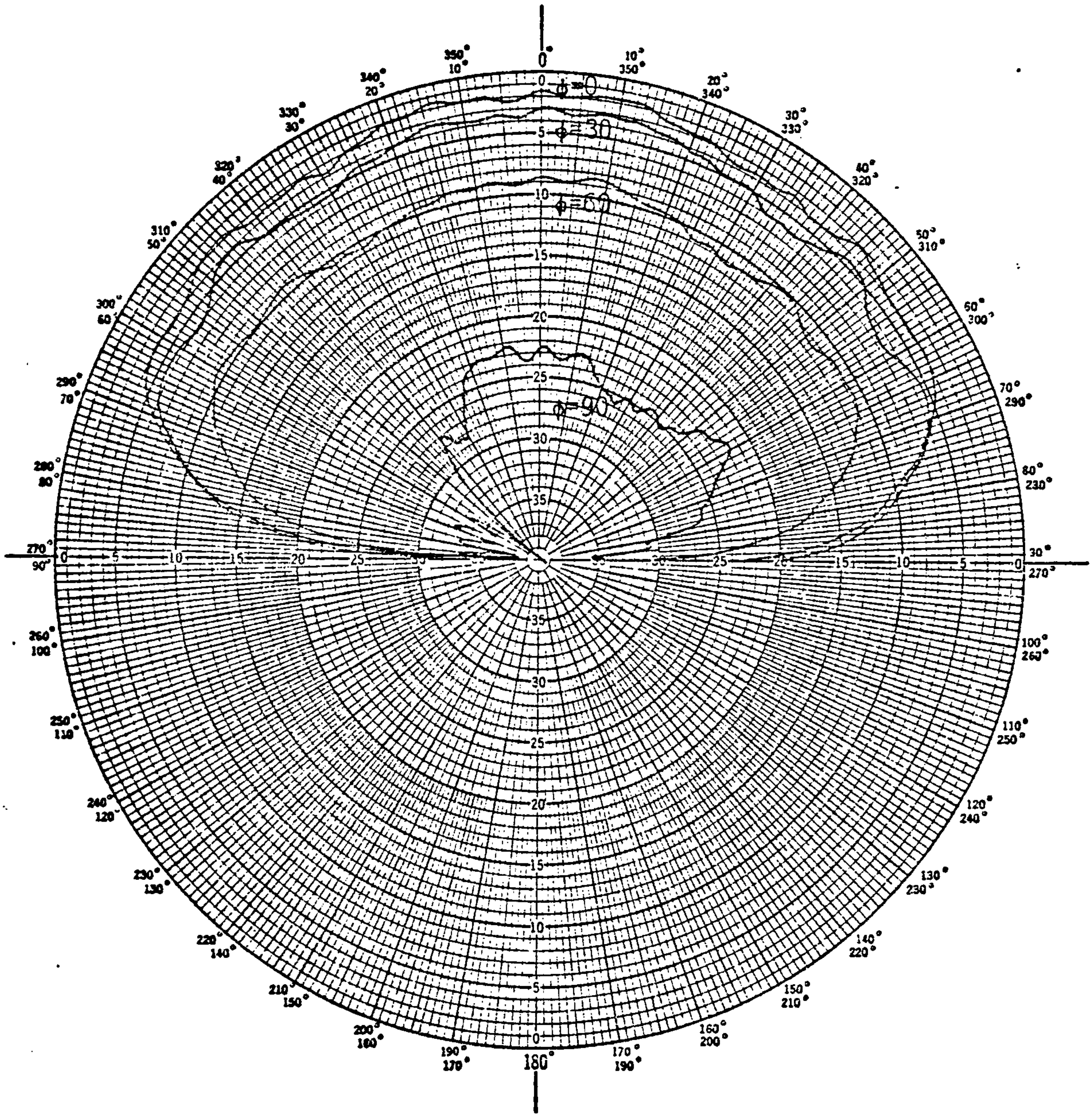

Figure 18: E_θ vs. θ for Different Values of ϕ
d: 0.16 cm.
Feed Point: R
Frequency: 2.815 GHz.

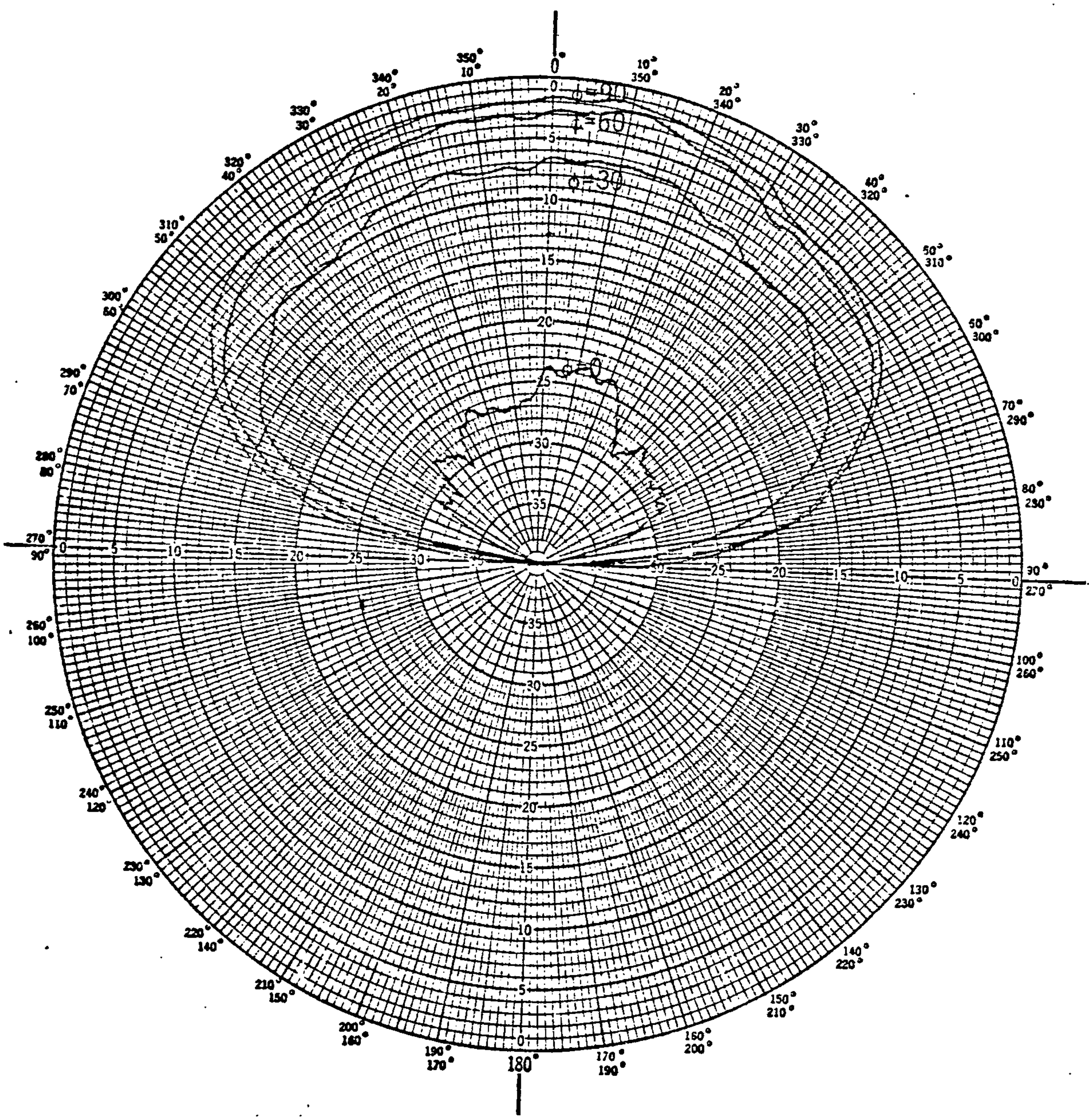

Figure 19: E_ϕ vs. θ for Different Values of ϕ
d: 0.16 cm.
Feed Point: R
Frequency: 2.815 GHz.

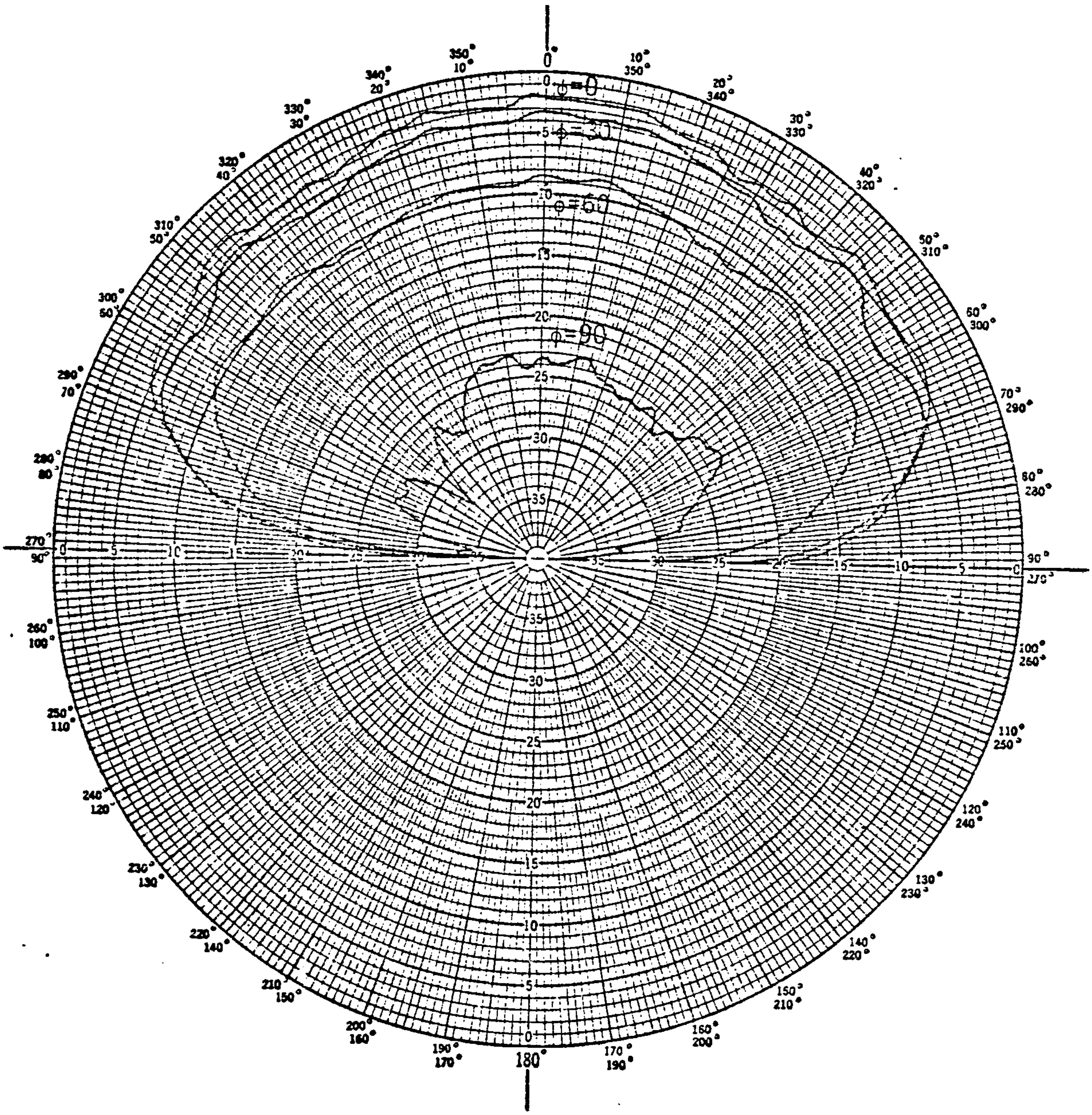

Figure 20: E_θ vs. θ for Different Values of ϕ
d: 0.16 cm.
Feed Point: 3/4R
Frequency: 2.82 GHz.

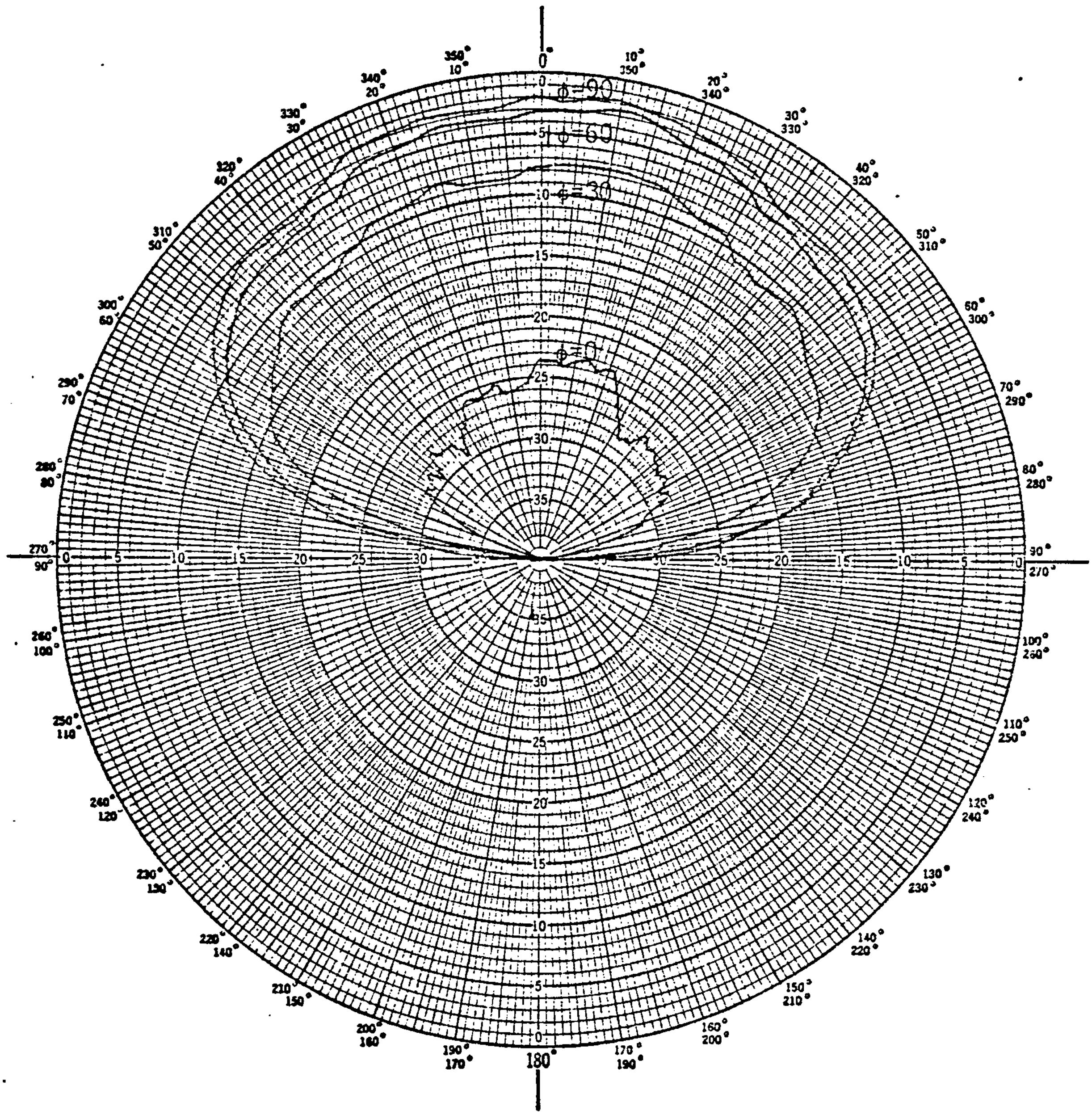

Figure 21: E_ϕ vs. θ for Different Values of φ
d: 0.16 cm.
Feed Point: 3/4R
Frequency: 2.82

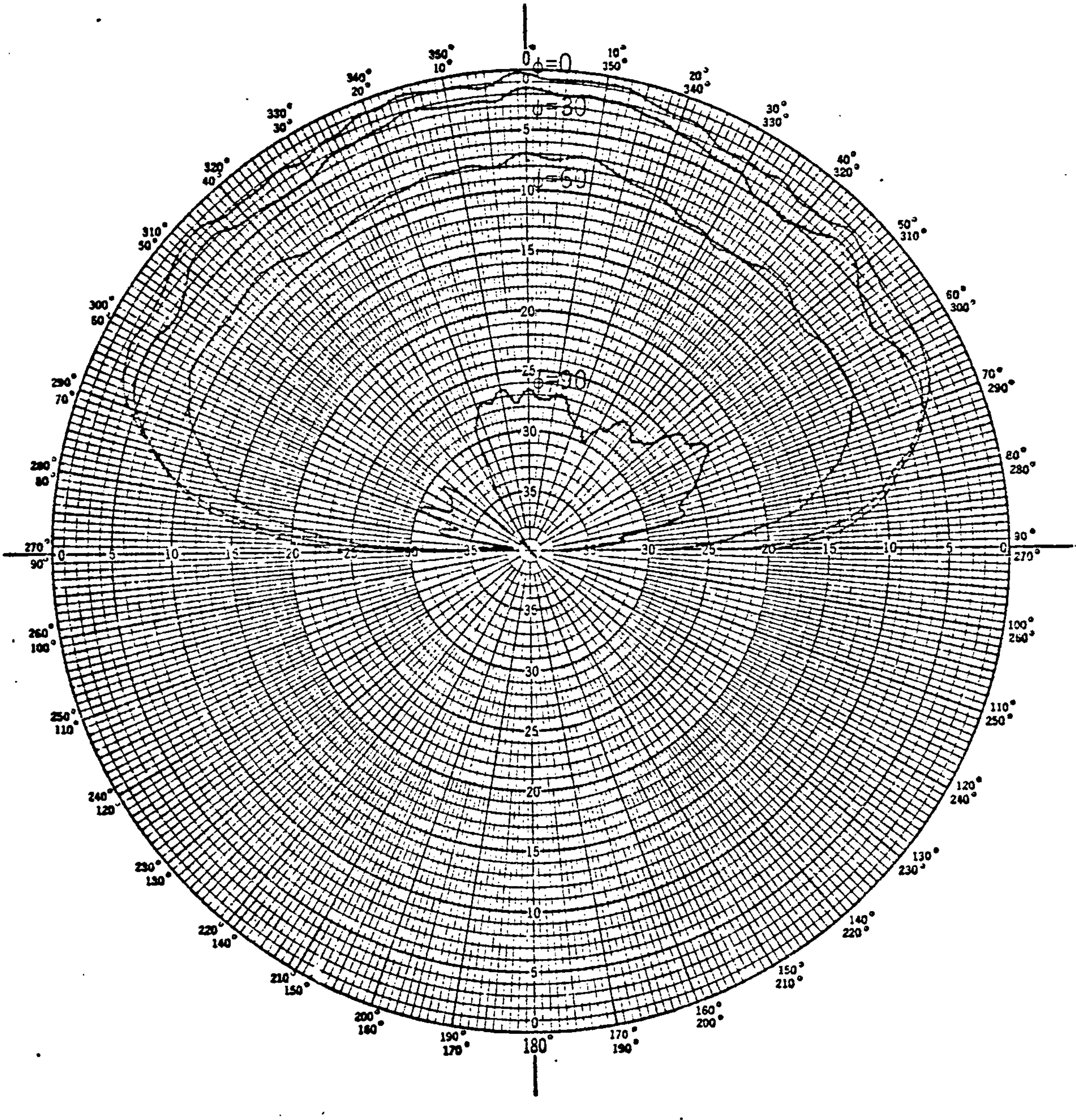

Figure 22: E_θ vs. θ for Different Values of φ
d: 0.16 cm.
Feed Point: 1/2R
Frequency: 2.818 GHz.

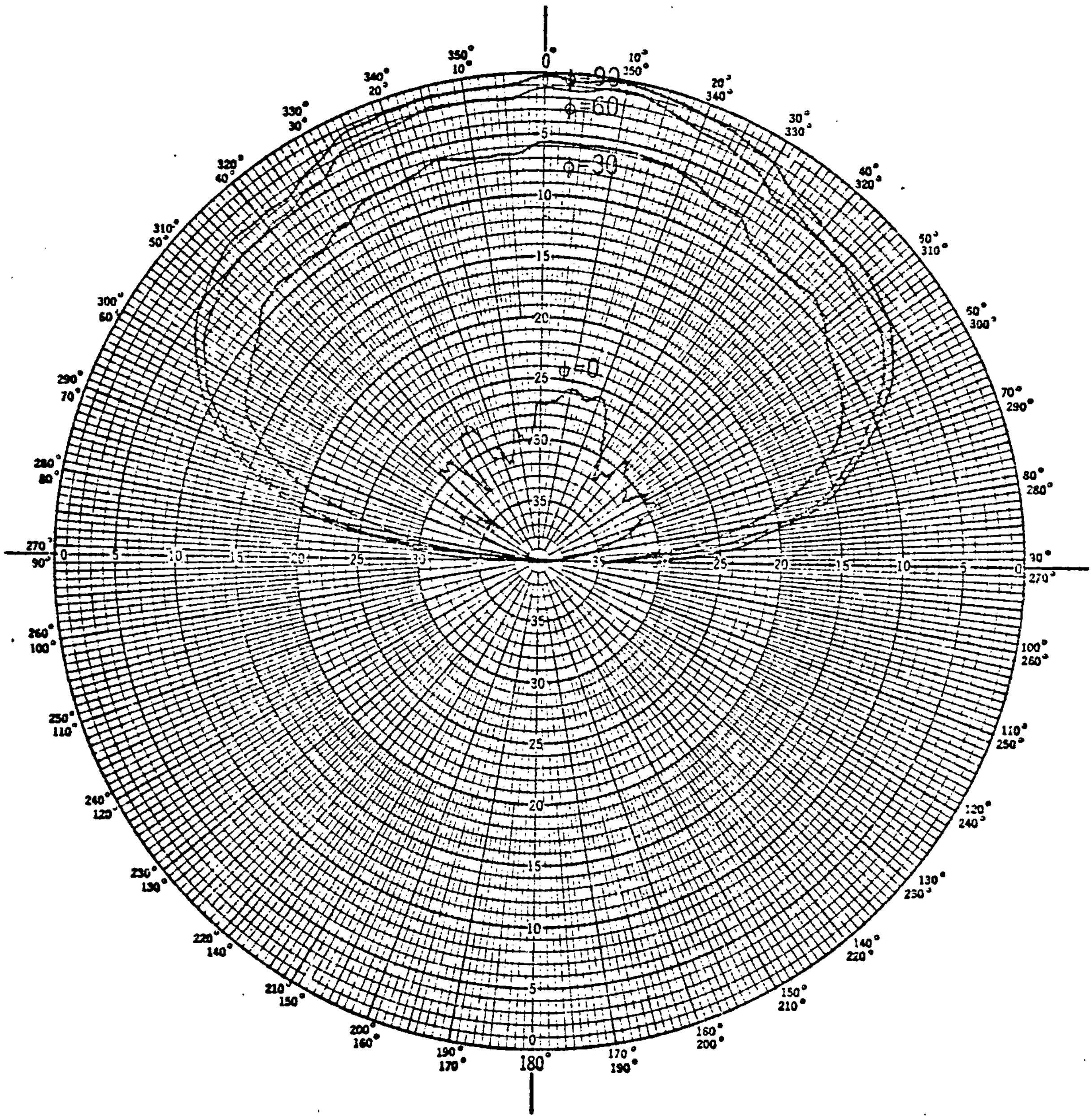

Figure 23: E_{ϕ} vs. θ for Different Values of φ
d: 0.16 cm.
Feed Point: 1/2R
Frequency: 2.818 GHz.

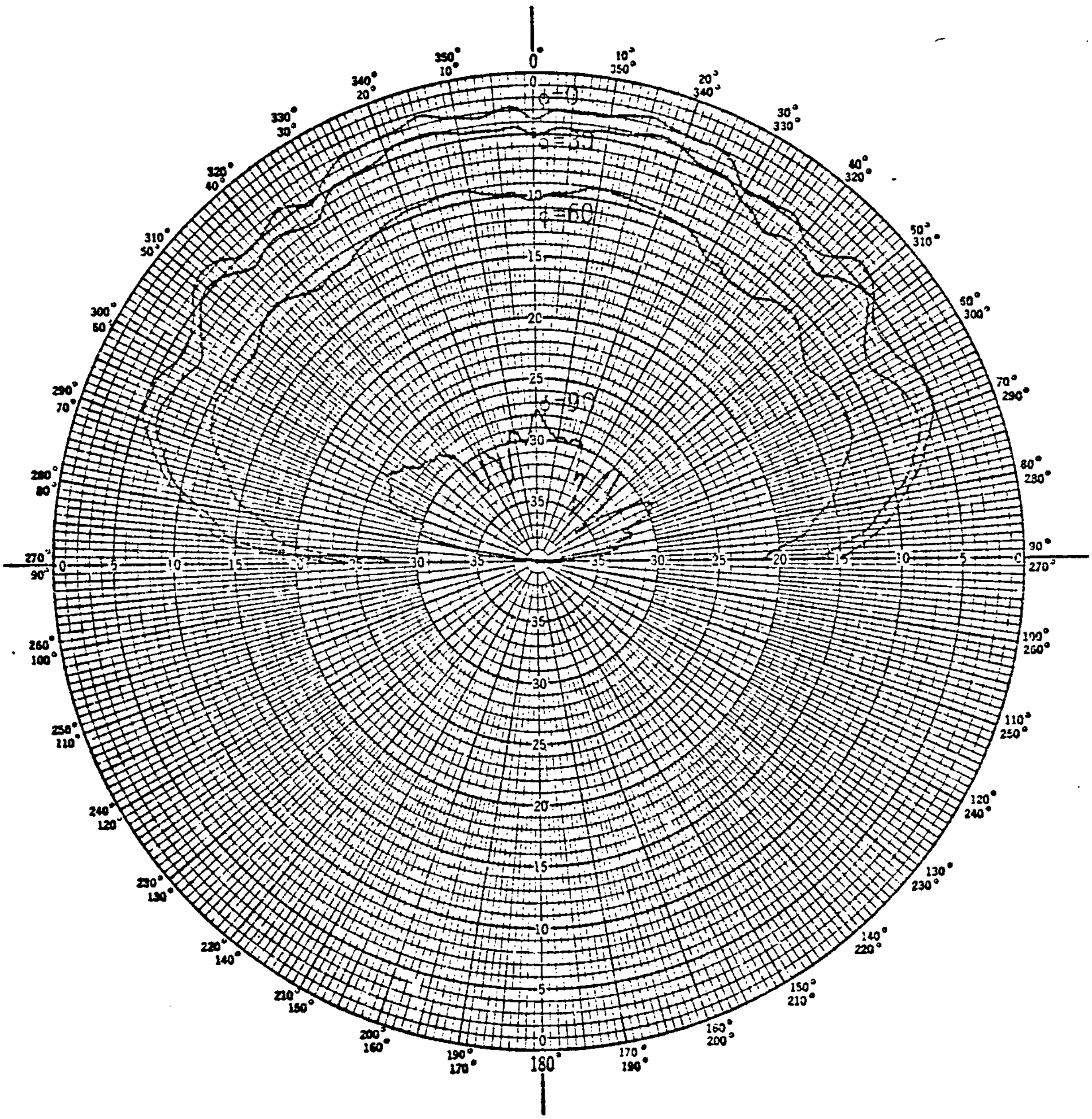

Figure 24: E_θ vs. θ for Different Values of ϕ
Without Absorber
d: 0.075 cm.
Feed Point: R
Frequency: 2.86 GHz.

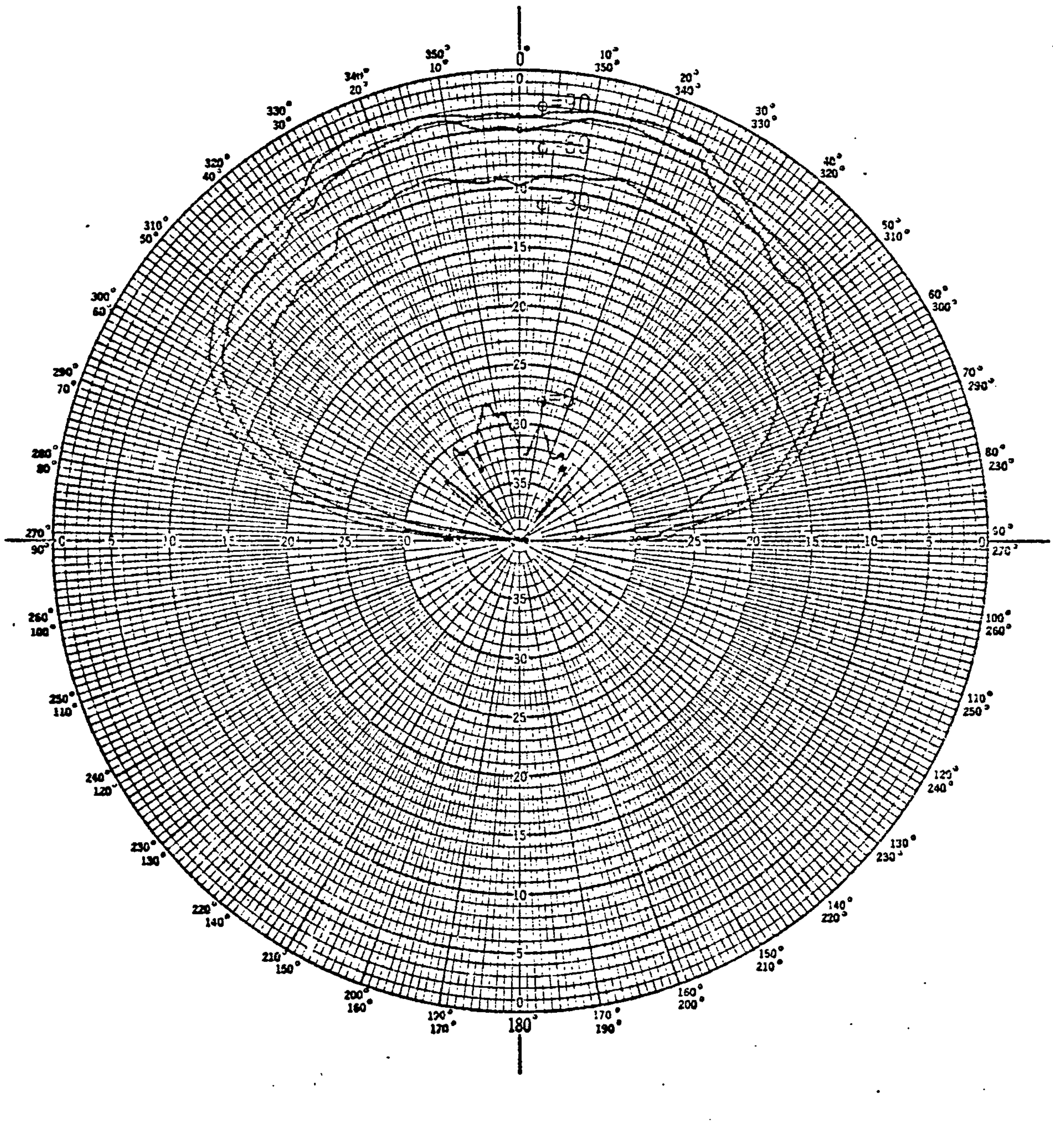

Figure 25: E_ϕ vs. θ for Different Values of ϕ
Without Absorber
d: 0.075 cm.
Feed Point: R
Frequency: 2.86 GHz.

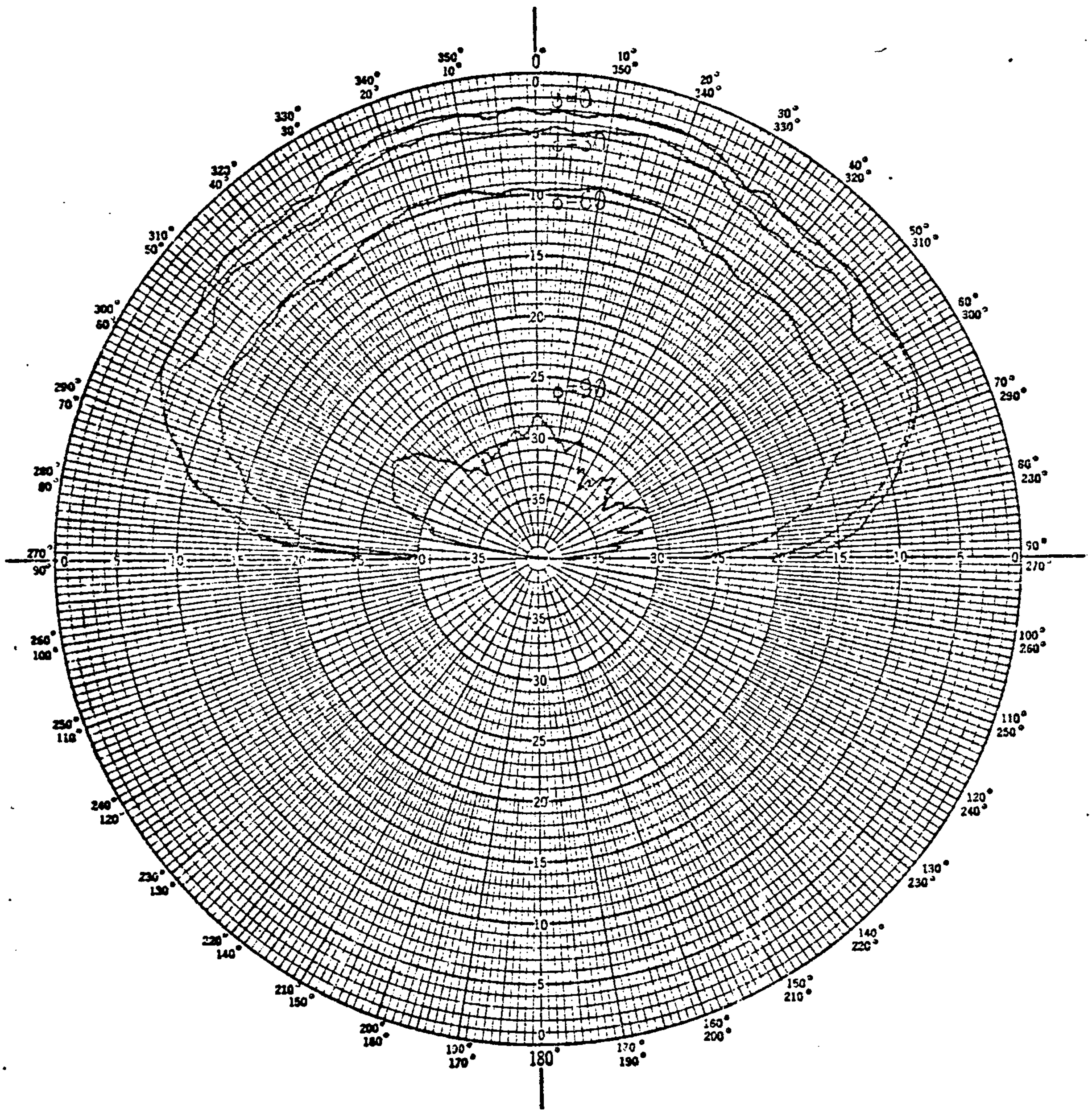

Figure 26: E_θ vs. θ for Different Values of ϕ
d: 0.075 cm.
Feed Point: R
Frequency: 2.86 GHz.

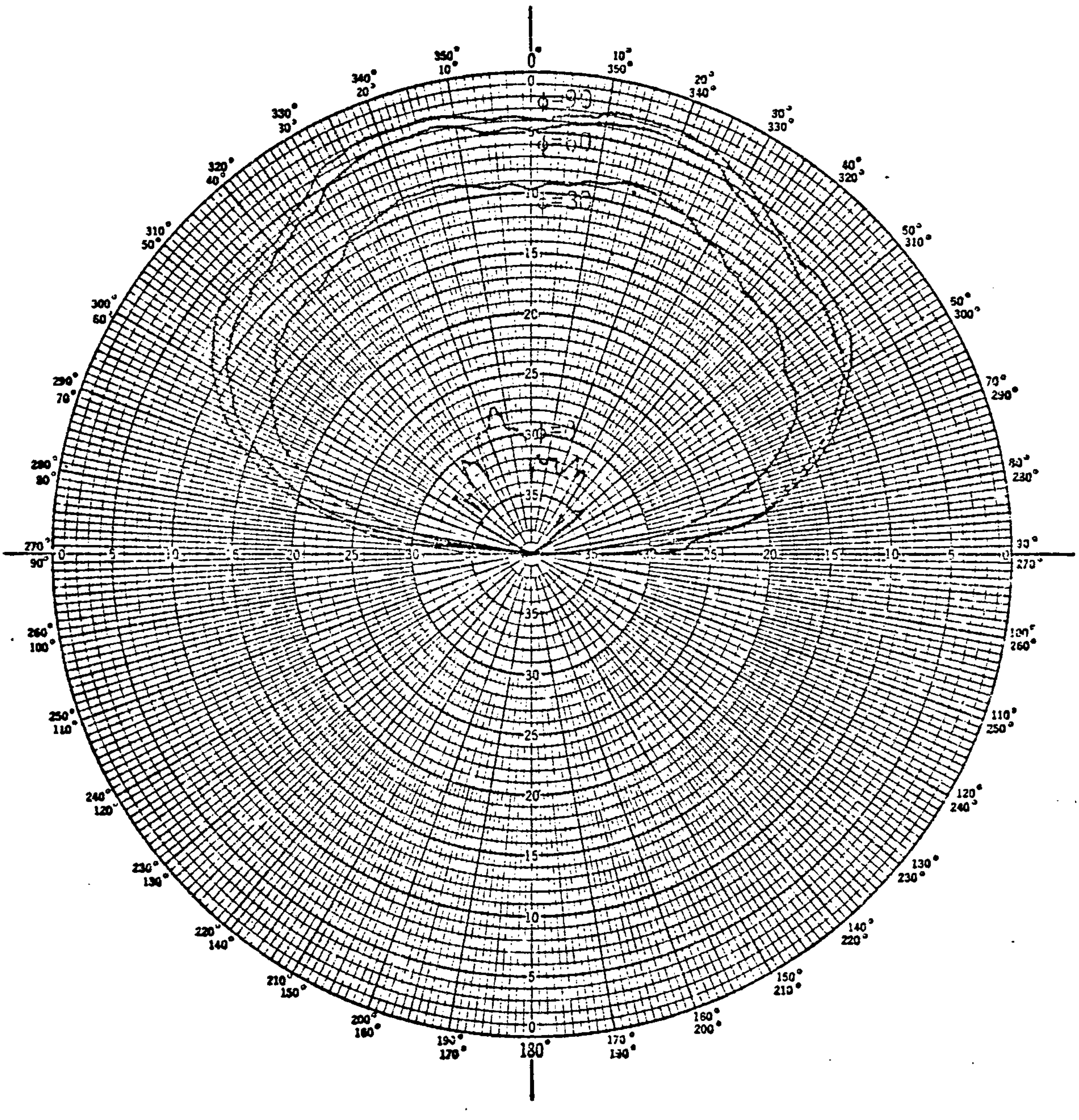

Figure 27: E_ϕ vs. θ for Different Values of ϕ
d: 0.075 cm.
Feed Point: R
Frequency: 2.86 GHz.

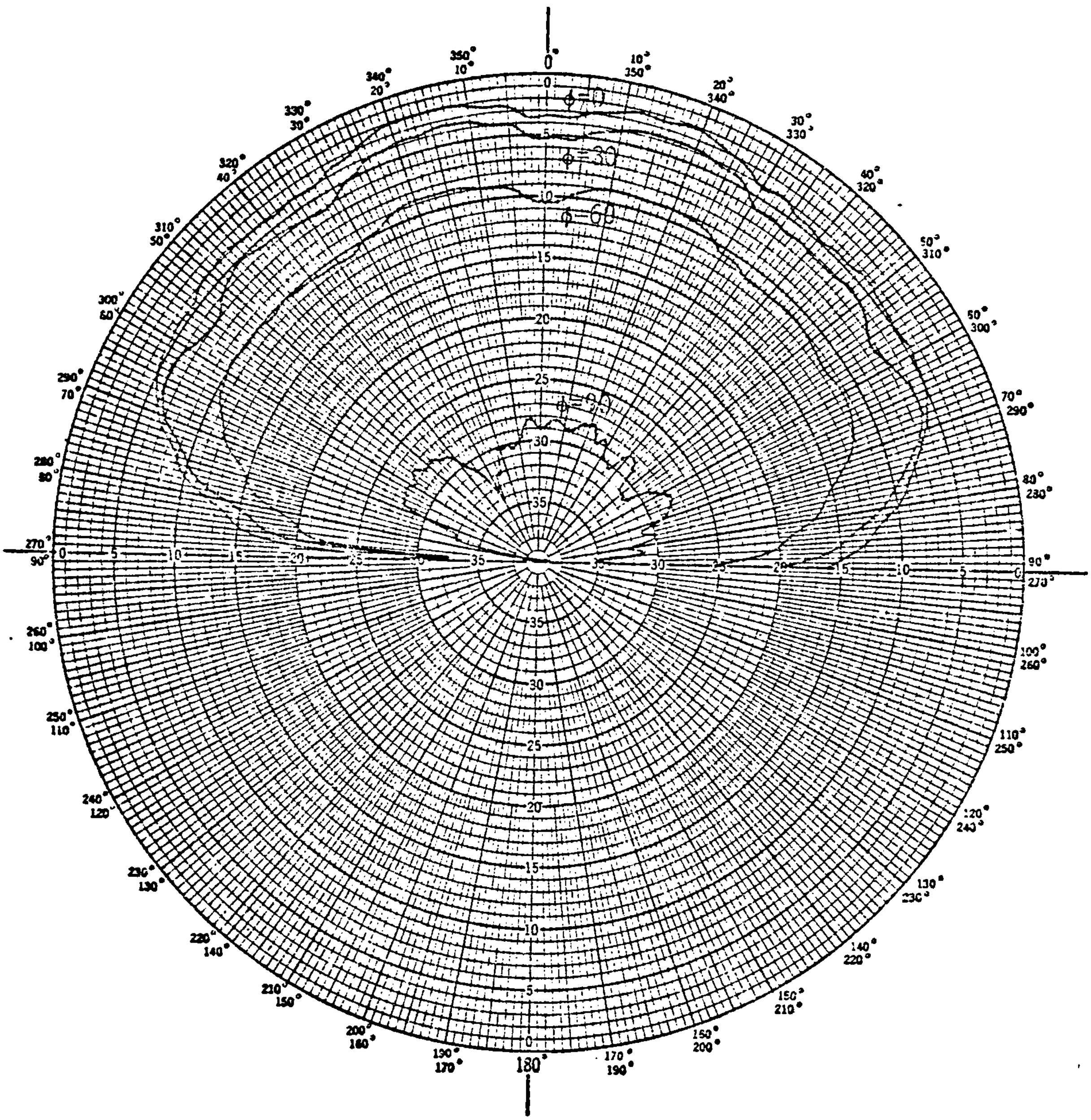

Figure 28: E_θ vs. θ for Different Values of ϕ
d: 0.075 cm.
Feed Point: 3/4R
Frequency: 2.869 GHz.

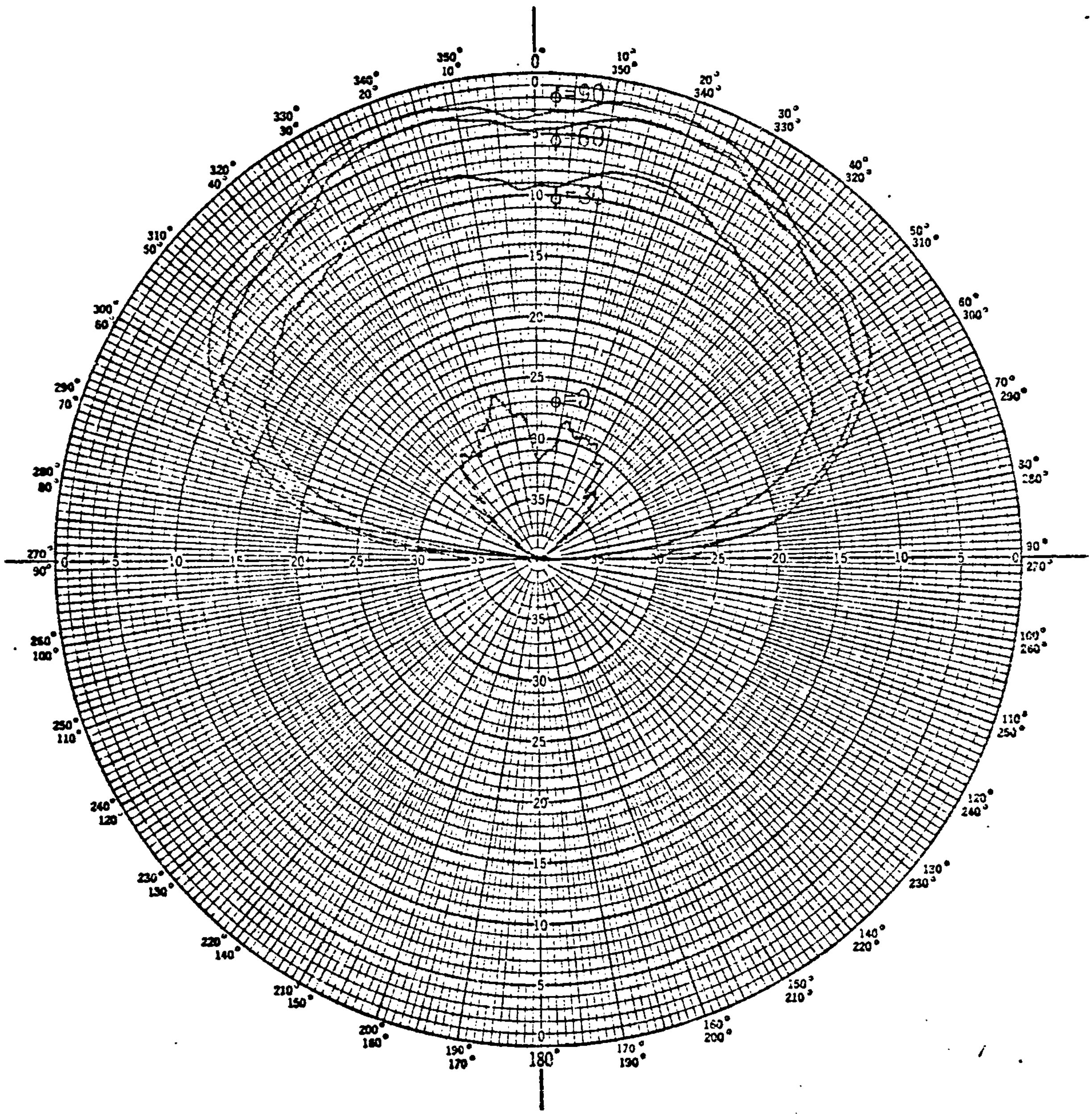

Figure 29: E_ϕ vs. θ for Different Values of ϕ
d: 0.075 cm.
Feed Point: 3/4R
Frequency: 2.869 GHz.

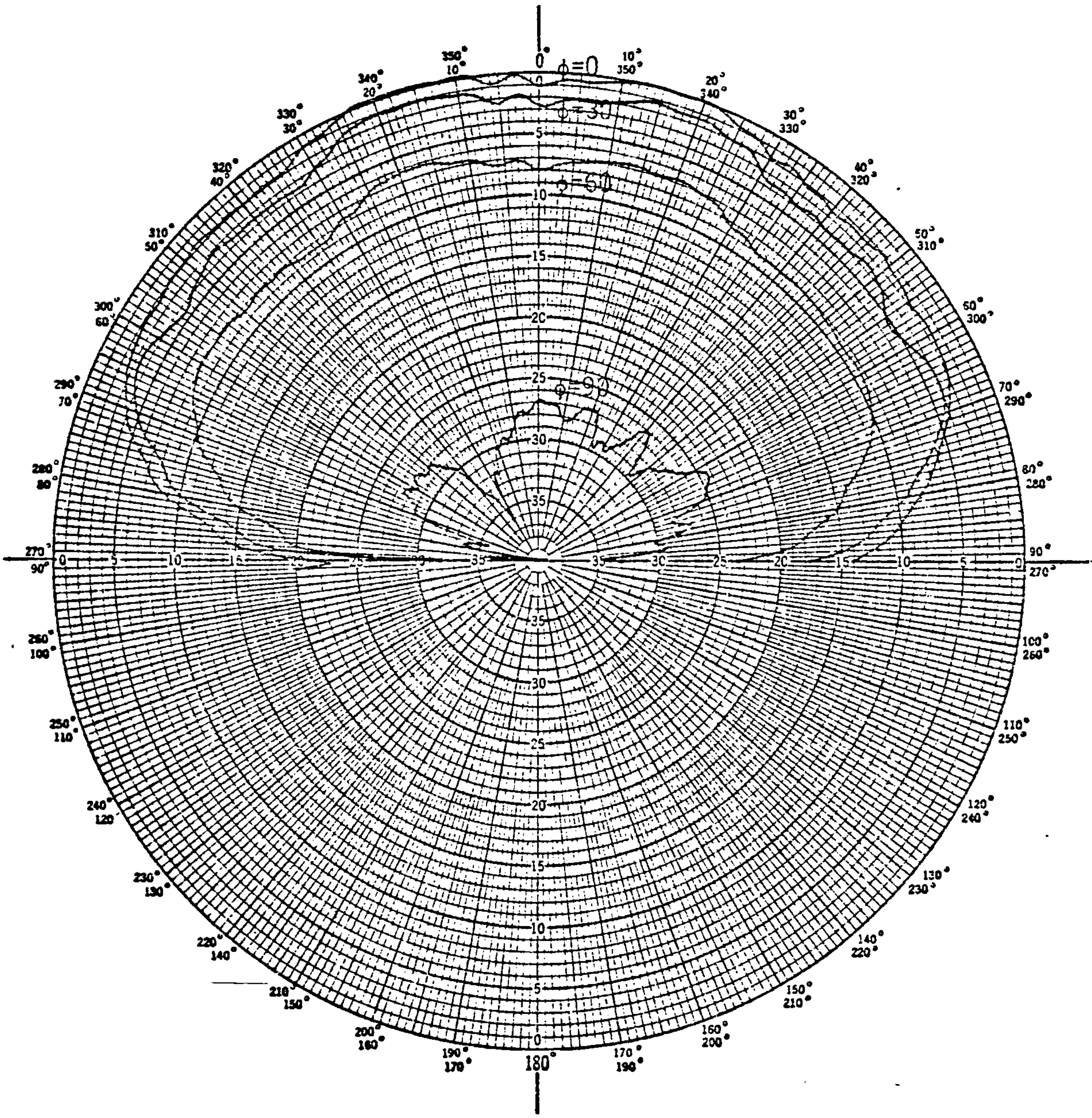

Figure 30: E_θ vs. θ for Different Values of ϕ
d: 0.075 cm.
Feed Point: 1/2R
Frequency: 2.88 GHz.

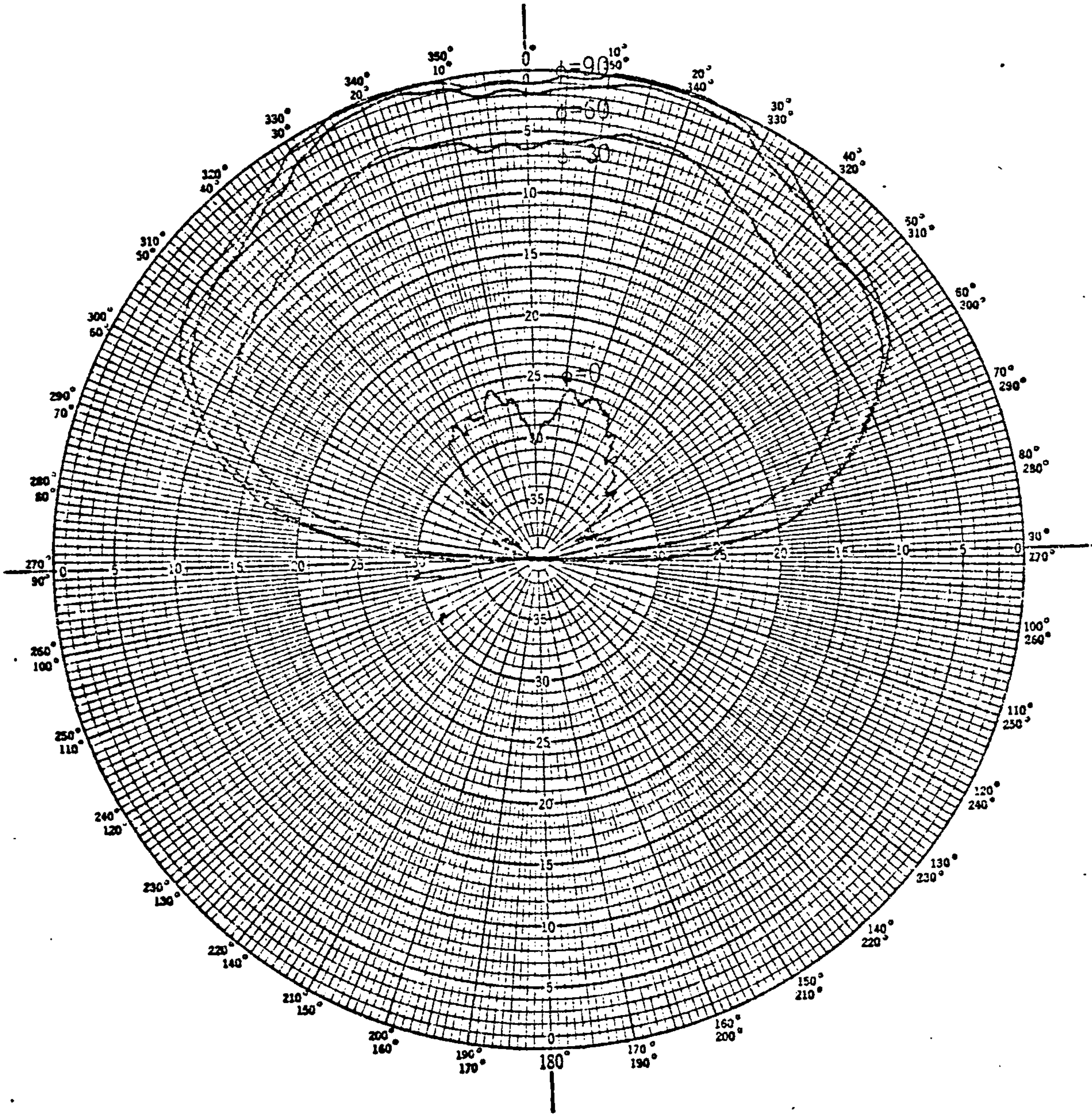

Figure 31: E_ϕ vs. θ for Different Values of ϕ
d: 0.075 cm.
Feed Point: 1/2R
Frequency: 2.88 GHz.

Figures 32 through 37 pertain to radiators that were fabricated on a substrate material with a thickness of 0.036 cm. Figures 32 and 33 show the electric fields of a radiator that was edge-fed and driven at its resonant frequency of 2.885 GHz. Figures 34 and 35 show the electric fields of an 3/4 R fed radiator at resonance. Its resonant frequency was measured to be 2.87 GHz. Finally, Figures 36 and 37 respectively, show $|E_\theta|$ vs θ and $|E_\phi|$ vs θ for a 1/2 R fed radiator driven at its resonant frequency of 2.864 GHz.

The most noticeable observation from Figures 18 through 37 is the general shape of the $|E_\theta|$ vs θ and the $|E_\phi|$ vs θ patterns. Regardless of the feed position or the ϕ angle, there was usually a finite value for $|E_\theta|$ at $\theta = 90°$ while $|E_\phi|$ at $\theta = 90°$ was usually zero. Also, in the $\phi = 0°$ plane, the principal plane cut for $|E_\theta|$ vs θ, and the $\phi = 90°$ plane, the principal plane cut for $|E_\phi|$ vs θ, the half-power beamwidth (measured between the -3 dB points of the beam maximum) was larger for the $\overline{E}_\theta$ component than for the $\overline{E}_\phi$ component for any given feed position or dielectric thickness.

IV.2b Effects of Feed Position on the Far Fields

For the three radiators fabricated on the dielectric substrate material with d = 0.16 cm, the position of the feed point, i.e. R, 3/4 R, 1/2 R, had little effect on the shapes of the $|E_\theta|$ vs θ or $|E_\phi|$ vs θ patterns regardless of the ϕ cut. The magnitudes of the patterns for radiators with different feed points could not be compared since the feed point movement caused a shift in the resonant frequency. This frequency change caused many other factors to change in the test configuration for measuring the patterns. A change in the output level of the signal generator, a change in the input impedance of the pyramidal

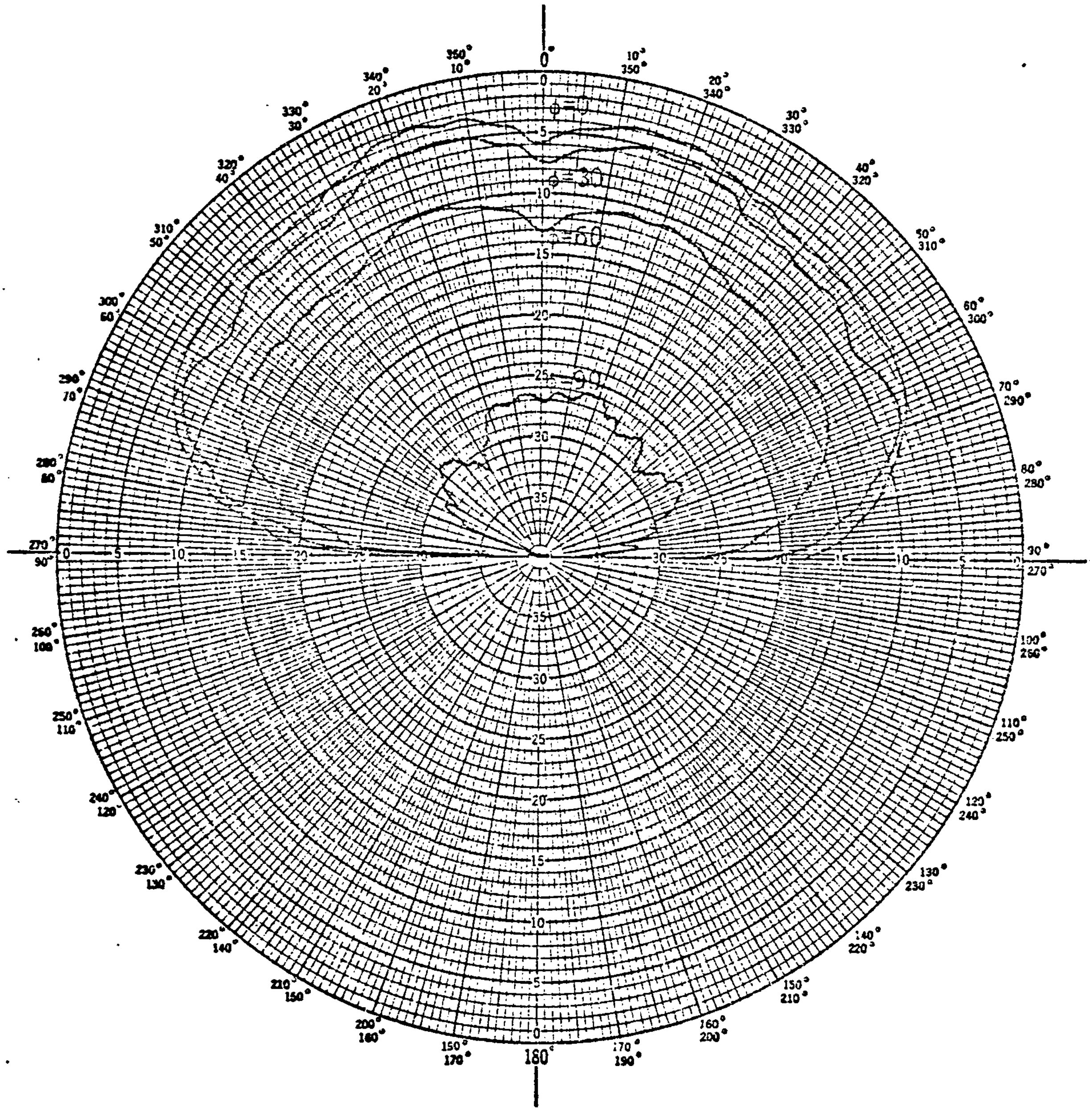

Figure 32: E_θ vs. θ for Different Values of ϕ
d: 0.036 cm.
Feed Point: R
Frequency: 2.885 GHz.

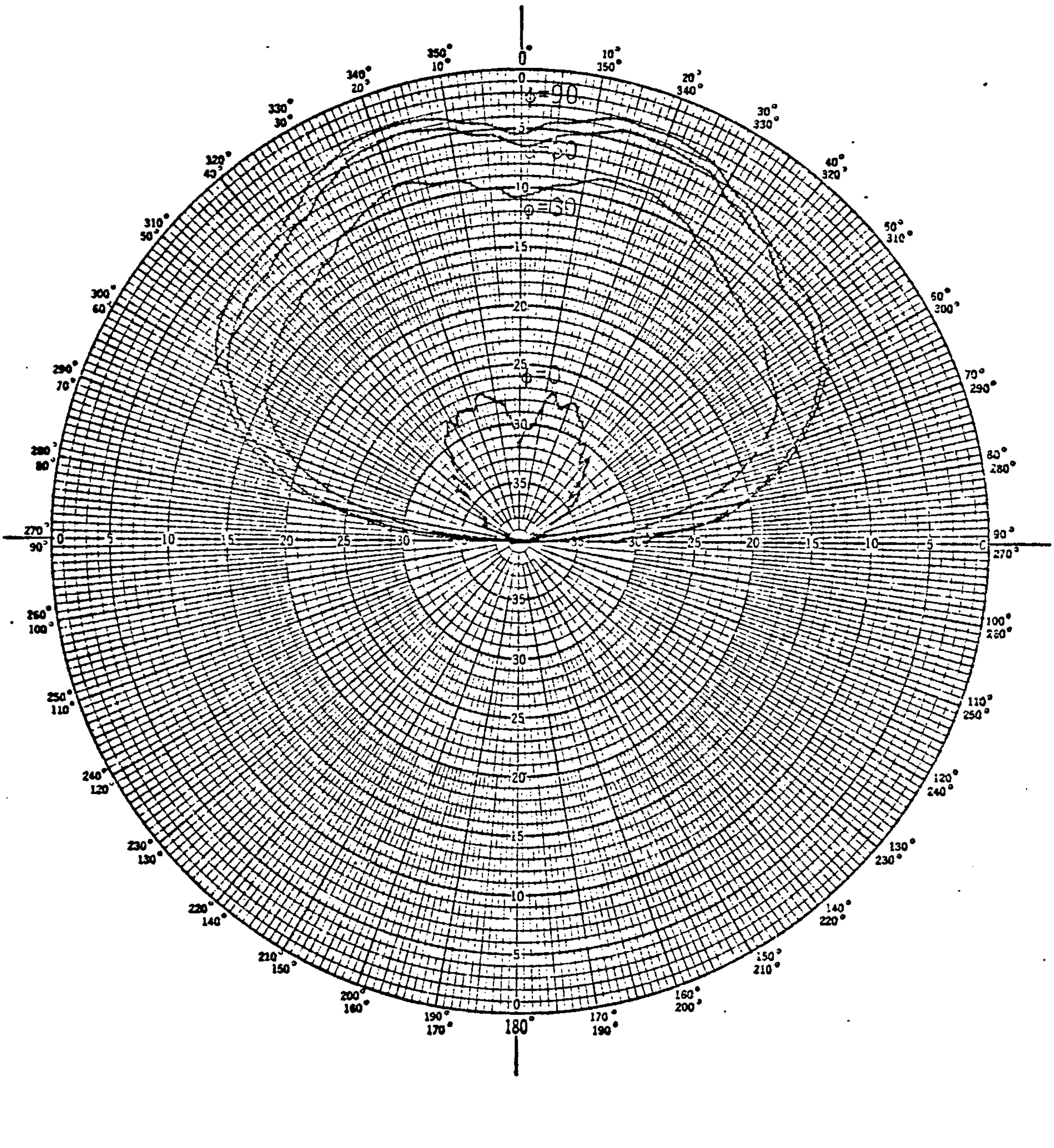

Figure 33: E_ϕ vs. θ for Different Values of φ
d: 0.036 cm.
Feed Point: R
Frequency: 2.885 GHz.

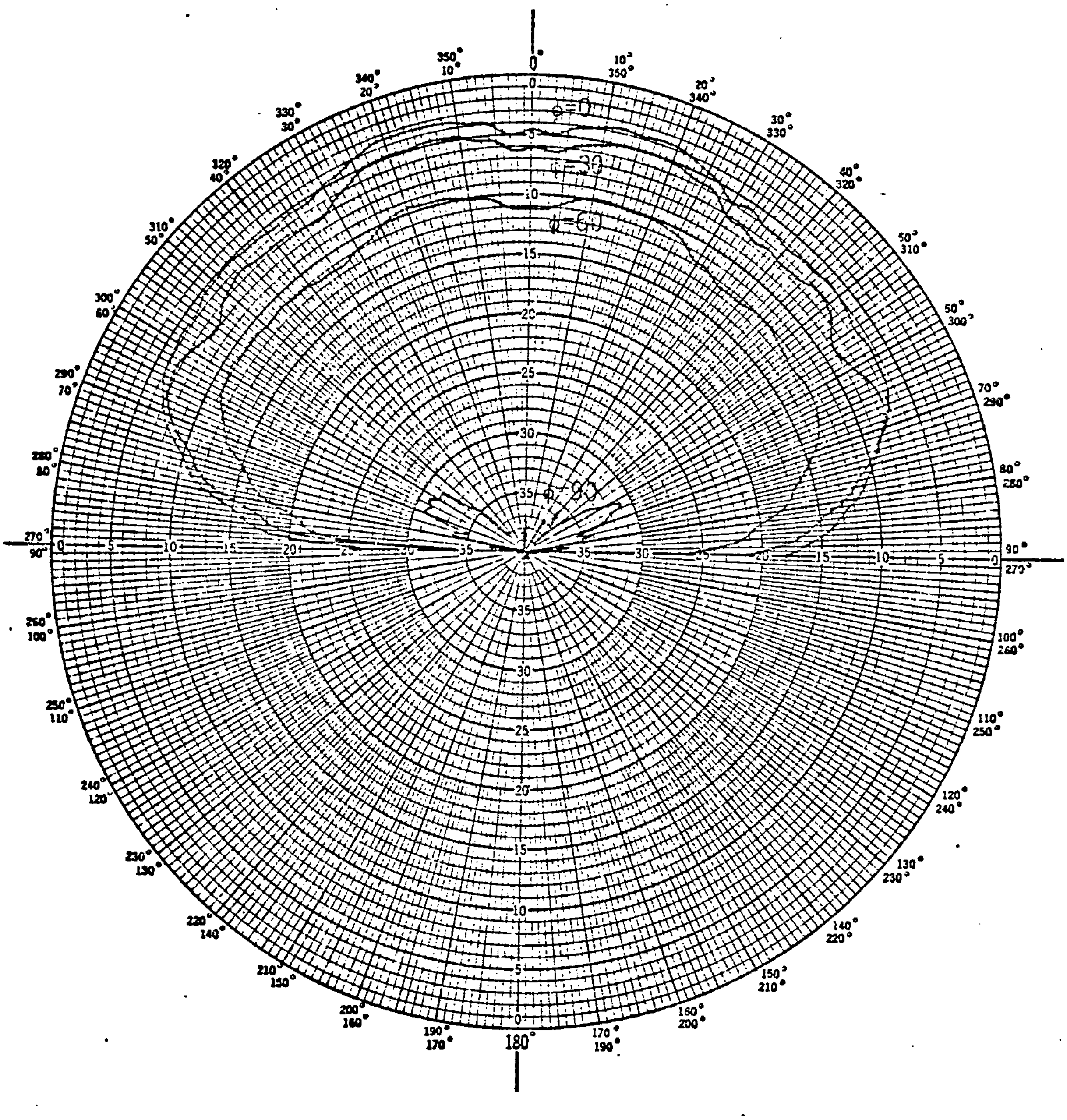

Figure 34: E_θ vs. θ for Different Values of ϕ
d: 0.036 cm.
Feed Point: 3/4R
Frequency: 2.87 GHz.

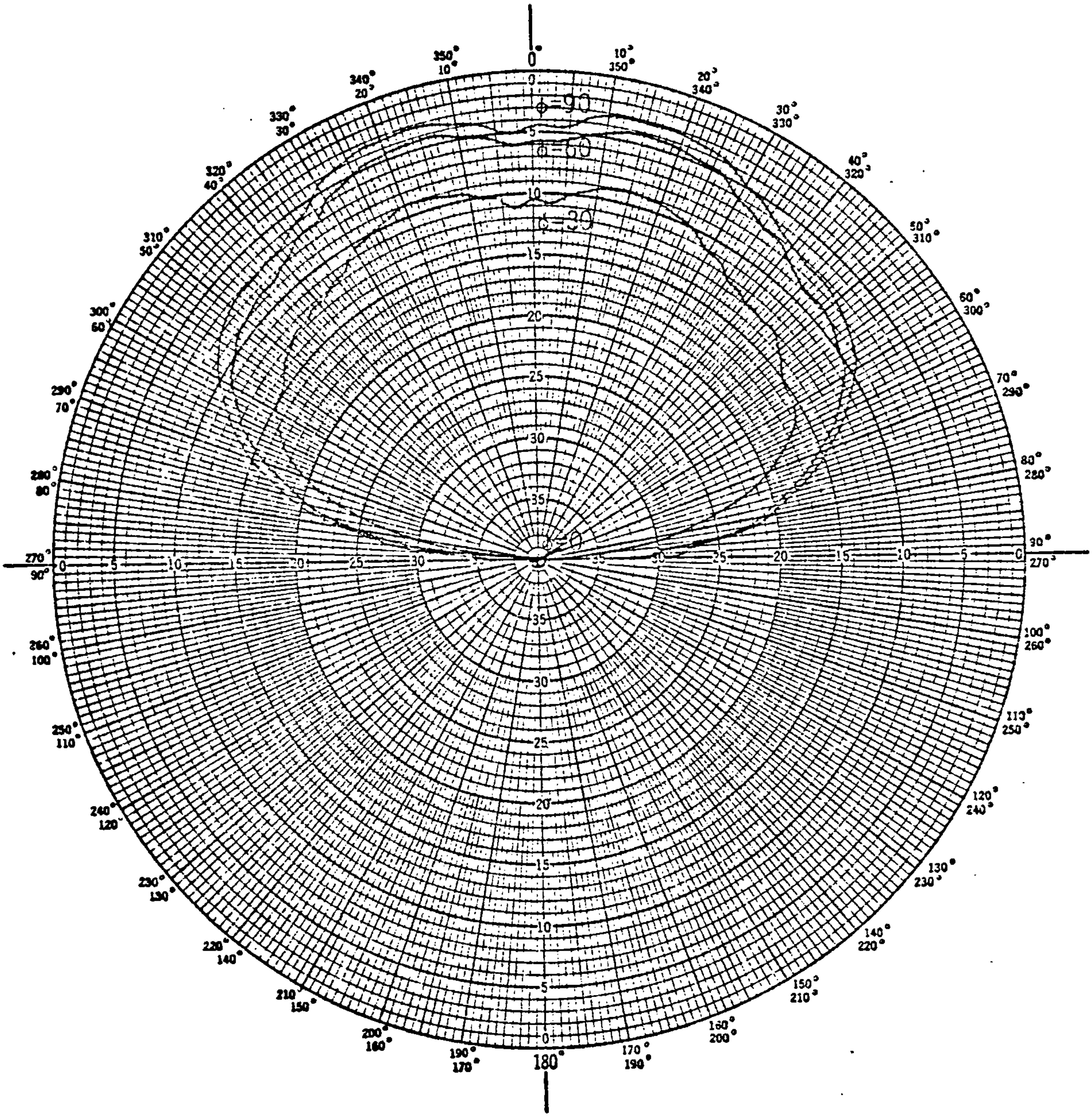

Figure 35: E_ϕ vs. θ for Different Values of ϕ
d: 0.036 cm.
Feed Point: 3/4R
Frequency: 2.87 GHz.

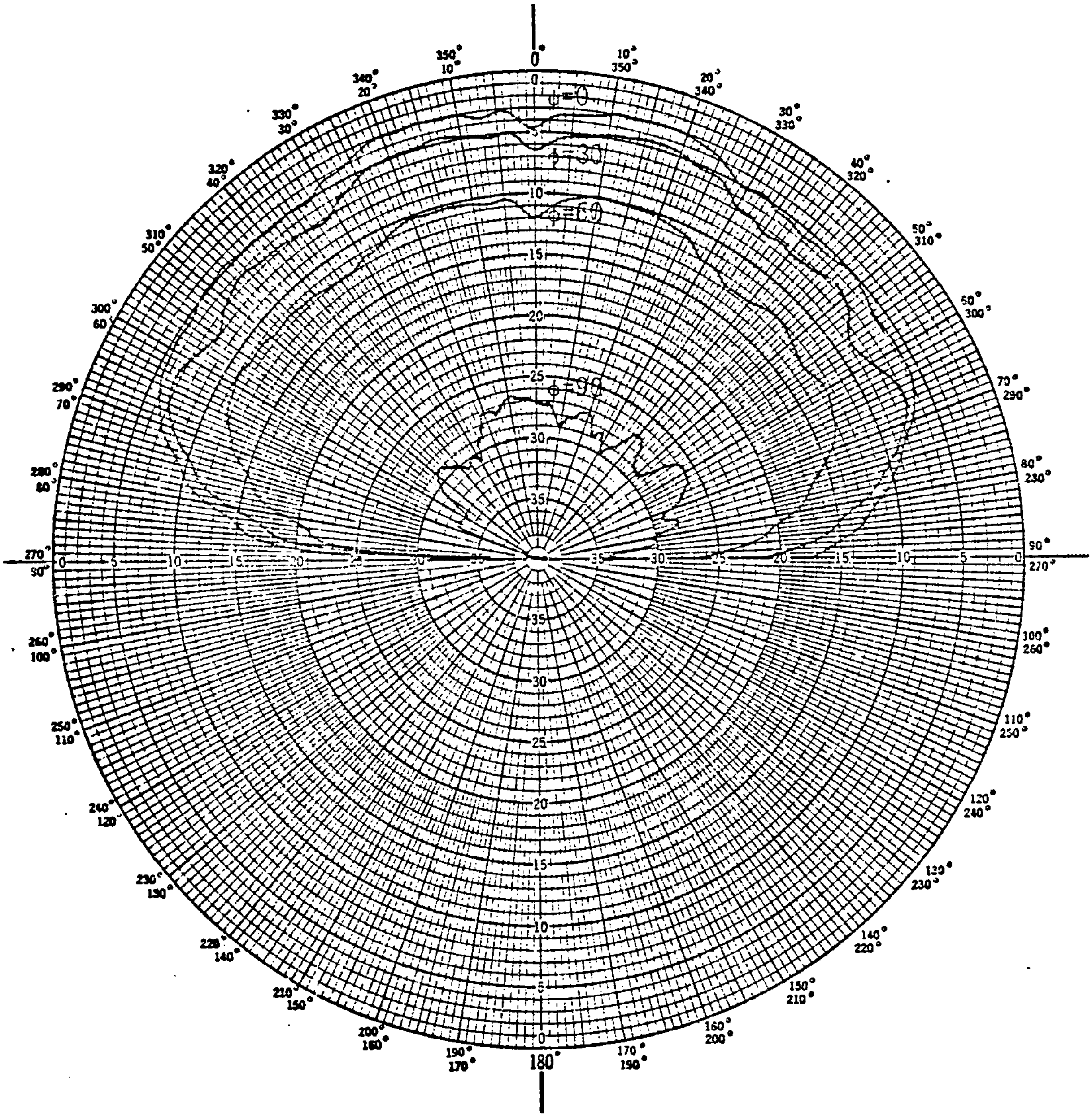

Figure 36: E_θ vs. θ for Different Values of ϕ
d: 0.036 cm.
Feed Point: 1/2R
Frequency: 2.864 GHz.

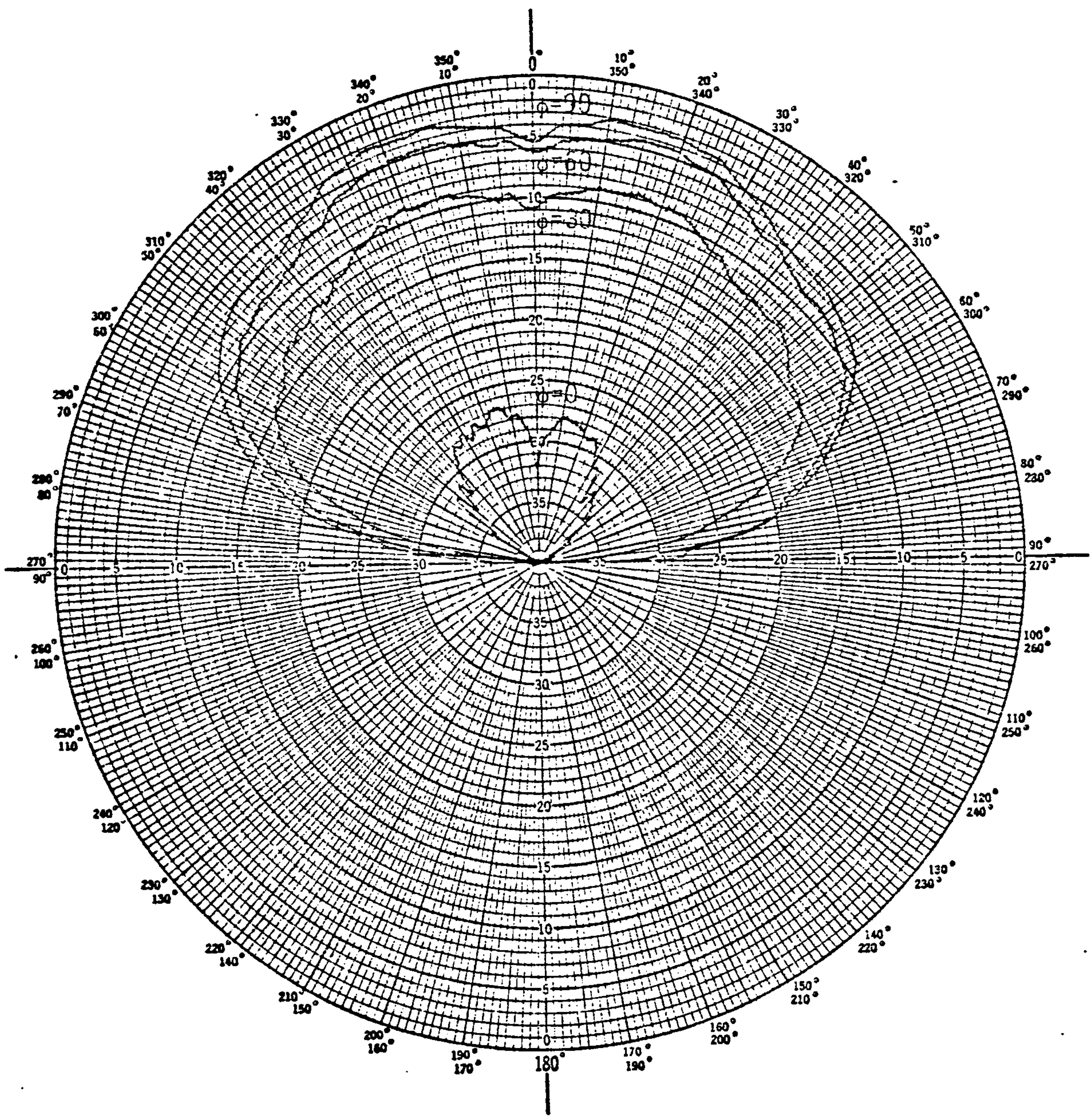

Figure 37: E_ϕ vs. θ for Different Values of ϕ
d: 0.036 cm.
Feed Point: 1/2R
Frequency: 2.864 GHz.

horn, and a change in the space loss between the transmitting horn and the receiving antenna were just a few of the factors that would prohibit any comparison of the magnitude of the electric fields for radiators with different feed points. Table IV.2 summarizes the 6 dB beamwidth of the electric fields for the d = 0.16 cm radiators.

ϕ Plane (deg.)	$\lvert E_\theta \rvert$ vs θ			$\lvert E_\phi \rvert$ vs θ		
	R FED	3/4R FED	1/2R FED	R FED	3/4R FED	1/2R FED
90	NA	NA	NA	119°	118°	117°
60	152°	151°	150°	120°	118°	118°
30	151°	152°	151°	119°	120°	120°
0	149°	147°	147°	NA	NA	NA

Table IV.2 6 dB Beamwidths for Various Feed Points (d = 0.16 cm)

For the three radiators fabricated on the dielectric material with a thickness of 0.075 cm, the position of the feed point once again had little effect on the shape of the far field patterns. A summary of the 6 dB beamwidths for various feed points is shown in Table IV.3.

ϕ Plane (deg.)	$\lvert E_\theta \rvert$ vs θ			$\lvert E_\phi \rvert$ vs θ		
	R FED	3/4R FED	1/2R FED	R FED	3/4R FED	1/2R FED
90	NA	NA	NA	117°	116°	117°
60	154°	150°	151°	115°	115°	114°
30	155°	153°	153°	113°	114°	111°
0	150°	148°	149°	NA	NA	NA

Table IV.3 6 dB Beamwidths for Various Feed Positions (d = 0.075 cm)

Table IV.4 summarizes the 6 dB beamwidths of the far field patterns for differently fed radiators fabricated on the dielectric material with d = 0.036 cm. Once again no drastic changes occur in the 6 dB beamwidth when the feed position is changed.

ϕ Plane (deg.)	$\lvert E_\theta \rvert$ vs θ			$\lvert E_\phi \rvert$ vs θ		
	R FED	3/4R FED	1/2R FED	R FED	3/4R FED	1/2R FED
90	NA	NA	NA	114°	115°	116°
60	147°	148°	150°	113°	114°	114°
30	150°	151°	151°	110°	112°	113°
0	147°	148°	149°	NA	NA	NA

Table IV.4 6 dB Beamwidths

for Various Feed Positions (d = 0.036 cm)

IV.2c Effects of Dielectric Thickness on the Far Field Patterns

By comparison of the appropriate figures, one can see that the far field patterns change for radiators at resonance with the same feed point but etched on different dielectric thicknesses. If one compares the 6 dB beamwidths on the patterns for radiators which were fed at the same point but etched on a different substrate thickness, this change is not obvious. However, for radiators driven at their resonant frequency, small dips start occurring at $\theta = 0$ in both $|E_\theta|$ vs θ and $|E_\phi|$ vs θ patterns as the dielectric thickness gets smaller. This data is summarized in Table IV.5. Values of these dips were rounded to the nearest 1/2 decibel. This dip at $\theta = 0$ for both $|E_\theta|$ and $|E_\phi|$ was not predicted

d (cm)	Feed Position	ϕ Cut (degrees)	$\|E_\theta$ dip$\|$ (dB)	$\|E_\phi$ dip$\|$ (dB)
0.16	R	90	NA	0
		60	0	.5
		30	0	0
		0	0	NA
	3/4 R	90	NA	0
		60	0	.5
		30	0	0
		0	0	NA
	1/2 R	90	NA	0
		60	0	0
		30	0	0
		0	0	NA
0.075	R	90	NA	1
		60	1	1.5
		30	1	2
		0	.5	NA
	3/4 R	90	NA	1.5
		60	1.5	2.0
		30	1.5	2.0
		0	1.5	NA
	1/2 R	90	NA	1.5
		60	2.0	2.0
		30	1.5	2.0
		0	1.5	NA
0.036	R	90	NA	2.5
		60	3.0	2.5
		30	3.0	3.0
		0	3.0	NA
	3/4 R	90	NA	1.5
		60	1.5	1.5
		30	1.5	1.5
		0	1.5	NA
	1/2 R	90	NA	2.0
		60	2.0	2.0
		30	2.0	2.0
		0	2.0	NA

Table IV.5 Magnitudes of the Electric Field Dips @ $\theta = 0°$ for Different Dielectric Thicknesses by Morel in his theoretical analysis of the far fields using Watkins' zeroth-order theory for the n=1 mode. Since all the patterns were measured at the resonant frequency of the individual radiators, one logical explanation for these dips is that the radiators fabricated on the 0.075 cm and the 0.036 cm dielectric thicknesses were being driven at a frequency such that higher order modes were generated in the region between the disc and the ground plane.

<u>IV.2d Effects of Frequency Variation on the Far Field Patterns</u>

To investigate the frequency dependence of the far fields, several measurements of $|E_\theta|$ vs θ and $|E_\phi|$ vs θ were made on an edge-fed radiator fabricated on a dielectric material with d = 0.16 cm. The results of these measurements are shown in Figures 38 through 51. Figures 38 and 39 show $|E_\theta|$ vs θ in the $\phi = 0°$ plane and $|E_\phi|$ vs θ in the $\phi = 90°$ plane, respectively. The operating frequency was 2.6 GHz, well below the resonant frequency of this radiator which was 2.815 GHz. Figures 40 and 41 show the electric field components for a frequency of 2.7 GHz. Figures 42 and 43 show the electric field components at the resonant frequency. Figures 44 and 45, respectively, show $|E_\theta|$ vs θ for $\phi = 0°$ and $|E_\phi|$ vs θ for $\phi = 90°$ measured at a frequency of 2.82 GHz. Figures 46 and 47, 48 and 49, and 50 and 51 show the electric field components for the edge-fed 0.16 cm radiator at 2.85 GHz, 2.96 GHz, and 3.0 GHz, respectively. Note that the electric field changed significantly as the frequency was deviated from the resonant frequency. Dips in the magnitude of the electric field began to occur at $\theta = 0$ as the frequency was increased above 2 815 GHz.

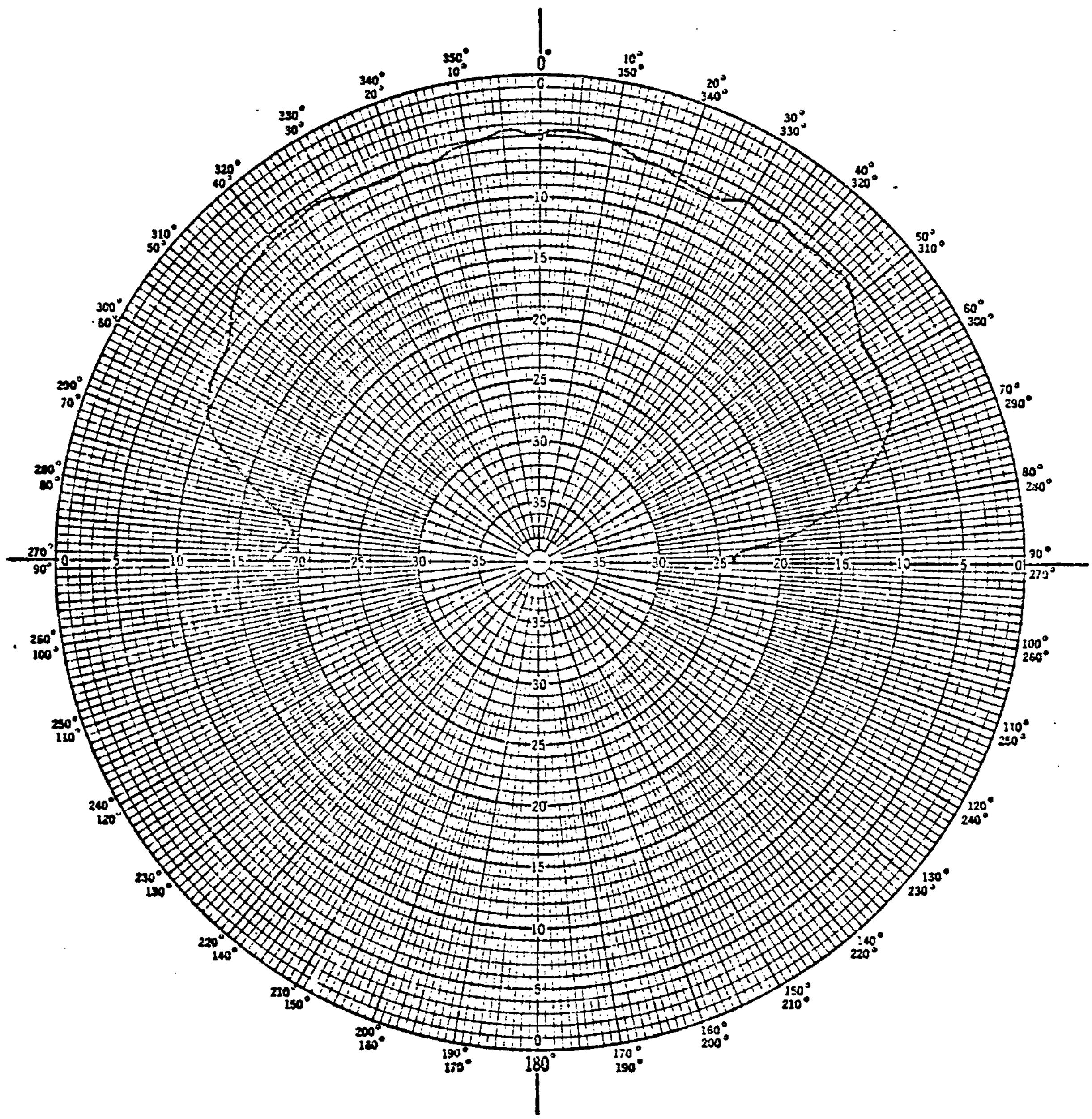

Figure 38: E_θ vs. θ for $\phi=0$
d: 0.16 cm.
Feed Point: R
Frequency: 2.6 GHz.

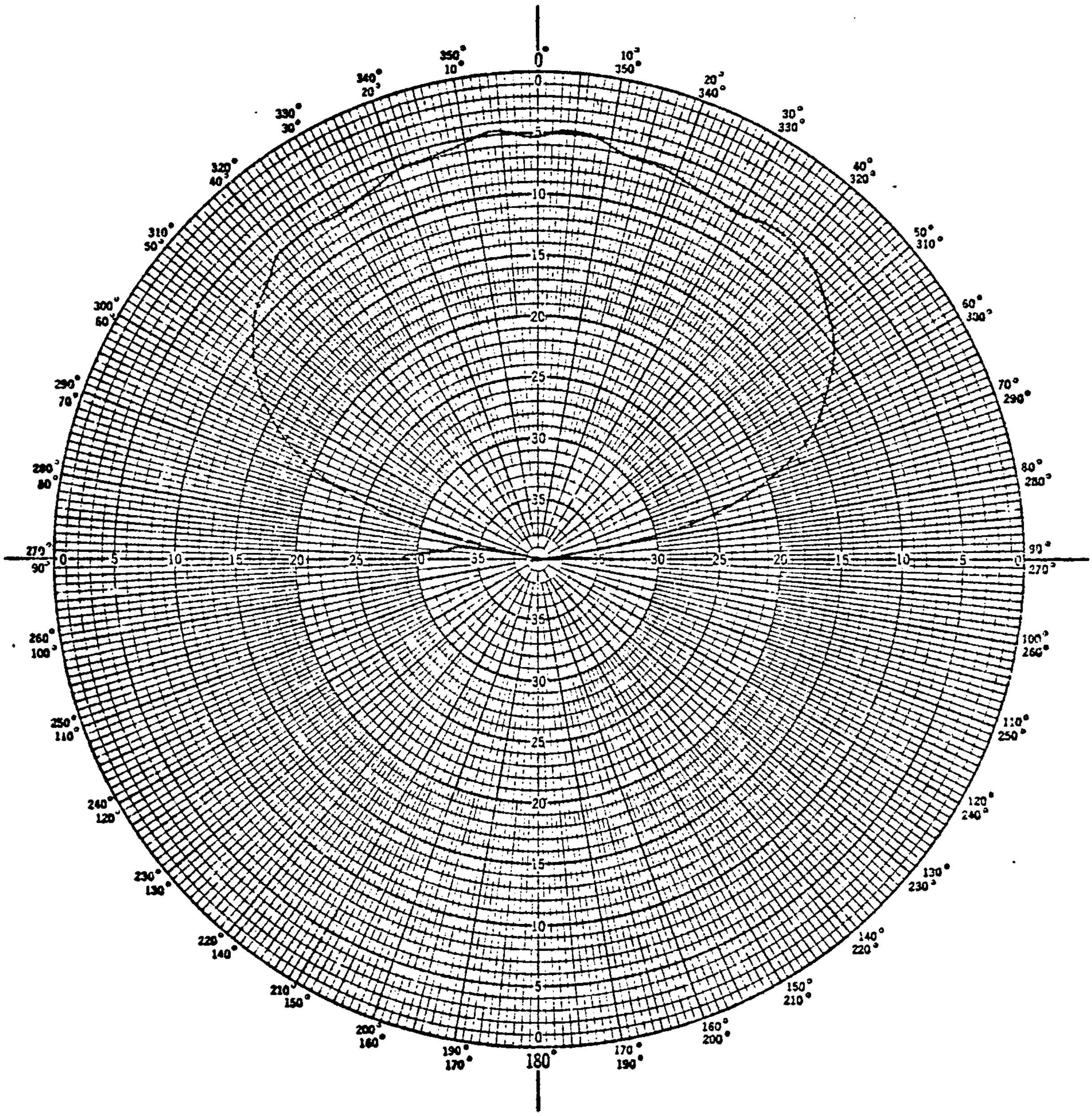

Figure 39: E_ϕ vs. θ for ϕ=90
d: 0.16 cm.
Feed Point: R
Frequency: 2.6 GHz.

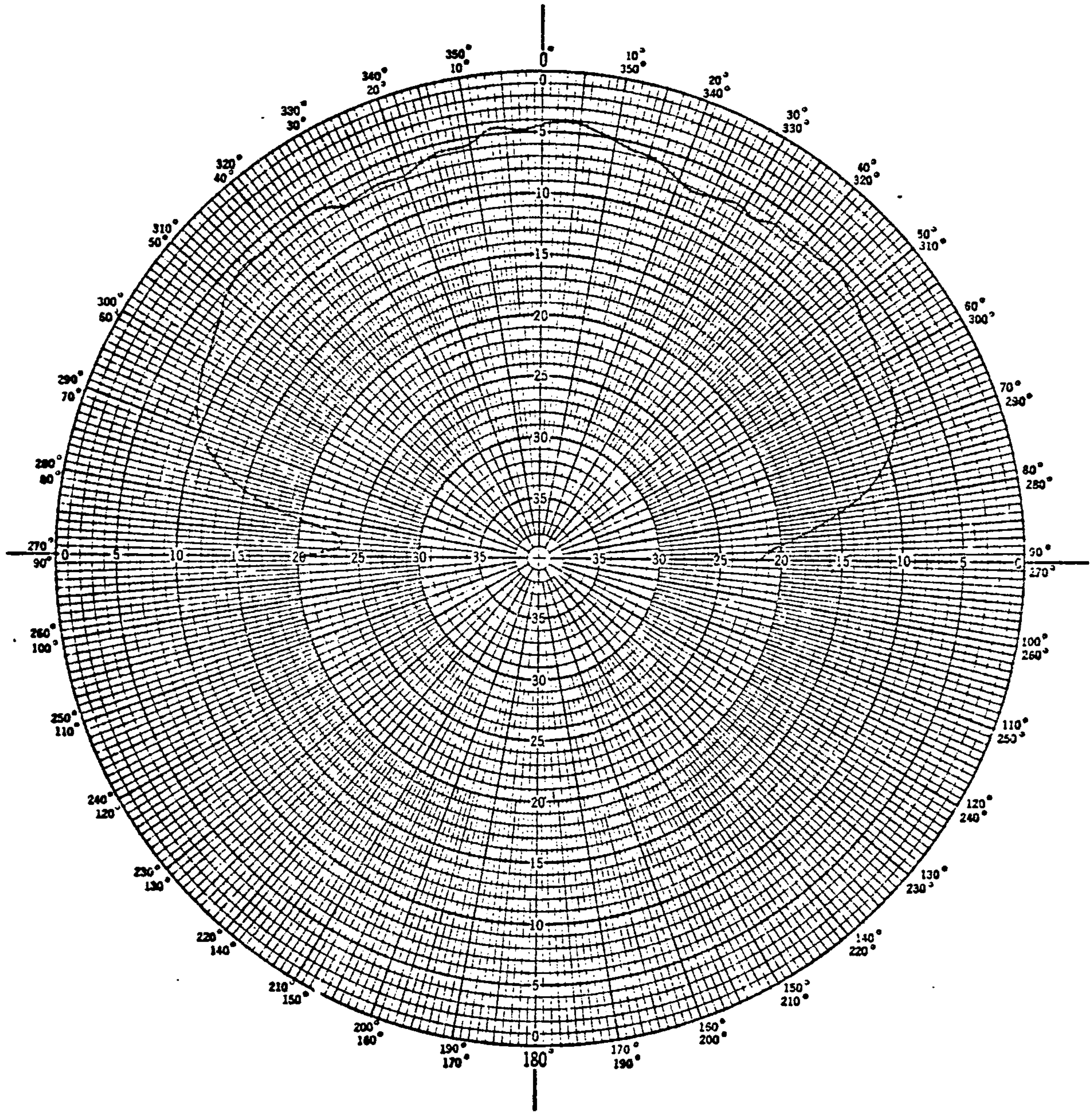

Figure 40: E_θ vs. θ for $\phi=0$
d: 0.16 cm.
Feed Point: R
Frequency: 2.7 GHz.

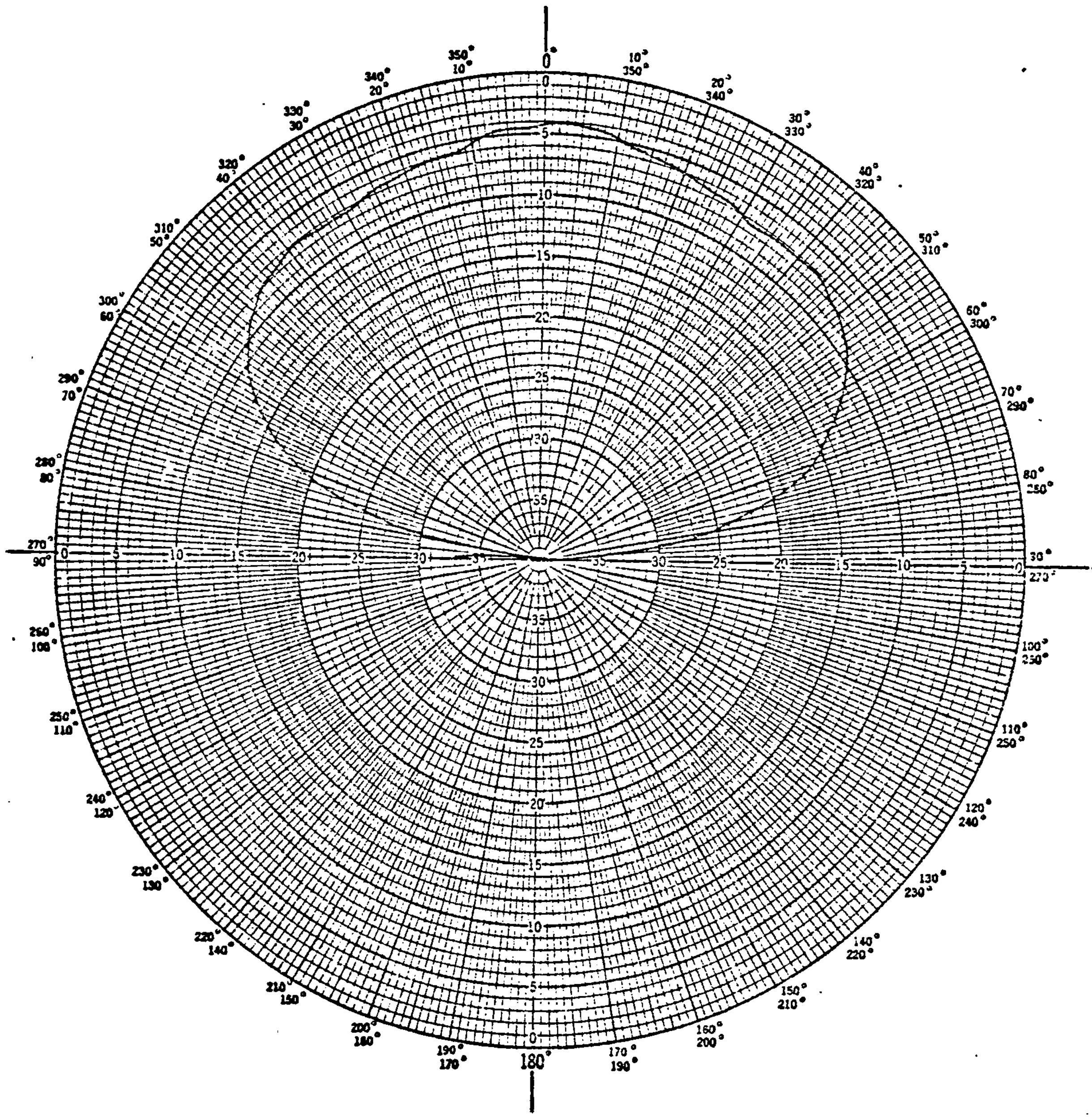

Figure 41: E_ϕ vs. θ for ϕ=90
d: 0.16 cm.
Feed Point: R
Frequency: 2.7 GHz.

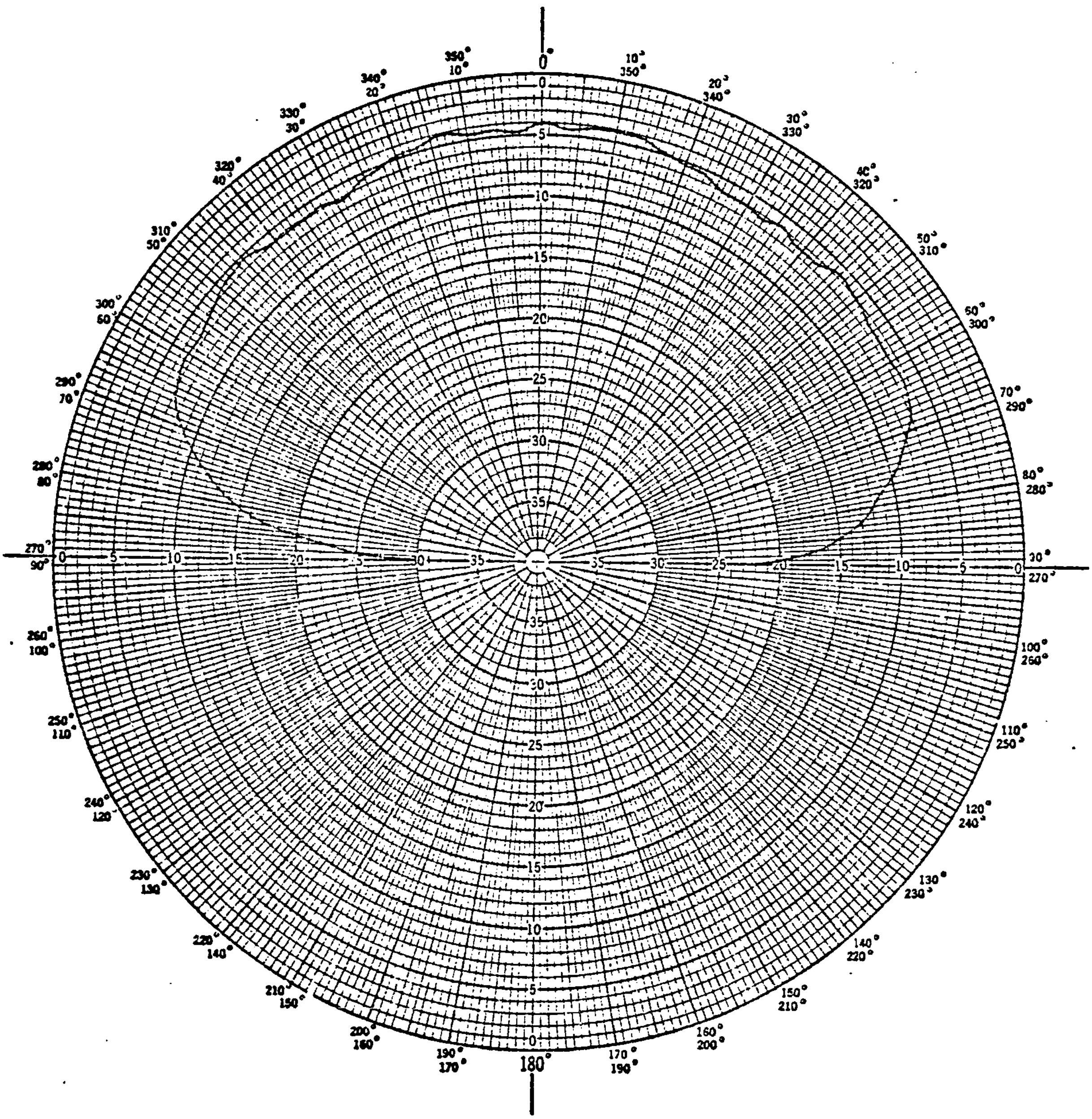

Figure 42: E_θ vs. θ for $\phi=0$

d: 0.16 cm.

Feed Point: R

Frequency: 2.815 GHz.

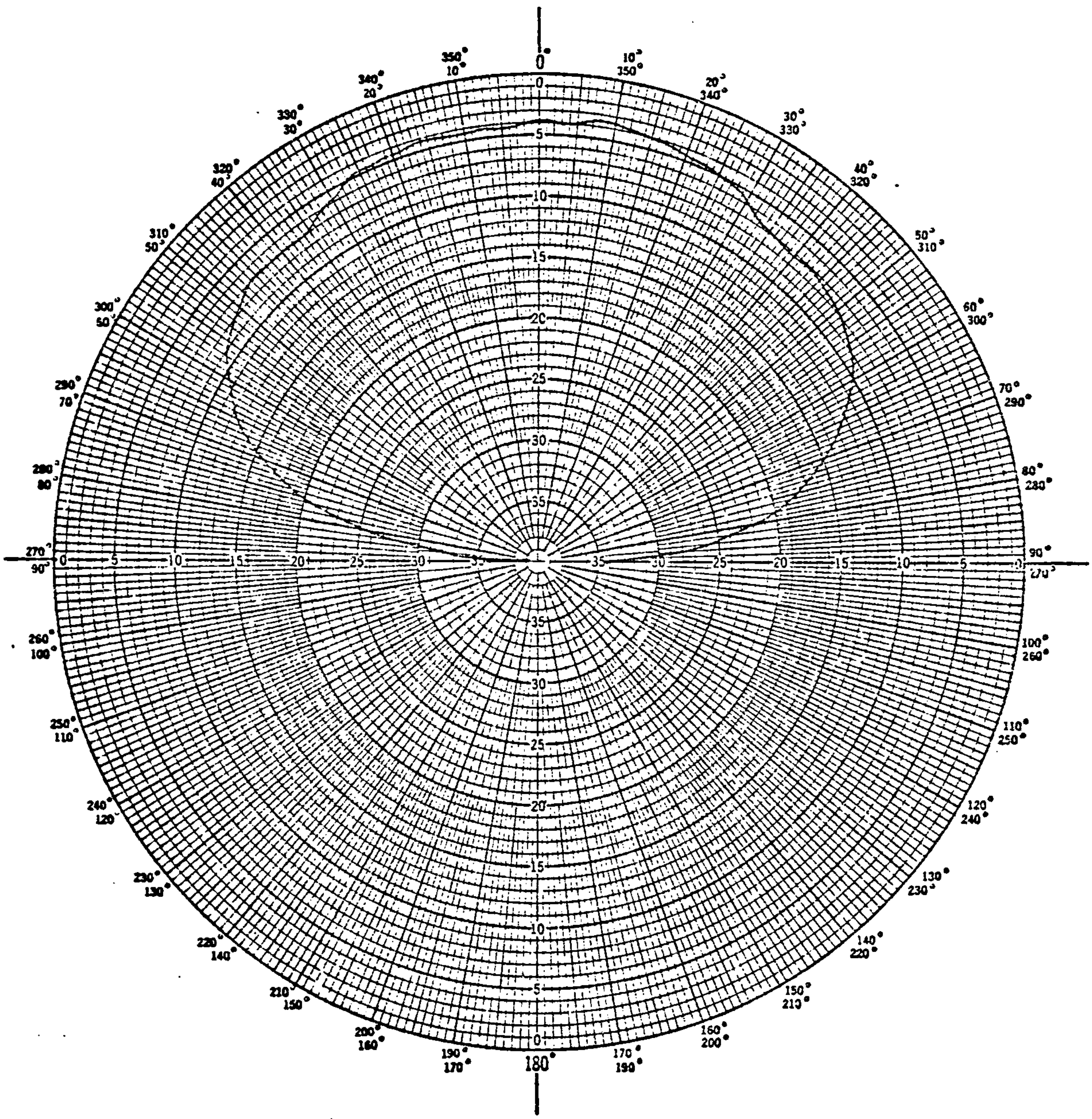

Figure 43: E_{ϕ} vs. θ for ϕ=90
d: 0.16 cm.
Feed Point: R
Frequency: 2.815 GHz.

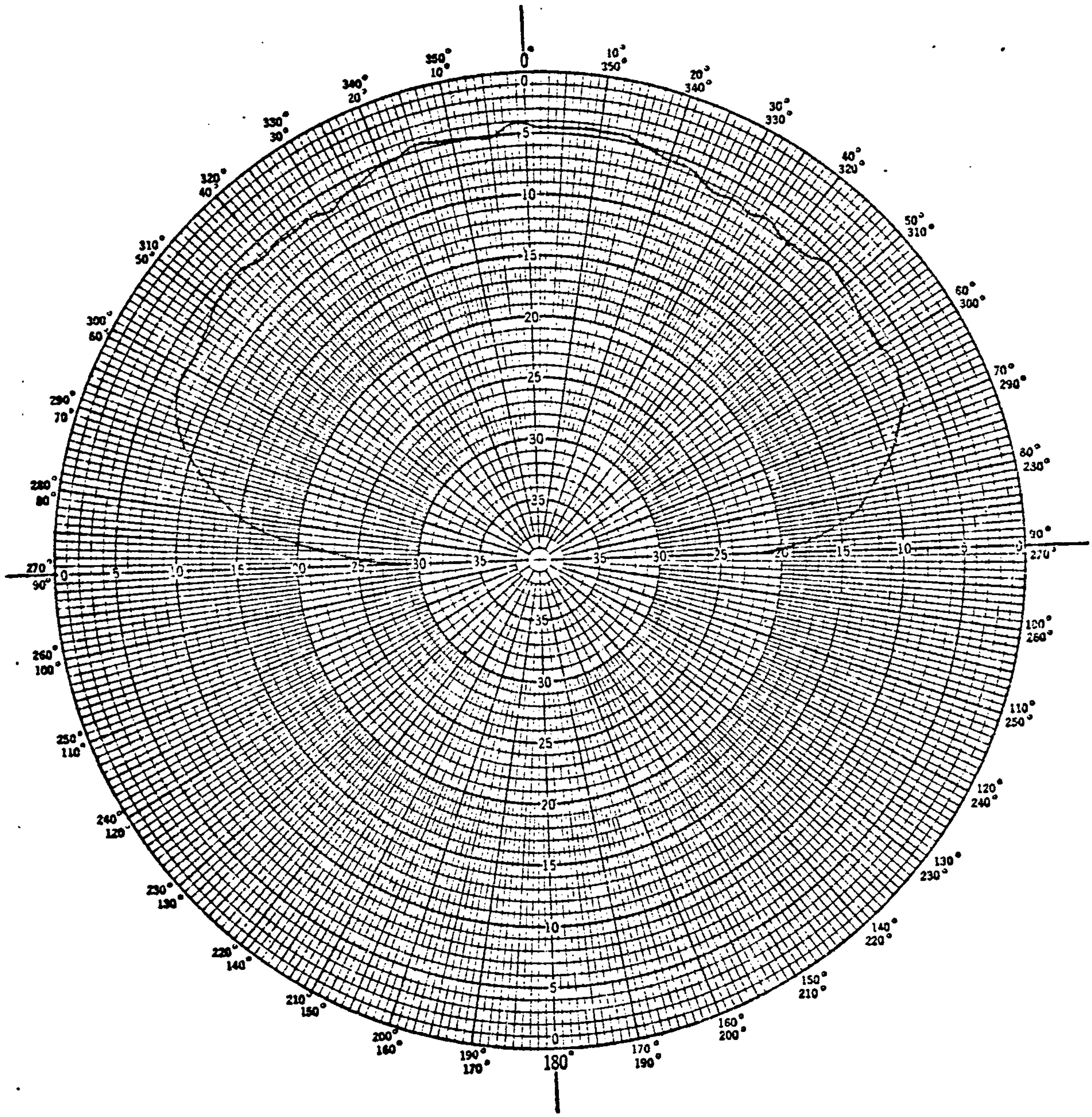

Figure 44: E_{θ} vs. θ for $\phi=0$

d: 0.16 cm.
Feed Point: R
Frequency: 2.82 GHz.

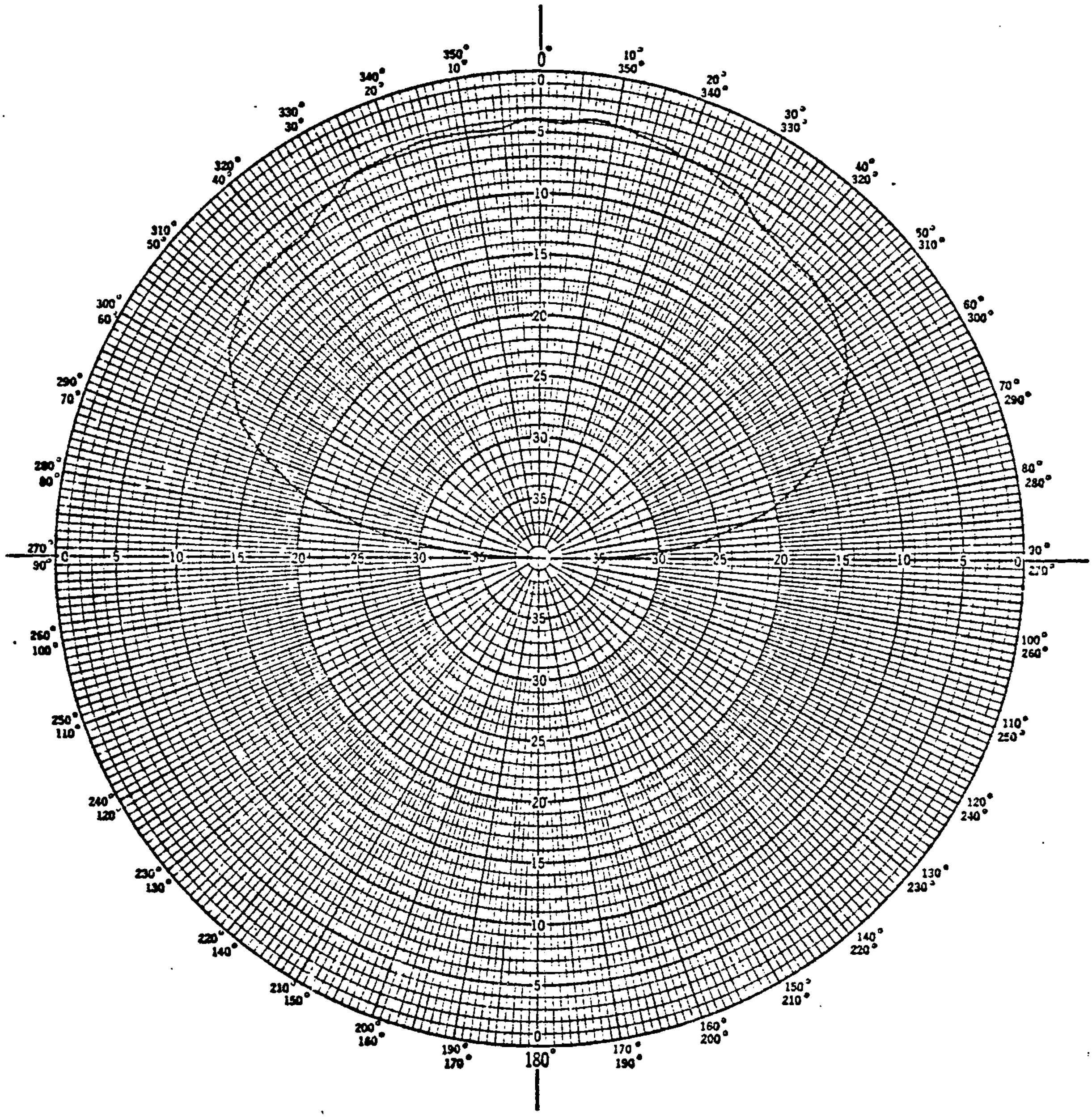

Figure 45: E_ϕ vs. θ for ϕ=90
d: 0.16 cm.
Feed Point: R
Frequency: 2.82 GHz.

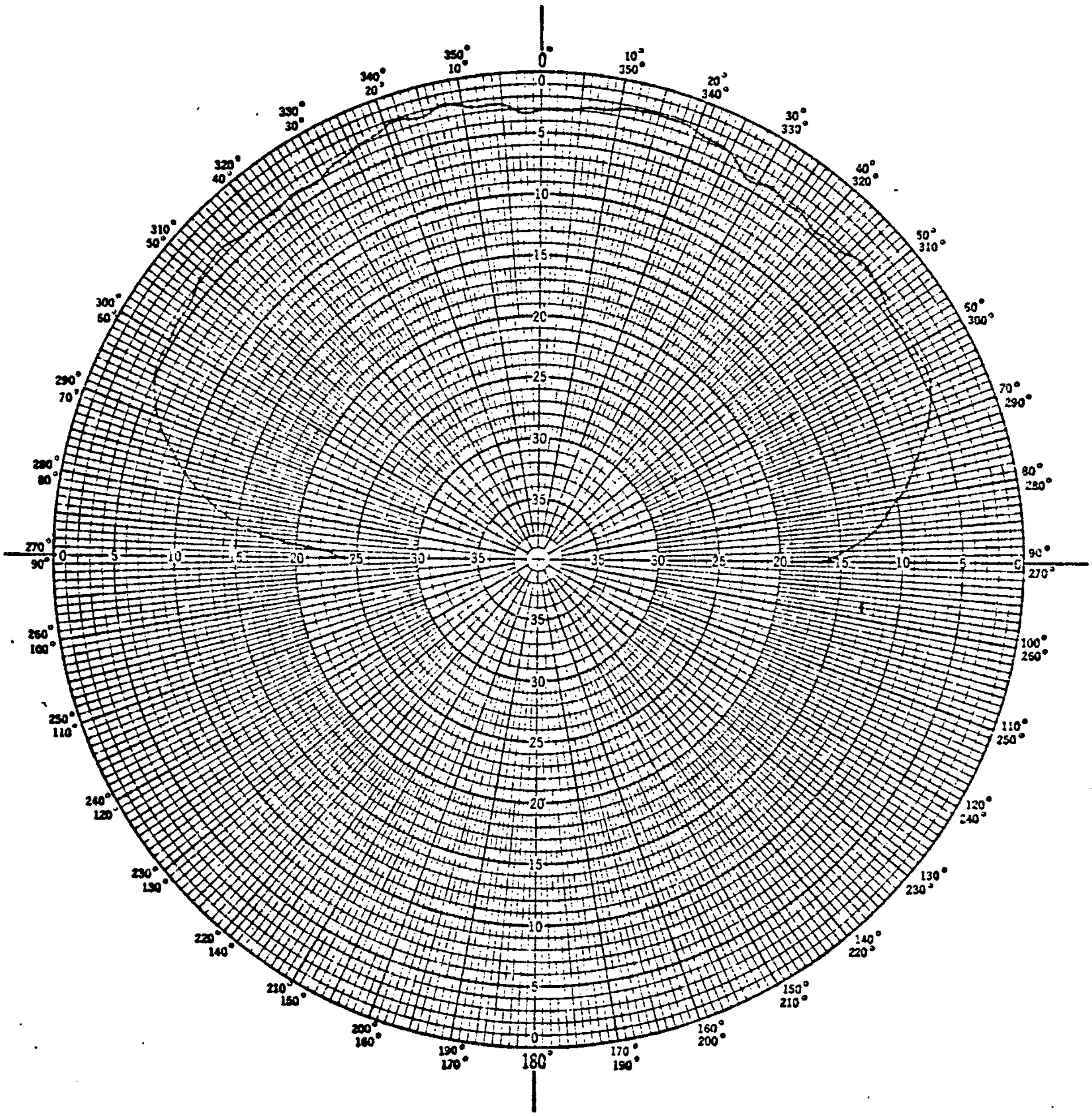

Figure 46: E_θ vs. θ for $\phi=0$

d: 0.16 cm.
Feed Point: R
Frequency: 2.85 GHz.

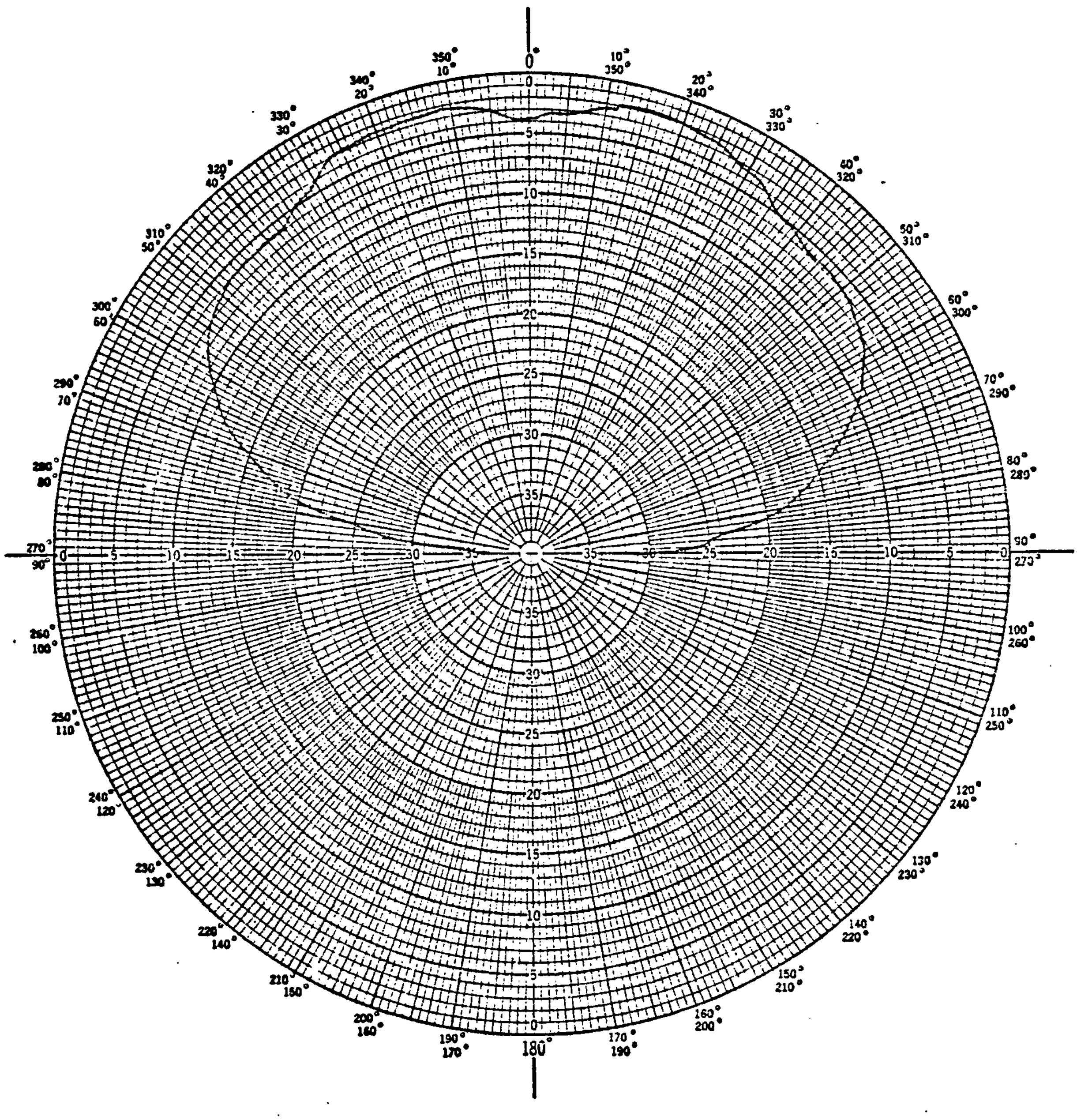

Figure 47: E_{ϕ} vs. θ for ϕ=90
d: 0.16 cm.
Feed Point: R
Frequency: 2.85 GHz.

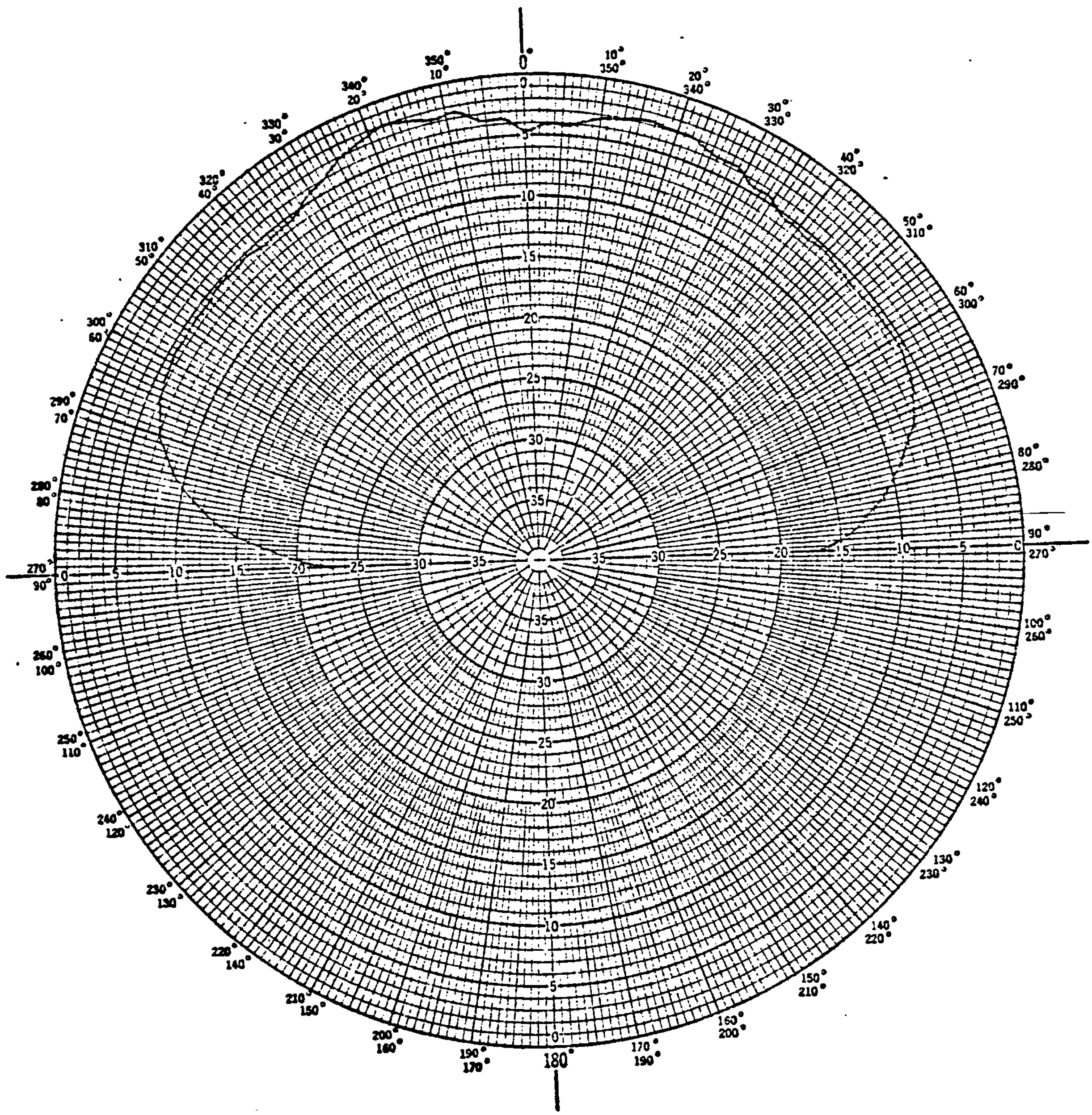

Figure 48: E_θ vs. θ for ϕ=0

d: 0.16 cm.
Feed Point: R
Frequency: 2.9 GHz.

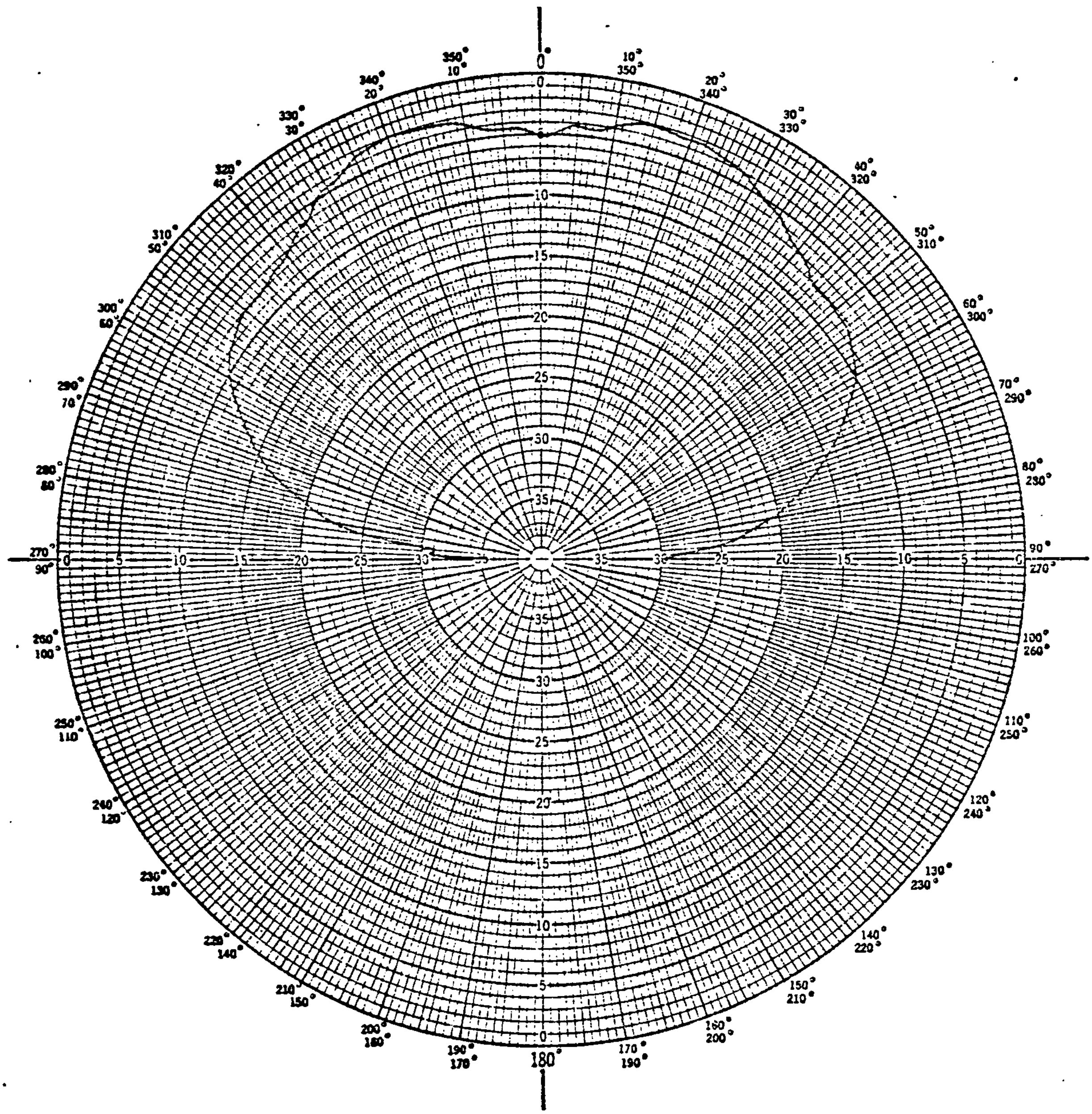

Figure 49: E_ϕ vs. θ for ϕ=90
d: 0.16 cm.
Feed Point: R
Frequency: 2.9 GHz.

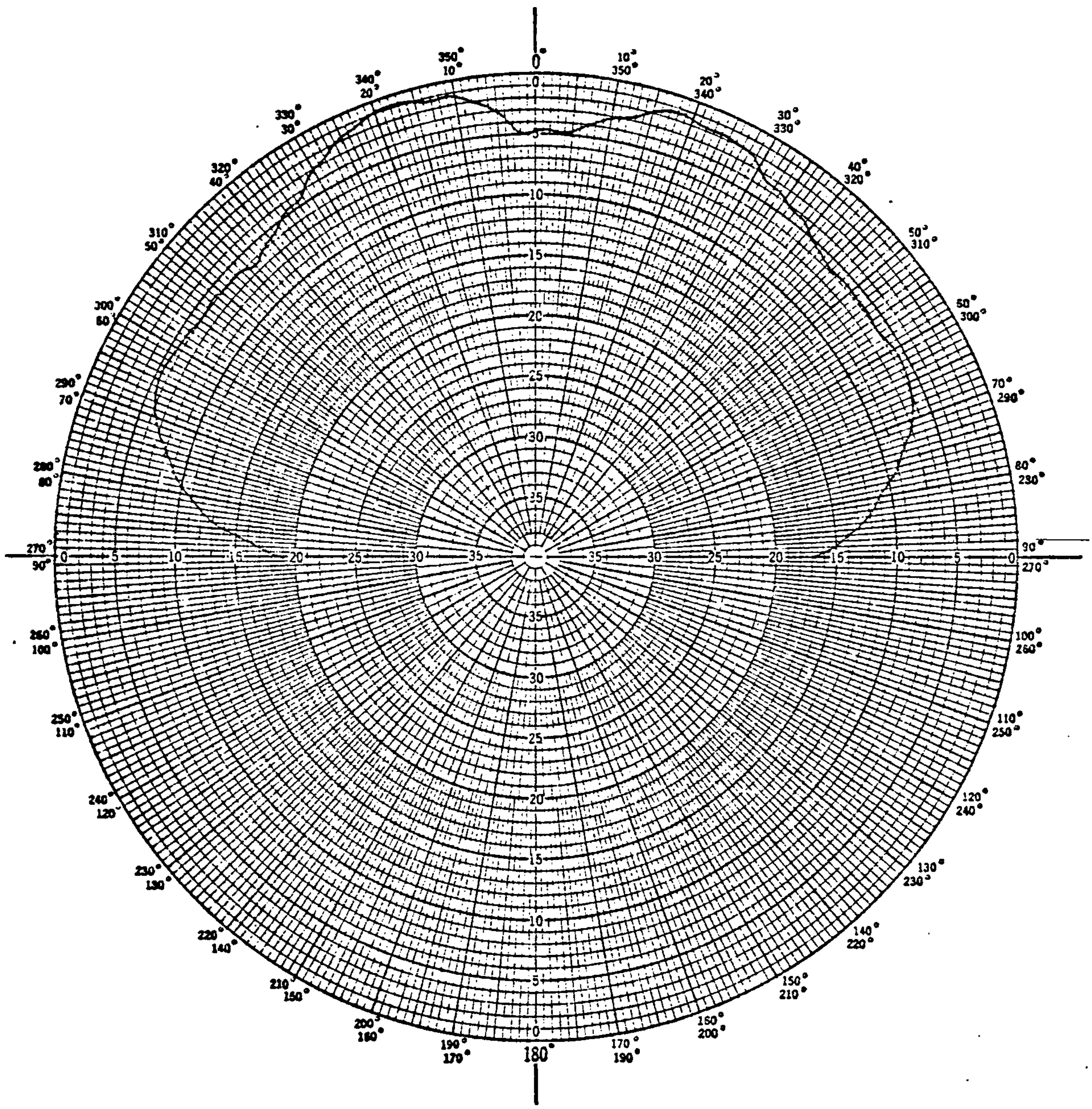

Figure 50: E_θ vs. θ for ϕ=0

d: 0.16 cm.
Feed Point: R
Frequency: 3.0 GHz.

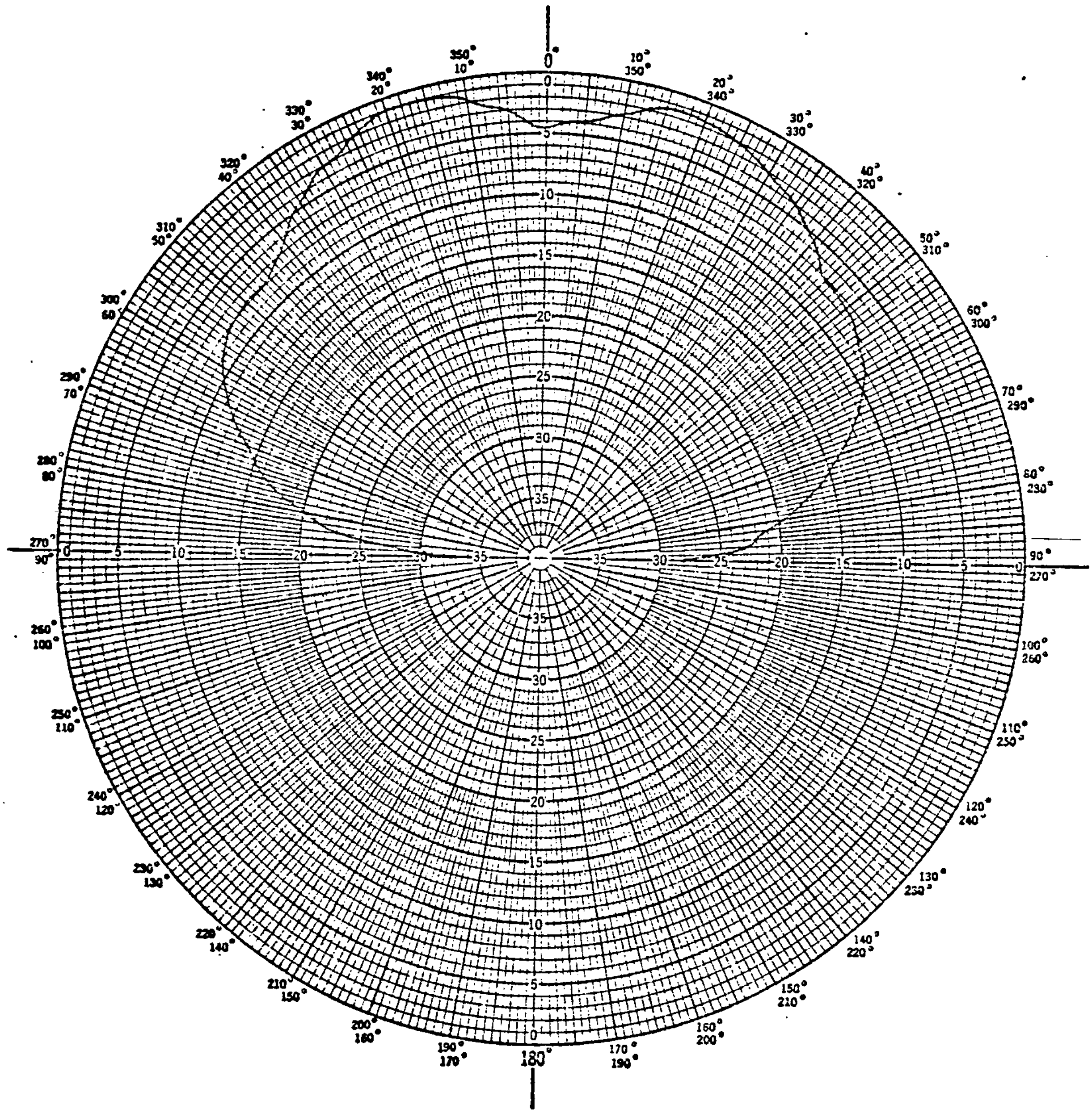

Figure 51: E_ϕ vs. θ for ϕ=90

d: 0.16 cm.

Feed Point: R

Frequency: 3.0 GHz.

IV. 3 Comparison of the Calculated and Measured Far Field Patterns

Using Watkins' zeroth-order theory for the n=1 mode, Morel calculated the far fields from the fictitious magnetic currents in the aperture between the disc and the ground plane.

These fields are given by the expressions:

$$E_\theta = \frac{-jE_o e^{-jk_o r} J_1(ka)\sin(k_o d\cos\theta)\, a\cos\phi\, J_1'(k_o a\sin\theta)}{r\cos\theta} \quad (5)$$

$$E_\phi = \frac{jE_o e^{-jk_o r} J_1(ka)\sin(k_o d\cos\theta)\sin\phi\, J_1(k_o a\sin\theta)}{k_o r\sin\theta} \quad (6)$$

where:

d = dielectric thickness

a = radius of the disc

k_o = free space wavenumber = $2\pi/\lambda$

ka = $k_o\sqrt{\varepsilon_r}\, a = 1.84118$

J_1 = first order Bessel function of the first kind

J_1' = derivitive of the first order Bessel function of the first kind

The expressions for $|E_\theta|$ and $|E_\phi|$ were normalized by a factor of $-jE_o\, e^{-jk_o r}\, 1/r$ and calculated for ϕ angles of 0°, 30°, 60°, and 90° as θ varied from 0° to 90° in 5° steps for each ϕ angle. Since the relative dielectric constants of the printed-circuit boards used in this experimental study were so closely matched, there was a negligible change in the calculated values of $|E_\theta|$ vs θ and $|E_\phi|$ vs θ for each ϕ plane as ε_r varied from 2.45 to 2.48. Thus, only one set of theoretical $|E_\theta|$ vs θ

and $|E_\phi|$ vs θ (normalized) patterns for different ϕ angles was calculated. These theoretical patterns are compared with the experimental patterns in Figures 52 and 53. The theoretical patterns were calculated using a dielectric constant of 2.47. The experimental patterns were measured on an edge fed circular disc antenna which had a substrate material with a dielectric constant of 2.47 and a thickness of 0.16 cm. Figure 52 shows both theoretical and experimental values of $|E_\theta|$ vs θ for the ϕ = 0°, 30°, 60°, and 90° angles. Figure 53 shows theoretical and experimental values of $|E_\phi|$ vs θ for the ϕ = 90°, 60°, 30°, and 0° angles.

The measured fields and the calculated fields are remarkably similar in the following ways. First, for $|E_\theta|$ vs θ there is good agreement between the theoretical and measured results for $\theta<70°$. For $\theta>70°$ the calculated $|E_\theta|$ is greater than the measured $|E_\theta|$. However, both the theoretical and measured patterns reveal a component of $|E_\theta|$ at θ = 90°. For $|E_\phi|$ vs θ , there is good agreement between the theoretical and measured results for values of $0° \leq \theta \leq 90°$. Note that both the calculated and measured results reveal that no component of $|E_\phi|$ exists at θ = 90°. Secondly, the measured and calculated patterns both reveal that the magnitude of E_θ decreases as the ϕ angle increases, and the magnitude of E_ϕ decreases as the ϕ angle decreases. Theoretically, there is a 1.25 dB drop in $|E_\theta|$as ϕ goes from 0° to 30° and a 6 dB drop in $|E_\theta|$ as ϕ goes from 0° to 60°. A 1.25 dB drop in $|E_\phi|$ also theoretically occurs as ϕ goes from 90° to 60° and a 6 dB drop can be calculated for $|E_\phi|$ as ϕ goes from 90° to 30°. Thirdly, both the theoretical and measured results show that the 3 dB beamwidths of E_θ are greater than those for E_ϕ. The theoretical and measured 3 dB

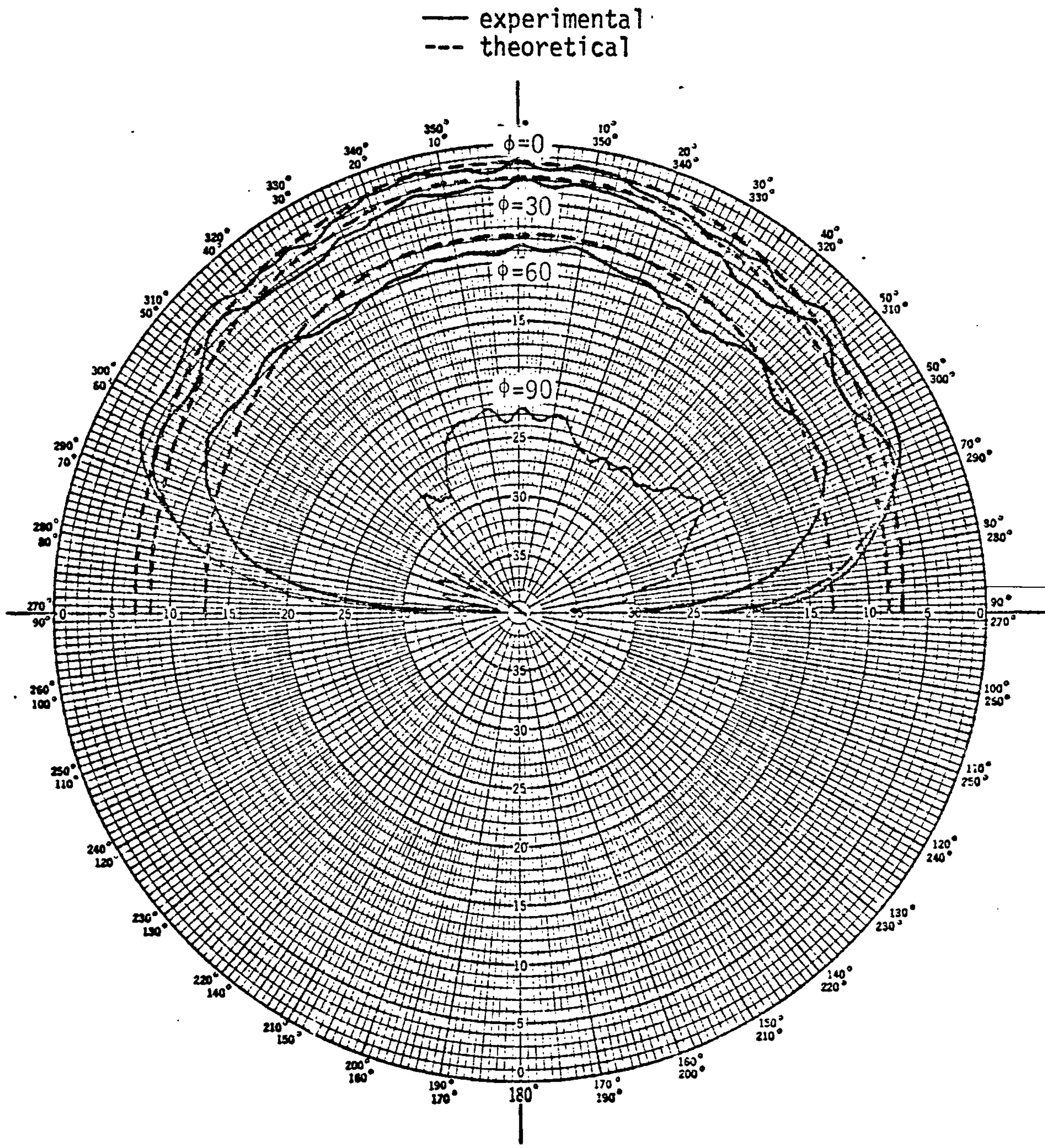

Figure 52: Theoretical and Experimental Values of $|E_\theta|$ vs θ for Different ϕ
$\varepsilon_r = 2.47$

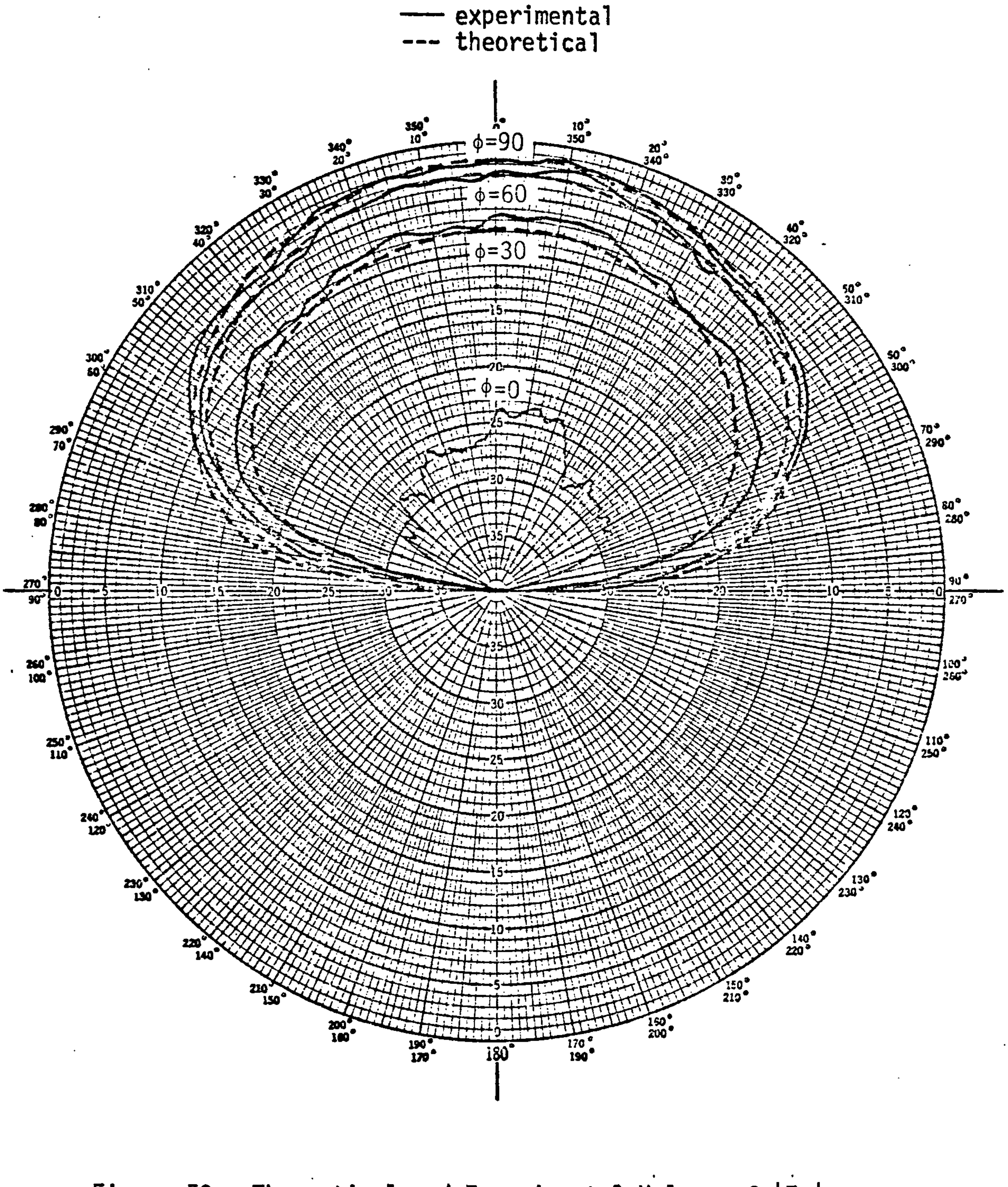

Figure 53: Theoretical and Experimental Values of $|E_\phi|$ vs θ for Different ϕ
$\varepsilon_r = 2.47$

beamwidths of a resonant edge fed circular disc radiator etched on three different substrate thicknesses are shown in Table IV.6.

substrate thickness (cm)	ϕ angle (degrees)	3 dB Beamwidths			
		Theoretical		Measured	
		E_θ	E_ϕ	E_θ	E_ϕ
0.16	0	100	NA	132	NA
	30	100	80	106	66
	60	100	80	136	65
	90	NA	80	NA	68
0.075	0	100	NA	132	NA
	30	100	80	107	70
	60	100	80	134	71
	90	NA	80	NA	72
0.036	0	100	NA	91	NA
	30	100	80	94	69
	60	100	80	119	70
	90	NA	80	NA	73

Table IV.6 Calculated and Measured 3 dB Beamwidths of Resonant Edge Fed Radiators

The measured fields and the calculated fields differ in that for the thinner dielectric materials, i.e. 0.075 cm and 0.036 cm, no dip occurs in the calculated $|E_\theta|$ vs θ and $|E_\phi|$ vs θ patterns at $\theta = 0^\circ$ as it does in the measured far field patterns.

IV.4 Polarization Measurements

Figures 18 and 19, respectively, show, among other things, $|E_\theta|$ vs θ for $\phi = 90^\circ$ and $|E_\phi|$ vs θ for $\phi = 0^\circ$. From Equations (5) and (6), one sees that $|E_\theta|$ vs θ for $\phi = 90^\circ$ and $|E_\phi|$ vs θ for $\phi = 0^\circ$ are both zero. Thus theoretically, for the n=1 mode, the printed-circuit, circular disc antennas are linearly polarized in the x direction for feed points along the x-axis. To test their polarization purity, the transmitting horn was cross-polarized with each printed-circuit, circular disc antenna for measurements of $|E_\theta|$ vs θ and $|E_\phi|$ vs θ. From Figure 18, one can observe that the ratio of $|E_\theta|$ @ $\theta = 0^\circ$, $\phi = 90^\circ$ to $|E_\theta|$ @ $\theta = 0^\circ$, $\phi = 0^\circ$ is approximately -21 dB or 0.089. From Figure 19, the ratio of $|E_\phi|$ @ $\theta = 0^\circ$, $\phi = 0^\circ$ to $|E_\phi|$ @ $\theta = 0^\circ$, $\phi = 90^\circ$ is approximately -22 dB or 0.079. These ratios were typical for all the printed-circuit, circular disc antennas that were fabricated. Thus, for all practical purposes, this type of antenna was experimentally found to be linearly polarized.

CHAPTER V

CONCLUSIONS

From the impedance measurements that were conducted in this experimental study, several conclusions can be drawn about using Watkins' zero-order theory for the n=1 mode in the design of the antennas. First, it was shown that the calculated resonant frequency was always higher than the measured resonant frequency regardless of the feed position or the dielectric thickness. However, the dielectric thickness affects both the resonant frequency and the magnitudes of the resistive and reactive components. For the edge-fed radiators and 3/4 R fed radiators, the measured resonant frequency approached the calculated resonant frequency as the dielectric thickness was decreased. For the 1/2 R fed radiators, the difference between the measured resonant frequency and the theoretical resonant frequency decreased as the dielectric thickness was decreased from 0.16 cm to 0.075 cm, but increased as the dielectric thickness was decreased from 0.075 cm to 0.036 cm. Also, it was shown that regardless of the feed point, the magnitudes of the resistance and reactance curves decreased for decreasing dielectric thickness. Secondly, it was shown that for a given thickness dielectric, the feed position changed the impedance magnitudes, but had a negligible effect as far as changing the resonant frequency of the printed-circuit, circular disc antennas. In general, for a given dielectric thickness, moving the feed point from the edge to a position closer to the center of the disc caused the magnitudes of both the resistance and reactance curves to decrease. However, no more than a ±0.7% change in the resonant frequency occurred when the feed point was moved from R to 1/2 R for any of the three dielectric thicknesses which were experimentally investigated.

Wadkins' zeroth-order theory for the n=1 mode was used by Morel to calculate the far fields, $\overline{E}_\theta$ and $\overline{E}_\phi$. When these theoretical patterns were plotted versus θ for different ϕ angles, it was discovered that radiation was maximum in a direction normal to the plane of the disc. Also, it was shown theoretically that there was a component of $\overline{E}_\theta$ at $\theta = 90°$ for all ϕ angles except 90° and no component of $\overline{E}_\phi$ at $\theta = 90°$ for all ϕ angles. Finally, the calculated patterns using the zeroth-order theory for the n=1 mode revealed that the beamwidth for $\overline{E}_\theta$ was greater than the beamwidth for $\overline{E}_\phi$. These theoretical predictions regarding the far fields were experimentally verified for the printed-circuit, circular disc antennas which were fabricated on a dielectric thickness of 0.16 cm. However, for the thinner dielectric materials, i.e. 0.075 cm and 0.036 cm, it was shown experimentally that radiation was not maximum in a direction normal to the plane of the disc. Dips began to occur at $\theta = 0°$ for the thinner dielectric materials.

Watkins' zeroth-order theory also predicted that the printed-circuit, circular disc antennas operating in the n=1 mode were linearly polarized. This was experimentally verified for three feed positions, R, 3/4 R, and 1/2 R, and three dielectric thicknesses 0.16 cm, 0.075 cm, and 0.036 cm.

BIBLIOGRAPHY

1. J. Watkins, "Circular Resonant Structures in Microstrip," Electronic Letters, Vol. 5, No. 21, October 16, 1969.

2. Robert E. Munson, "Conformal Microstrip Antennas and Microstrip Phased Arrays," IEEE Transactions on Antennas and Propagation, Vol. AP-22, pp. 74-78, January 1974.

3. John Q. Howell, "Microstrip Antennas," IEEE Transactions on Antennas and Propagation, Vol. AP-23, pp. 90-93, January 1975.

4. "PC Board Etching Instructions," Lockheed Company Pamphlet, 1969.

5. Microwave Network Analyzer Applications, Hewlett Packard, June 1970.

6. S. Ramo, J. R. Whinnery, and T. VanDuzer, Fields and Waves in Communications Electronics, New York: Wiley and Sons, p. 33, 1967.

7. Pierre B. Morel, "A Theoretical Investigation of the Circular Printed Circuit Antenna," M. S. Thesis, University of Houston, 1976.

APPENDIX 1

DATA SHEETS

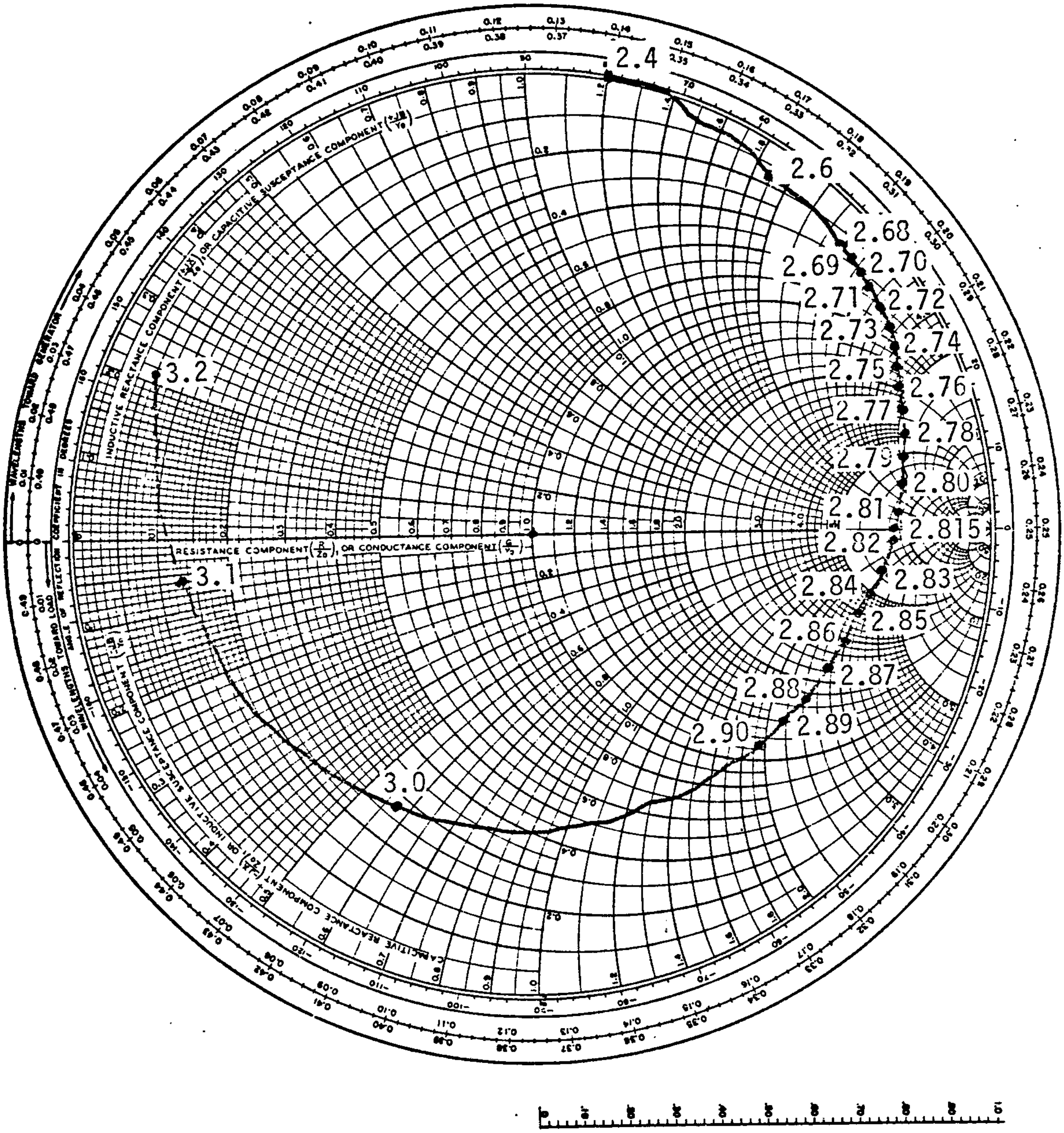

d: 0.16 cm.

ε_r: 2.47

R Fed Radiator

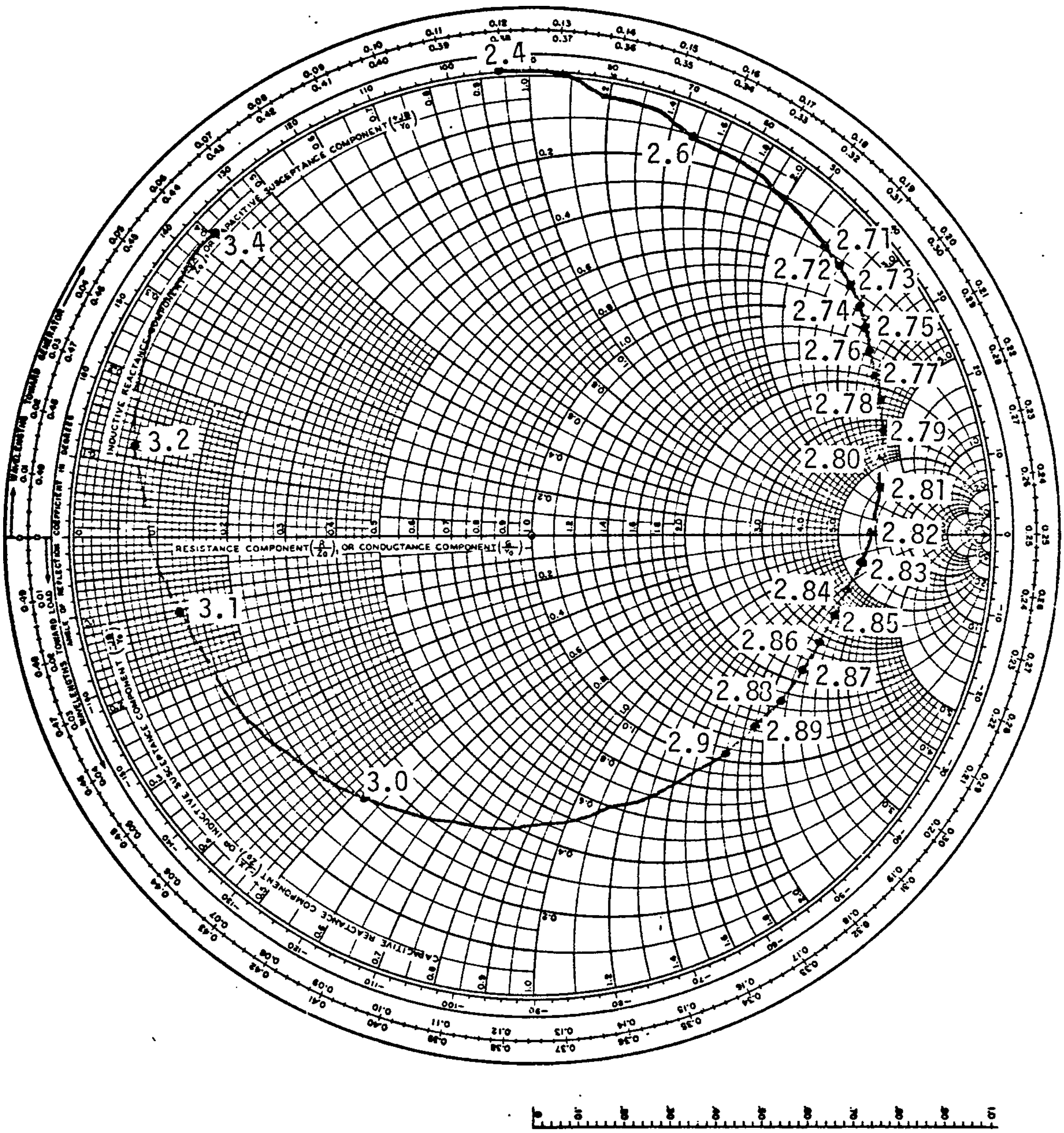

d: 0.16 cm.
ε_r: 2.47
3/4R Fed Radiator

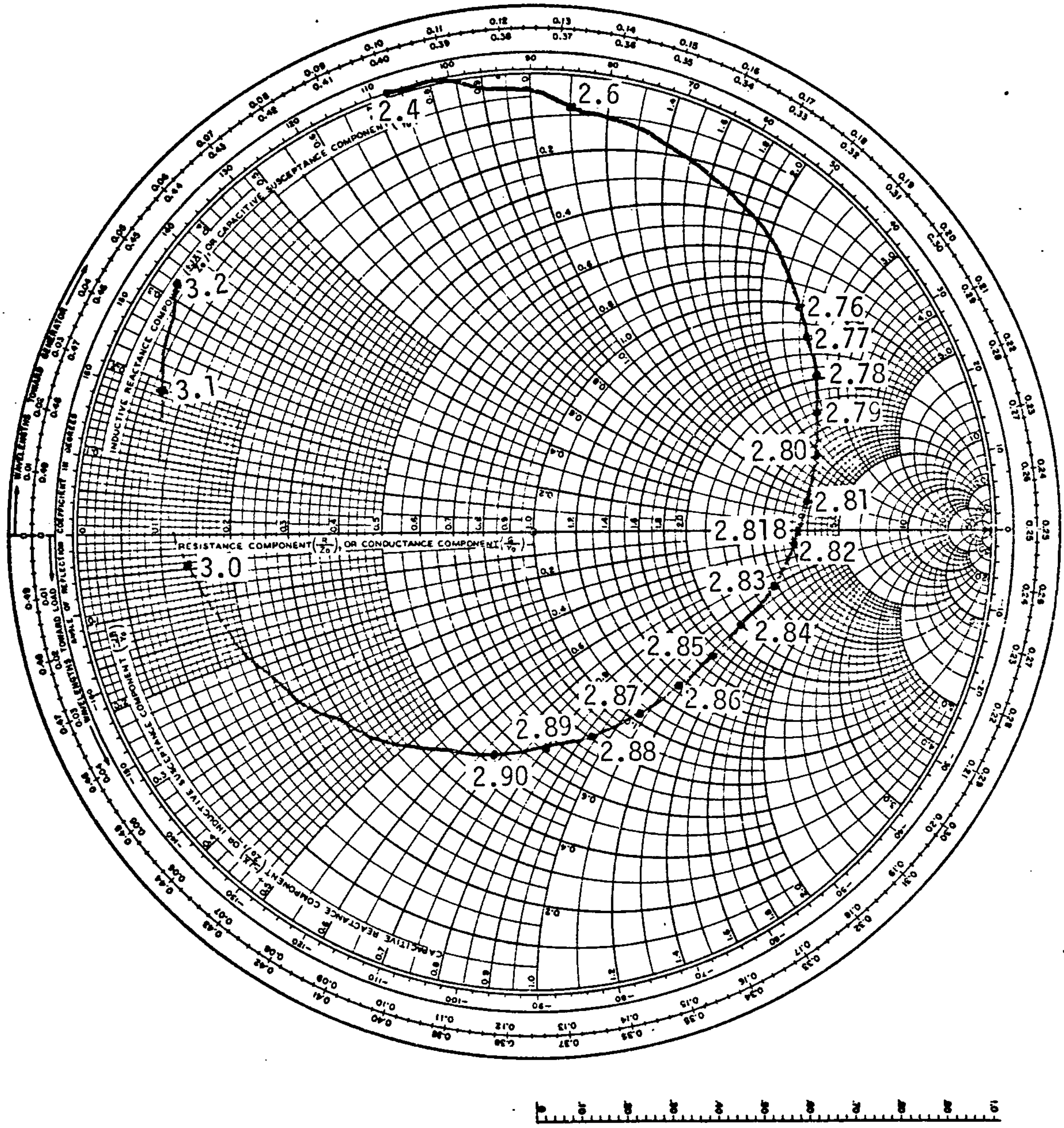

d: 0.16 cm.
ε_r: 2.47
1/2R Fed Radiator

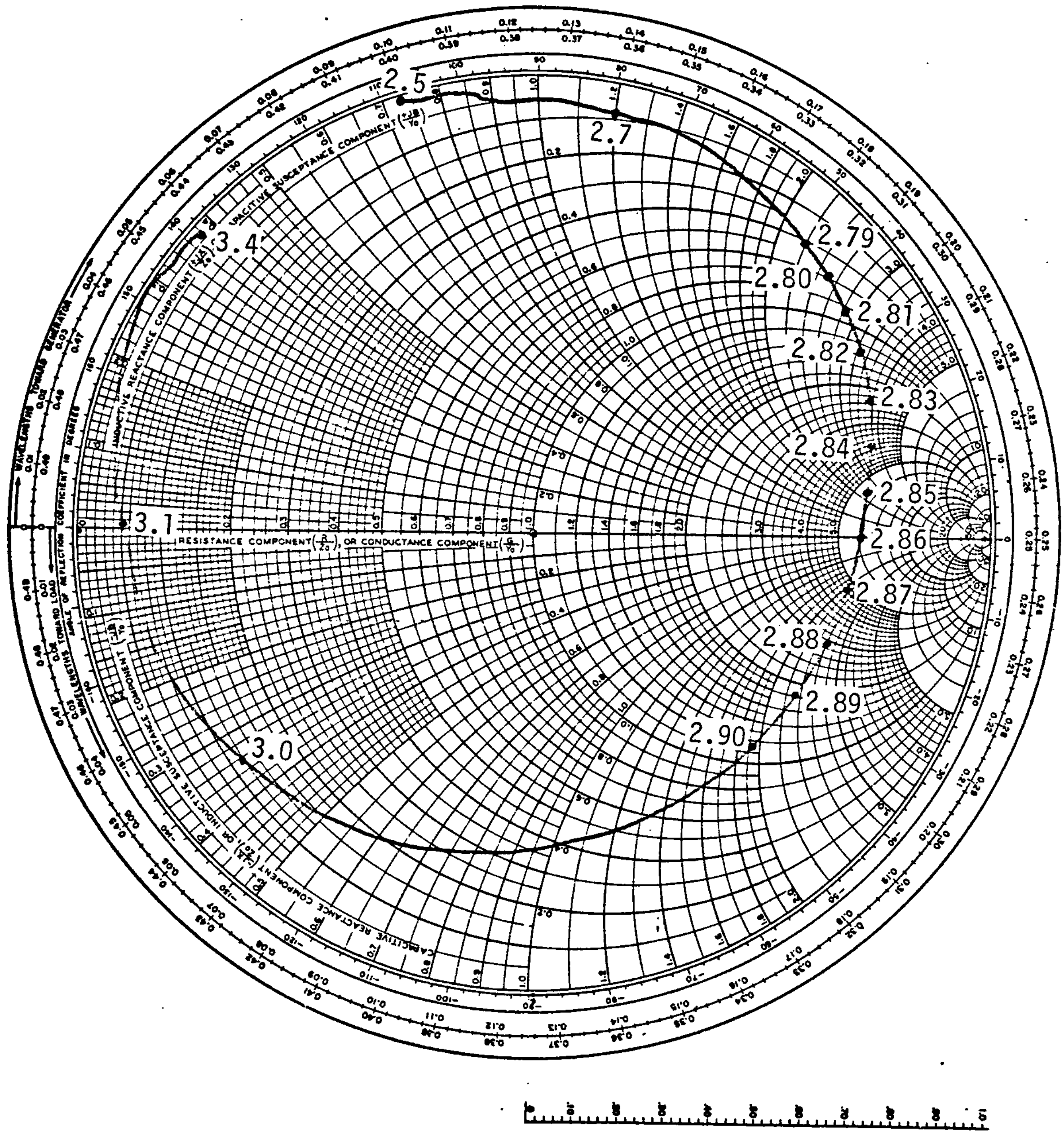

d: 0.075 cm.
ε_r: 2.48
R Fed Radiator

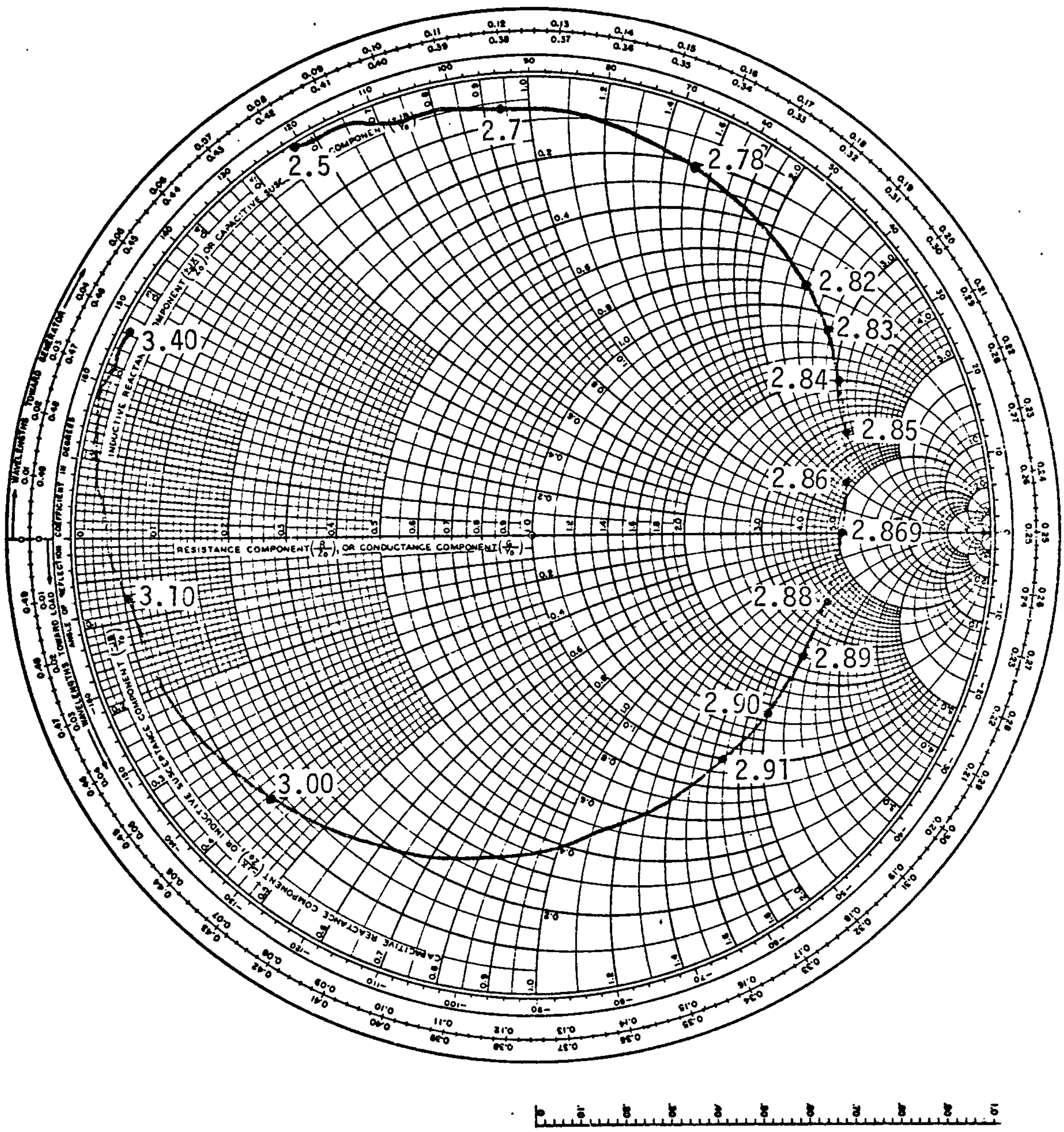

d: 0.075 cm.

ε_r: 2.48

3/4R Fed Radiator

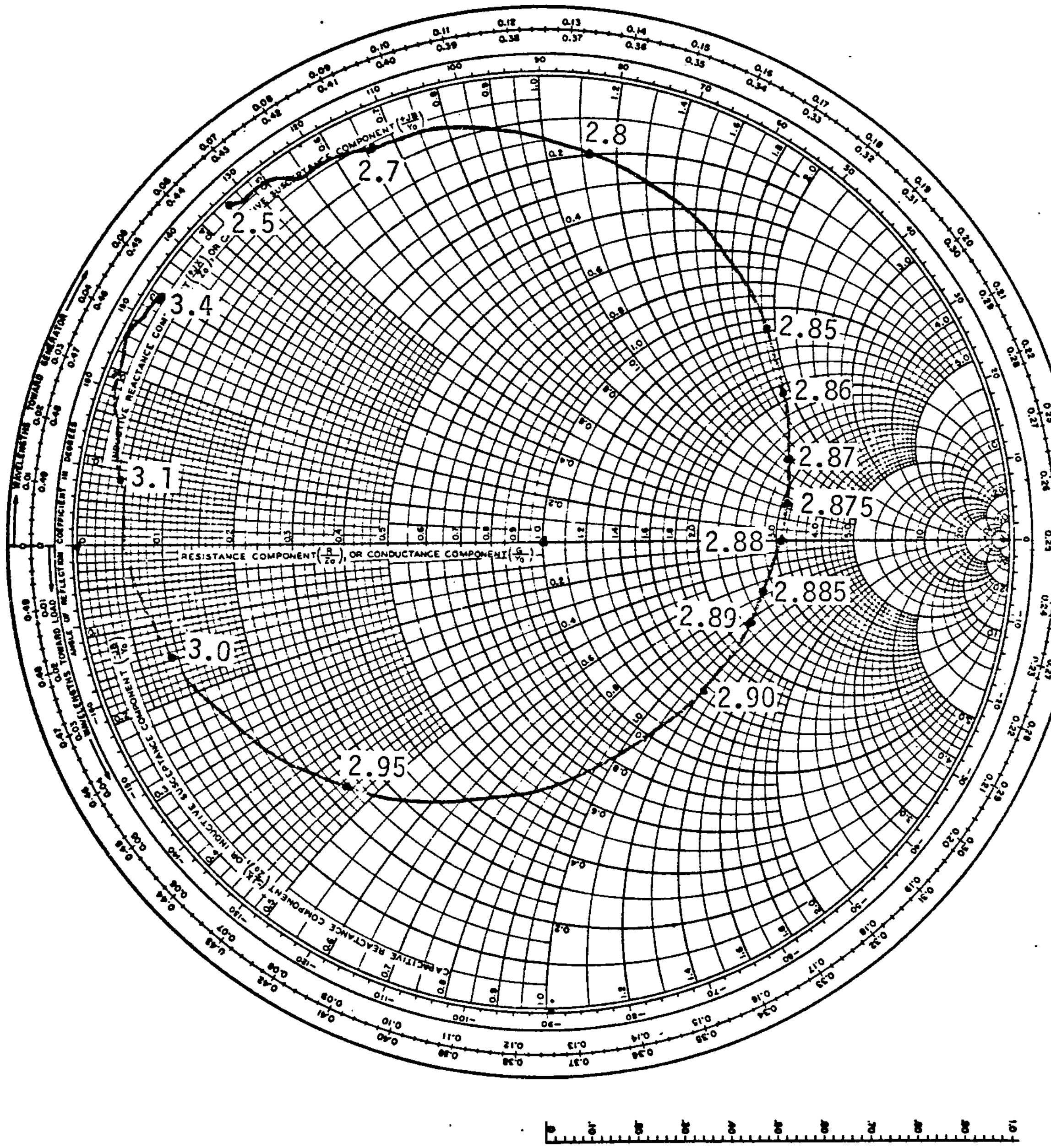

d: 0.075 cm.

ε_r: 2.48

1/2R Fed Radiator

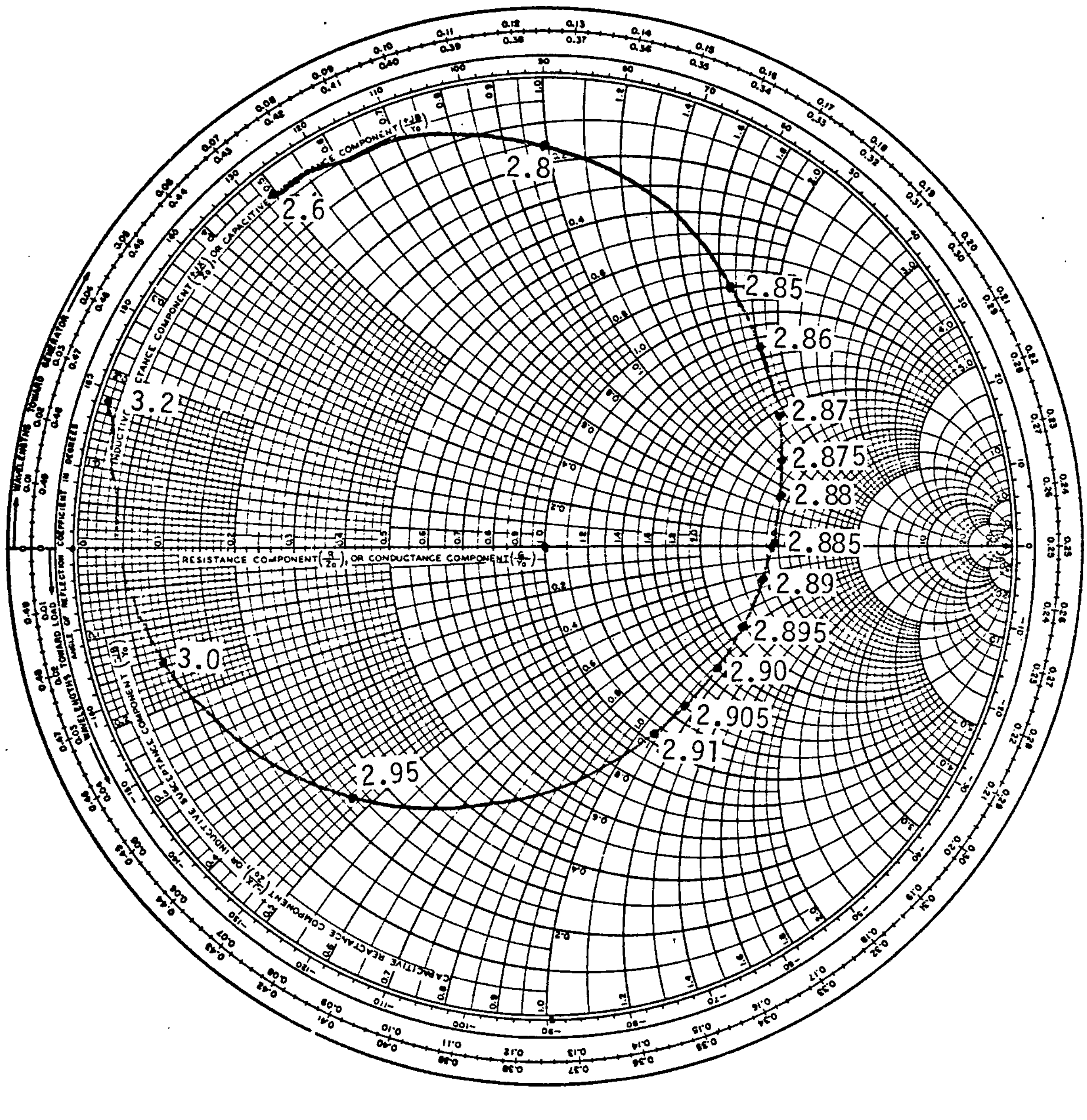

d: 0.036 cm.
ϵ_r: 2.45
R Fed Radiator

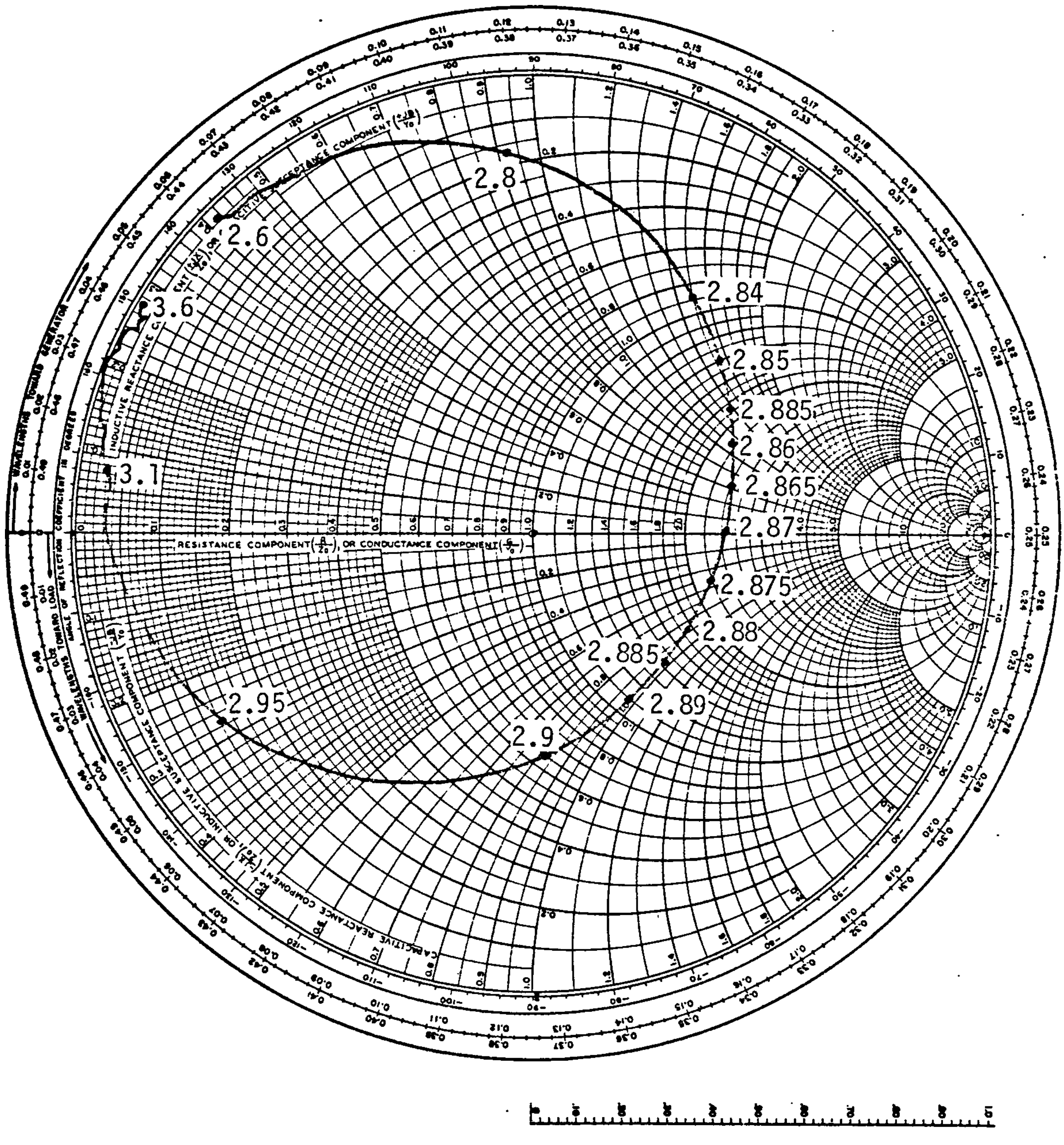

d: 0.036 cm.
ε_r: 2.45
3/4R Fed Radiator

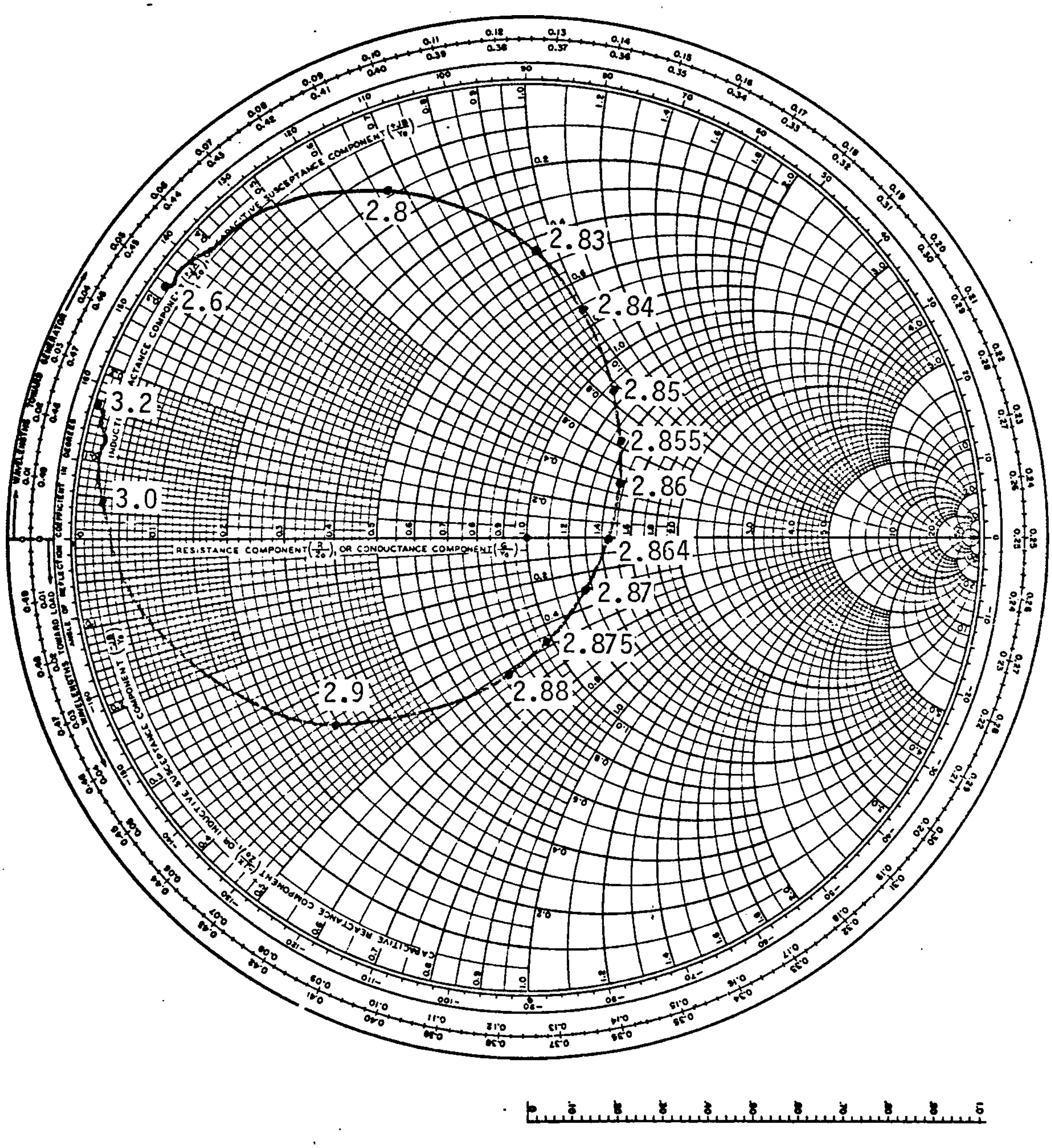

d: 0.036 cm.
ε_r: 2.45
1/2R Fed Radiator

APPENDIX 2

WANG 720C COMPUTER PROGRAM

0	MARK
1	00 02
2	UP
3	9
4	0
5	-
6	DOWN
7	MARK
8	00 03
9	UP
10	3
11	6
12	0
13	DIVIDE
14	DOWN
15	INTEGER X
16	-
17	4
18	x
19	DOWN
20	INTEGER X
21	-
22	WRITE ALPHA
23	SQRT X
24	PI
25	x
26	2
27	DIVIDE
28	DOWN
29	X^2
30	STORE DIRECT
31	REGISTER 3
32	1
33	6
34	UP
35	1
36	STORE DIRECT
37	REGISTER 0
38	MARK
39	15 14
40	RECALL DIRECT
41	REGISTER 3
42	x DIRECT
43	REGISTER 0
44	DOWN
45	DIVIDE DIRECT
46	REGISTER 0
47	1
48	-
49	DOWN
50	CHANGE SIGN
51	DIVIDE DIRECT
52	REGISTER 0
53	1
54	-
55	+ DIRECT
56	REGISTER 0
57	WRITE ALPHA
58	WRITE
59	SEARCH
60	15 14
61	RECALL Y
62	REGISTER 0
63	.
64	5
65	SET EXP
66	CHANGE SIGN
67	1
68	1
69	-
70	-
71	DOWN
72	WRITE ALPHA
73	END PROG
74	SEARCH
75	15 15
76	MARK
77	00 07
78	WRITE ALPHA
79	CLEAR X
80	UP
81	.
82	5
83	SKIP IF Y GE X
84	WRITE ALPHA
85	X^2
86	1
87	+
88	STORE Y
89	REGISTER 0
90	2
91	-
92	RECALL DIRECT
93	REGISTER 0
94	DIVIDE
95	DOWN
96	STORE Y
97	REGISTER 1
98	x
99	STORE Y

100	REGISTER 0
101	1
102	STORE DIRECT
103	REGISTER 3
104	1
105	5
106	UP
107	8
108	STORE DIRECT
109	REGISTER 2
110	MARK
111	15 13
112	RECALL DIRECT
113	REGISTER 0
114	x DIRECT
115	REGISTER 3
116	RECALL DIRECT
117	REGISTER 2
118	x DIRECT
119	REGISTER 2
120	EXCHANGE DIRECT
121	REGISTER 2
122	x DIRECT
123	REGISTER 3
124	DOWN
125	+ DIRECT
126	REGISTER 3
127	2
128	-
129	1
130	- DIRECT
131	REGISTER 2
132	EXCHANGE DIRECT
133	REGISTER 3
134	DIVIDE DIRECT
135	REGISTER 3
136	RECALL DIRECT
137	REGISTER 2
138	WRITE ALPHA
139	LOG e X
140	SEARCH
141	15 13
142	RECALL Y
143	REGISTER 1
144	RECALL DIRECT
145	REGISTER 3
146	x
147	WRITE ALPHA
148	GO
149	x
150	4
151	5
152	WRITE ALPHA
153	10^x
154	DOWN
155	WRITE ALPHA
156	END PROG
157	SEARCH
158	15 15
159	MARK
160	00 04
161	STORE DIRECT
162	REGISTER 1
163	00 02
164	EXCHANGE DIRECT
165	REGISTER 1
166	00 03
167	DIVIDE DIRECT
168	REGISTER 1
169	RECALL DIRECT
170	REGISTER 1
171	RETURN
172	MARK
173	00 05
174	03 00
175	00 07
176	RETURN
177	MARK
178	03 00
179	STORE DIRECT
180	REGISTER 3
181	/x/
182	UP
183	1
184	SKIP IF Y EQ X
185	SEARCH
186	15 12
187	RECALL DIRECT
188	REGISTER 3
189	SET EXP
190	2
191	0
192	SEARCH
193	15 15
194	MARK
195	15 12
196	DOWN
197	x^2
198	CHANGE SIGN
199	UP

```
200    1
201    +
202    DOWN
203    SQRT X
204    DIVIDE DIRECT
205    REGISTER   3
206    RECALL DIRECT
207    REGISTER   3
208    SEARCH
209    15 15
210    MARK
211    00 06
212    03 00
213    00 07
214    UP
215    9
216    0
217    EXCHANGE
218    -
219    DOWN
220    SEARCH
221    15 15
222    MARK
223    00 00
224    UP
225    WRITE ALPHA
226    STOP
227    MARK
228    15 11
229    x
230    DOWN
231    SEARCH
232    15 15
233    MARK
234    00 01
235    UP
236    WRITE ALPHA
237    GO
238    SEARCH
239    15 11
240    MARK
241    00 09
242    STORE DIRECT
243    REGISTER   1
244    00 03
245    x
246    DOWN
247    EXCHANGE DIRECT
248    REGISTER   1
249    12 15
250    14 08
251    00 02
252    x
253    RECALL DIRECT
254    REGISTER   1
255    RETURN
256    MARK
257    00 08
258    WRITE ALPHA
259    WRITE
260    SEARCH
261    15 05
262    WRITE ALPHA
263    SET EXP
264    EXCHANGE
265    RETURN
266    CHANGE SIGN
267    UP
268    1
269    8
270    0
271    RETURN
272    MARK
273    15 05
274    WRITE ALPHA
275    LOG e X
276    SEARCH
277    15 04
278    1
279    SET EXP
280    CHANGE SIGN
281    9
282    5
283    MARK
284    15 04
285    WRITE ALPHA
286    e^x
287    DIVIDE
288    x^2
289    STORE DIRECT
290    REGISTER   0
291    12 05
292    14 08
293    x^2
294    + DIRECT
295    REGISTER   0
296    RECALL DIRECT
297    REGISTER   0
298    EXCHANGE
299    WRITE ALPHA
```

300	LOG 10 X
301	1/x
302	CHANGE SIGN
303	00 07
304	STORE DIRECT
305	REGISTER 0
306	1
307	WRITE ALPHA
308	LOAD PROG
309	UP
310	9
311	0
312	x
313	RECALL DIRECT
314	REGISTER 0
315	+
316	12 05
317	14 08
318	SQRT X
319	EXCHANGE
320	RETURN
321	MARK
322	00 10
323	03 01
324	-
325	MARK
326	15 09
327	2
328	DIVIDE
329	DOWN
330	SEARCH
331	15 15
332	MARK
333	03 01
334	e^x
335	UP
336	1/x
337	RETURN
338	MARK
339	00 11
340	03 01
341	+
342	SEARCH
343	15 09
344	MARK
345	00 12
346	03 01
347	STORE Y
348	REGISTER 3
349	-
350	+ DIRECT
351	REGISTER 3
352	RECALL DIRECT
353	REGISTER 3
354	DIVIDE
355	DOWN
356	SEARCH
357	15 15
358	MARK
359	00 13
360	03 02
361	+
362	MARK
363	15 10
364	DOWN
365	SQRT X
366	RECALL Y
367	REGISTER 3
368	+
369	DOWN
370	LOG e X
371	SEARCH
372	15 15
373	MARK
374	03 02
375	STORE DIRECT
376	REGISTER 3
377	x^2
378	UP
379	1
380	RETURN
381	MARK
382	00 14
383	03 02
384	-
385	SEARCH
386	15 10
387	MARK
388	00 15
389	UP
390	CHANGE SIGN
391	STORE DIRECT
392	REGISTER 3
393	1
394	+
395	+ DIRECT
396	REGISTER 3
397	RECALL DIRECT
398	REGISTER 3
399	DIVIDE

400	DOWN
401	LOG e X
402	UP
403	2
404	DIVIDE
405	DOWN
406	MARK
407	15 15
408	12 15
409	14 08
410	RETURN
411	MARK
412	LOG e X
413	STOP
414	STORE DIRECT
415	REGISTER 10
416	WRITE ALPHA
417	01 02
418	00 02
419	00 02
420	00 02
421	00 14
422	01 13
423	02 05
424	00 04
425	02 14
426	02 05
427	02 06
428	02 12
429	00 01
430	00 02
431	00 02
432	00 02
433	00 02
434	01 13
435	02 05
436	00 14
437	02 09
438	02 05
439	02 12
440	02 07
441	01 04
442	01 09
443	02 06
444	00 02
445	00 02
446	00 02
447	01 13
448	02 05
449	00 14
450	02 09
451	02 05
452	02 12
453	02 07
454	01 04
455	01 09
456	02 06
457	00 02
458	00 02
459	00 02
460	01 04
461	01 15
462	00 05
463	02 05
464	02 13
465	01 12
466	02 06
467	02 12
468	02 05
469	00 02
470	00 02
471	00 02
472	00 02
473	01 04
474	01 15
475	00 05
476	02 05
477	02 13
478	01 12
479	02 06
480	02 12
481	02 05
482	01 08
483	00 02
484	00 02
485	00 02
486	00 02
487	00 02
488	01 03
489	03 00
490	00 15
491	02 01
492	01 02
493	03 07
494	01 03
495	03 01
496	01 02
497	00 02
498	00 02
499	00 02

500	00 02
501	00 02
502	00 02
503	02 12
504	01 09
505	02 05
506	00 14
507	00 14
508	01 04
509	02 12
510	01 04
511	02 05
512	02 06
513	02 07
514	00 02
515	00 02
516	02 12
517	01 09
518	02 05
519	00 14
520	00 14
521	01 04
522	02 12
523	01 04
524	02 05
525	02 06
526	02 07
527	00 02
528	00 02
529	01 13
530	02 05
531	01 12
532	02 09
533	00 02
534	00 05
535	01 12
536	01 13
537	02 07
538	00 02
539	00 02
540	01 04
541	01 15
542	01 12
543	00 15
544	01 04
545	02 06
546	01 12
547	01 13
548	00 01
549	00 02
550	00 05
551	01 12
552	01 13
553	02 07
554	01 08
555	END ALPHA
556	WRITE
557	12 15
558	WRITE ALPHA
559	00 02
560	00 02
561	01 15
562	01 12
563	00 15
564	02 06
565	01 04
566	02 07
567	02 14
568	02 13
569	02 05
570	END ALPHA
571	WRITE
572	12 06
573	WRITE ALPHA
574	01 12
575	02 06
576	00 15
577	02 09
578	02 05
579	01 08
580	01 08
581	END ALPHA
582	MARK
583	e^x
584	STOP
585	STORE DIRECT
586	REGISTER 27
587	STOP
588	STORE DIRECT
589	REGISTER 11
590	STOP
591	STORE DIRECT
592	REGISTER 12
593	RECALL Y
594	REGISTER 11
595	RECALL DIRECT
596	REGISTER 12
597	00 09
598	STORE Y
599	REGISTER 13

```
600   STORE DIRECT
601   REGISTER 14
602   RECALL DIRECT
603   REGISTER 13
604   CHANGE SIGN
605   STORE DIRECT
606   REGISTER 15
607   RECALL DIRECT
608   REGISTER 14
609   CHANGE SIGN
610   STORE DIRECT
611   REGISTER 16
612   RECALL DIRECT
613   REGISTER 14
614   UP
615   1
616   +
617   STORE Y
618   REGISTER 17
619   RECALL DIRECT
620   REGISTER 16
621   UP
622   1
623   +
624   STORE Y
625   REGISTER 18
626   RECALL Y
627   REGISTER 13
628   RECALL DIRECT
629   REGISTER 17
630   00 08
631   STORE Y
632   REGISTER 19
633   STORE DIRECT
634   REGISTER 20
635   RECALL Y
636   REGISTER 15
637   RECALL DIRECT
638   REGISTER 18
639   00 08
640   STORE Y
641   REGISTER 21
642   STORE DIRECT
643   REGISTER 22
644   RECALL Y
645   REGISTER 19
646   RECALL DIRECT
647   REGISTER 21
648   DIVIDE
649   STORE Y
650   REGISTER 23
651   RECALL Y
652   REGISTER 20
653   RECALL DIRECT
654   REGISTER 22
655   -
656   STORE Y
657   REGISTER 24
658   RECALL Y
659   REGISTER 23
660   RECALL DIRECT
661   REGISTER 24
662   00 09
663   STORE Y
664   REGISTER 25
665   STORE DIRECT
666   REGISTER 26
667   RECALL DIRECT
668   REGISTER 10
669   x DIRECT
670   REGISTER 25
671   x DIRECT
672   REGISTER 26
673   RECALL DIRECT
674   REGISTER 27
675   WRITE
676   05 03
677   WRITE ALPHA
678   00 02
679   00 02
680   00 02
681   END ALPHA
682   RECALL DIRECT
683   REGISTER 11
684   WRITE
685   06 02
686   WRITE ALPHA
687   00 02
688   00 02
689   00 02
690   END ALPHA
691   RECALL DIRECT
692   REGISTER 12
693   WRITE
694   09 00
695   WRITE ALPHA
696   00 02
697   00 02
698   00 02
699   00 02
```

```
700    00 02
701    00 02
702    00 02
703    END ALPHA
704    RECALL DIRECT
705    REGISTER  26
706    UP
707    INTEGER X
708    -
709    .
710    5
711    EXCHANGE
712    SKIP IF Y LT X
713    SEARCH
714    1/x
715    1
716    + DIRECT
717    REGISTER  26
718    MARK
719    1/x
720    RECALL DIRECT
721    REGISTER  26
722    WRITE
723    04 00
724    WRITE ALPHA
725    00 02
726    00 02
727    00 02
728    00 02
729    00 02
730    END ALPHA
731    RECALL DIRECT
732    REGISTER  25
733    UP
734    INTEGER X
735    -
736    .
737    5
738    EXCHANGE
739    SKIP IF Y LT X
740    SEARCH
741    PI
742    1
743    + DIRECT
744    REGISTER  25
745    MARK
746    PI
747    RECALL DIRECT
748    REGISTER  25
749    WRITE
750    06 00
751    WRITE ALPHA
752    01 08
753    END ALPHA
754    SEARCH
755    e^x
756    END PROG
```